TR N33 04 5060

NUREG/CR-5060
AAEC/C49

An Approach to the Mathematical Modelling of the Uranium Series Redistribution Within Ore Bodies

Australian Atomic Energy Commission

Prepared for
U.S. Nuclear Regulatory
Commission

COMPLETED

ORIGINAL

BEST COPY AVAILABLE

NOTICE

This report was prepared as an account of work sponsored by an agency of the United States Government. Neither the United States Government nor any agency thereof, or any of their employees, makes any warranty, expressed or implied, or assumes any legal liability of responsibility for any third party's use, or the results of such use, of any information, apparatus, product or process disclosed in this report, or represents that its use by such third party would not infringe privately owned rights.

NOTICE

Availability of Reference Materials Cited in NRC Publications

Most documents cited in NRC publications will be available from one of the following sources:

1. The NRC Public Document Room, 1717 H Street, N.W. Washington, DC 20555
2. The Superintendent of Documents, U.S. Government Printing Office, Post Office Box 37082, Washington, DC 20013-7082
3. The National Technical Information Service, Springfield, VA 22161

Although the listing that follows represents the majority of documents cited in NRC publications, it is not intended to be exhaustive.

Referenced documents available for inspection and copying for a fee from the NRC Public Document Room include NRC correspondence and internal NRC memoranda; NRC Office of Inspection and Enforcement bulletins, circulars, information notices, inspection and investigation notices; Licensee Event Reports; vendor reports and correspondence; Commission papers; and applicant and licensee documents and correspondence.

The following documents in the NUREG series are available for purchase from the GPO Sales Program: formal NRC staff and contractor reports, NRC-sponsored conference proceedings, and NRC booklets and brochures. Also available are Regulatory Guides, NRC regulations in the *Code of Federal Regulations*, and *Nuclear Regulatory Commission Issuances*.

Documents available from the National Technical Information Service include NUREG-series reports and technical reports prepared by other federal agencies and reports prepared by the Atomic Energy Commission, forerunner agency to the Nuclear Regulatory Commission.

Documents available from public and special technical libraries include all open literature items, such as books, journal and periodical articles, and transactions. *Federal Register* notices, federal and state legislation, and congressional reports can usually be obtained from these libraries.

Documents such as theses, dissertations, foreign reports and translations, and non-NRC conference proceedings are available for purchase from the organization sponsoring the publication cited.

Single copies of NRC draft reports are available free, to the extent of supply, upon written request to the Division of Information Support Services, Distribution Section, U.S. Nuclear Regulatory Commission, Washington, DC 20555.

Copies of industry codes and standards used in a substantive manner in the NRC regulatory process are maintained at the NRC Library, 7920 Norfolk Avenue, Bethesda, Maryland, and are available there for reference use by the public. Codes and standards are usually copyrighted and may be purchased from the originating organization or, if they are American National Standards, from the American National Standards Institute, 1430 Broadway, New York, NY 10018.

NUREG/CR-5060
AAEC/C49
RW

An Approach to the Mathematical Modelling of the Uranium Series Redistribution Within Ore Bodies

Manuscript Completed: June 1986
Date Published: December 1987

Prepared by
P. L. Airey, C. Golian, D. A. Lever*

Australian Atomic Energy Commission
Lucas Heights Research Laboratories
Lucas Heights, NSW 2232, Australia

*Visiting Scientist from UKAERE Harwell

Prepared for
Division of Engineering
Office of Nuclear Regulatory Research
U.S. Nuclear Regulatory Commission
Washington, DC 20555
NRC FIN B6661
Under Contract No. NRC-04-81-172

II

ABSTRACT

The distributions of the uranium series isotopes in the Koongarra ore body were "predicted" by a simple one-dimensional model of isotopic migration parameters. Controlling the "predictions" were the retardation factors and the groundwater flow rates. The conditions modelled were a groundwater flow rate of 1 meter per year, retardation factors of 1×10^4 for ^{238}U and of 1.2×10^4 for ^{234}U, and ^{230}Th is immobile. For this set of conditions, an exceptionally good agreement was observed between field-measured isotope ratios and "predicted" isotope ratios.

A multiphase model adequately describes the redistribution of uranium and daughter radionuclides in the weathered zone of the ore bodies. It redistributes U, Th and Ra isotopes among an aqueous phase, an amorphous iron phase, a crystalline phase and a "phase" of clay and quartz.

CONTENTS

EXECUTIVE SUMMARY xiii

1. INTRODUCTION 1

1.1 Approach to Modelling 1
1.2 The Study Region 3

1.2.1 Ranger One ore body 4
1.2.2 Jabiluka ore deposits 4
1.2.3 Nabarlek ore body 5
1.2.4 Koongarra deposit 5

2. MATHEMATICAL MODELLING OF THE UPPER SEQUENCES OF THE ORE BODY 6

2.1 General Description of the Model 6
2.2 Mathematical Formulation of the Model 7
2.3 Output of the Model 9

3. VALIDITY OF THE MODEL 11

3.1 Independent Assessment of the Assumptions of the Model 11

3.1.1 Four-zone classification 11
3.1.2 Separation of leaching and depositional zones . 11
3.1.3 Comparison with independent geomorphological evidence (erosion) 12

3.2 Mathematical Correlation with Other Open-system Models 12

3.2.1 Mathematical correlation between the current model and the uranium trend model (UTDM) . . 13
3.2.2 Mathematical correlation with Hille's open-system model 15

3.3 Application of the Model to Open-system Dating . . 16

3.3.1 Dating of soil profiles 16
3.3.2 Examples of open-system dating 18

4. EXTENSION OF THE MODEL TO MULTIPHASE SYSTEMS . . . 19

4.1 Formulation of the Multiphase Model 19
4.2 Application to Experimental Data 23
4.3 Discussion of the Multiphase Model 25

4.3.1 Radionuclide transport between phases - the parameter ϕ_e 25
4.3.2 A mechanism for enhanced retardation on clays over long timescales 28
4.3.3 Transferability of information from the analogue to the repository site 28

5. KOONGARRA SECONDARY MINERALIZATION - MODELLING OF A ROLL FRONT 30

5.1 Uranium Series Fractionation within the Secondary Mineralization 30
5.2 A Simple Migration Model 31
5.3 General Solutions 32
5.4 Analysis of Rock Activity Ratios 35
5.5 Estimates of the Migration Time 36
5.6 Analysis of Lead Data 38
5.7 Application of Laplace Transform Techniques . . . 39
5.8 Concluding Remarks 42

6. APPLICATION OF THE MODEL TO THE DEVELOPMENT AND REFINEMENT OF THE ANALOGUE 44

6.1 Calculation of Source Terms 44
6.2 Interpretation of Laboratory Data in Terms of Time-dependent Retardation Factors 45
6.3 Separation of Authigenic and Allogenic Components of Uranium Series Elements 46
6.4 Transferability of Information from the Analogue to the Repository Site 46
6.5 Validation of Geochemical Transport Codes . . . 47

7. REFERENCES 48

FIGURES

1	The location of the principal uranium ore bodies and prospects in the Alligator Rivers region of the Northern Territory of Australia.	51
2	Generalized geologic plan of the Ranger One ore bodies and prospects.	52
3	Generalized geologic plan and cross-sections of the Jabiluka One and Two ore bodies.	53
4	Location of the sampling wells at Nabarlek.	54
5A	Location of the sampling wells at the Koongarra deposit.	55
5B	A section between wells PH 78 and PH 94 showing the location of a major fault, the extent of the uranium deposits, the boundary of surface oxidation and the groundwater flow paths.	55
6A	Composite illustration of the variation with depth of the $^{230}Th/^{234}U$ activity ratios from the Ranger One, Jabiluka One and Nabarlek ore bodies.	56
6B	Schematic representation of the four-zone model.	56
7	Variation of the isotope ratios with the erosion parameter ξ/λ_4 (Equation (3)).	57
8	Variation of the $^{234}U/^{238}U$ activity ratios in selectively extracted phases from samples from the S1/146 core of the Ranger One ore body.	58
9	Variation of the $^{230}Th/^{234}U$ activity ratios in selectively extracted phases from samples from the S1/146 core of the Ranger One ore body.	59
10	Schematic representation of the variation of X (=(^{238}U-^{230}Th)/^{238}U) and Y (=(^{238}U-^{234}U)/^{234}U) since the development of the soil horizon.	60
11	Variation of the leaching parameter ξ with the intercept X_i for conditions of leaching and deposition.	61
12	Variation of the reciprocal of the leaching parameter ξ^{-1} with the intercept X_i for different ages and selected values of the parameter R (Equation (3)).	62
13	The range of validity of the leaching (or deposition) parameter ξ/time variation for $^{234}U/^{238}U$ and $^{230}Th/^{234}U$ ratios shown in the key. Measurement accuracies of ±0.02 are assumed. Three values of the parameter R (Equation (3)) have been used. Figure 13A applies to leaching, and 13B to deposition.	63

14 The domain of validity of the leaching parameter ξ/time relationship for $^{234}U/^{238}U = 0.90$ and $^{230}Th/^{234}U = 1.25$ assuming isotopic equilibrium at zero time. A value of R (Equation (3)) of 1.15 has been chosen. The effect of measurement uncertainties of 0.02, 0.03 and 0.05 on the range of parameter values is shown. 64

15 Comparison of interpretation of data for Quaternary deposits in Nevada[22]. 65

16 Dating of shells (data of Rosholt and Szabo[17]). Comparison of Hille's[15] model results and time-leaching domains obtained using the current model. 66

17 Schematic diagram of the microscopic four-phase model of uranium series nuclide geochemistry on the weathered surfaces of crystalline rocks. 67

18A Variation of the $^{234}U/^{238}U$ excess in clay/quartz ($Rt_{CQ} - 1$) (Equation (56), with the ratio of uranium on the iron phases to that on clay/quartz (U_{AX}/U_{CQ}). 68

18B Variation of the parameter $(Rt_{CQ} - 1)/U_{CQ}$ with the uranium ratio U_{AX}/U_{CQ}. 68

19 Variation of $^{AX}Re^{CQ}$ (Equation (55)), the probability that the product of α-recoil from a parent originating in the iron phases AX will be found in the clay/quartz phases CQ. 69

20 The flux of uranium between specified separable phases within the weathered ore. 70

21 Schematic plot of the distribution of activity of ^{238}U, ^{234}U and ^{230}Th in the region of secondary mineralization and corresponding plot of the $^{234}U/^{238}U$ against $^{230}Th/^{238}U$ activity ratios for the case $R_{238} < R_{234}$ and $R_{238} < R_{230}$. 71

22 Schematic plot of the distribution of activity of ^{238}U, ^{234}U and ^{230}Th in the region of secondary mineralization and corresponding plot of the $^{234}U/^{238}U$ against $^{230}Th/^{238}U$ activity ratios for the case $R_{234} < R^{\infty}_{234}$ and $R_{238} < R_{230}$ ("fast" system). 72

23 Schematic plot of the distribution of activity of ^{238}U, ^{234}U and ^{230}Th in the region of secondary mineralization and corresponding plot of the $^{234}U/^{238}U$ against $^{230}Th/^{238}U$ activity ratios for the case $R^{\infty}_{234} < R_{234} < R_{238} < R_{230}$ ("slow" system). 73

24 Plot of $^{234}U/^{238}U$ and $^{230}Th/^{238}U$ activity ratios found at Koongarra showing best linear fit ($R_{234} = 1.2\ R_{238}$, $R_{230} = \infty$). 74

25 Example of numerical application of Laplace transform technique to the case of a pulse input ${}_0C_{238}(t) = t\ e^{-\zeta t}$, showing the corresponding activity ratio plot. 75

TABLES

1	Four-zone Model of the Upper Sequences of the Ore Bodies	76
2	Ranger: Comparison of Predicted Uranium Geochemistry from Mineralogical and Isotope Data	77
3	Drill Core Samples - Model Parameters	78
4	Uranium Series Fractionation in Separable Phases from Drill Core S1/146, Ranger One	79
5	Comparison of Uranium Series Fractionation on Koongarra and Ranger One (S1/146) Drill Core	80
6	Experimental Verification of the Multiphase Model	81
7	Koongarra Groundwater - Isotopic Data	82
8	Estimates of Migration Time from Analysis of Lead Data	83

APPENDICES

APPENDIX A	SOLUTION OF THE URANIUM TRANSPORT EQUATIONS	A-1	84
APPENDIX B	COMPUTER PROGRAM - MAIN MODEL	B-1	87
APPENDIX C	CORRELATION BETWEEN THE PRESENT MODEL AND THE URANIUM TREND DATING MODEL	C-1	89
APPENDIX D	ALGEBRAIC EXPRESSION FOR THE INTERCEPT OF THE URANIUM TREND LINE	D-1	90
APPENDIX E	ANALYTICAL SOLUTIONS OF THE SIMULTANEOUS DIFFERENTIAL EQUATIONS DESCRIBING THE DISTRIBUTION OF ^{238}U, ^{234}U AND ^{230}Th IN AMORPHOUS AND CRYSTALLINE IRON	E-1	91
APPENDIX F	COMPUTER PROGRAM - MULTIPHASE	F-1	95
APPENDIX G	LIST OF SYMBOLS	G-1	100

BLANK PAGE

EXECUTIVE SUMMARY

A number of mathematical approaches have been developed to model radionuclide transport around uranium ore bodies in the Alligator Rivers Region of the Northern Territory of Australia. The extensive region of secondary mineralization with the Koongarra deposit represents a very interesting system which may be used as an analogue for high-level radioactive waste repositories. Modelling of this system has been undertaken so that general hydraulic transport models can be adapted for use in repository safety assessments. It is important that the two inherent classes of data (generic and site-specific) be recognized and interpreted so that their relevance can be evaluated and the transferability of the information (to a repository site) can be maximized.

The principal aim of the study was to quantify the rate of mobilization of the radionuclides by estimating the net rate of leaching (or accumulation) of uranium due to groundwater flow and the weathering of crystalline rock. In addition, the timescale for transport under open system conditions was determined. In the latter case the residence time of uranium within a particular zone of the ore deposits is based on radioisotope and mineralogical data.

The general nature of the generating equations allowed the model to be applied to other related problems, e.g. dating of bones, shells, and the development of soil profiles.

The validation of modelling work has been attempted by establishing correlations with other open-system models (uranium trend model, J. Rosholt; Hille's model) and by comparing its predictions with field observations.

The mathematical studies have been extended to model multiphase systems. As a result of experimental evidence, differences in the accessibility of uranium in the amorphous and the crystalline iron phases to groundwater are allowed; the recoil effect and exchange between phases are also included. A better understanding of the migration of radionuclides through clays is therefore possible.

1. INTRODUCTION

The aim of the project is to contribute to the scientific basis for the long-term prediction of the migration of radionuclides. A natural analogue approach has been used. Uranium ore bodies in the Alligator Rivers Region of the Northern Territory of Australia have been evaluated as analogues of high-level radioactive waste repositories. Accounts of the project have been presented in Annual Reports to the US Nuclear Regulatory Commission and in a number of general presentations[1-6].

To predict the transport of radionuclides, two basic parameters are required:

- the net velocity of the mobile phase;
- the retardation factor, i.e. the relative rate of migration of the mobile phase and the solute.

Over the timescale of interest in the transport of radionuclides, a number of additional factors need to be considered. These may be classified as follows:

(i) Changes in the hydraulics. Even in the far-field, long-term changes in the hydraulics are expected, owing to

- climatic change, and
- changes in the porosity or the hydraulic conductivity due to processes of dissolution on precipitation.

(ii) Changes in the retardation factor of the radionuclide, owing to

- changes in the mineralogy of the accessible surfaces, and
- the effect of recoil on the initial distribution of authigenic radionuclides formed by α-decay.

Of equal importance is to determine whether the mathematical procedures for interpreting these parameters in terms of the rate of radionuclide transport are suitable for making long-term predictions. As a significant step, an attempt will be made to verify the Sandia waste-isolation flow and transport code, SWIFT[7] using the natural analogue system. Specifically, this entails investigation of the extent to which the code can predict the distribution of uranium and its daughter products down-gradient of the region of primary mineralization.

1.1 Approach to Modelling

This report outlines the mathematical approaches which have been used to support the analogue study. The investigation can be described in a number of roughly chronological stages:

Stage 1 It was first necessary to obtain a quantitative description of the redistribution of uranium within the ore bodies in order to establish the relative importance of

- leaching, and
- erosion

as mechanisms of radionuclide transport. As there were no models which could be readily adapted to the current application, some pioneering work was necessary. Attempts have been made to validate the model by

- establishing mathematical correlations with other open-system models, and
- comparing model predictions with field observations.

Stage 2 Because of the general nature of the model, it can be applied to a number of related problems, including

- the dating of bones, shells and other open systems, and
- the development of soil profiles.

Stage 3 The model developed in stage 1 is by its nature global, as it is used to describe the redistribution of uranium through the upper sequences of the ore bodies. The matrix is assumed to be homogeneous. This simplification severely limits the usefulness of the analogues because many of the factors affecting radionuclide migration over very long periods, which are not apparent at laboratory timescales, are associated with the non-homogeneity of the host rock. For instance, in the weathered zone, iron minerals are of particular significance. Microscale modelling has been undertaken to understand the observed uranium series fractionation between identifiable phases within the ore. In particular, it provides a basis for an assessment of the relative importance of

- α-recoil,
- molecular diffusion, and
- change in mineralogy,

when determining the effect of geological time on radionuclide distribution coefficients.

Modelling on the microscale is particularly important when relating the findings from the uranium ore body to the proposed repository site. The principles will be elaborated in section 4 of this report.

Stage 4 As mentioned previously, one of the principal aims of the investigation is to test the applicability of currently used transport codes for long-term prediction of radionuclide migration. In this approach, the correctness of the computational procedures has been assumed. Emphasis has therefore been placed on assessing the validity of the generating equations which are dependent on a number of assumptions including the following:

- Interaction between the 'dissolved' radionuclides and the host rock may be described by a linear equilibrium isotherm in which kinetic adsorption effects are neglected.

- The predictions of the code are valid despite the presence of groundwater colloids.

A simple quantitative model for the evolution of the zone of secondary mineralization associated with the Koongarra deposit is being developed by Lever. When the concentration of uranium in the groundwater varies only slowly with distance, an approximate solution for $^{234}U/^{238}U$ and $^{230}Th/^{234}U$ on the host rock has been developed, from which the retarded uranium velocity may be calculated. This parameter may be compared with that calculated independently from the groundwater velocity and measured uranium sorption coefficients. Comparison of the value of a single parameter calculated by two independent means provides the basis for an independent assessment of both procedures.

1.2 The Study Region

The uranium deposits of the East Alligator River (Figure 1) are the most significant mineral resources of the Pine Creek geosyncline[8]. The geosyncline comprises about 14 km of Lower Proterozoic sediments with interlayered tuff units, and rests on granitic late Archean complexes[9]. The sediments were regionally deformed and metamorphosed at 1800 My BP. Cover rocks of Middle Proterozoic and younger ages rest unconformably on these rocks. The Lower Proterozoic sediments are mainly pelites (75 per cent) which are commonly carbonaceous, lesser psammites and carbonates and minor rudites. The environment of deposition ranges from shallow marine to supratidal and fluvial for most of the sequence.

In the Alligator Rivers region, most of the uranium mineralization is in the base of the Cahill Formation which forms part of the Namoona group within the Lower Proterozoic sediments. The deposits are located in zones of chloritization and adjacent to lenses of massive dolomite and/or magnetite. It has been suggested that the common proximity of the uranium

deposits to the carbonate rocks may be relevant to ore genesis[9]. It is also believed that association with the granitic Archean basement is also important[10].

The study region, in common with much of far northern Australia, has a monsoonal climate. Almost all the rainfall occurs in the wet season between November and March. Both the East and the South Alligator Rivers have their headwaters in a rugged sandstone formation, in the south-east of the region, which rises about 250 m above adjoining lowlands. Wet season flow comprises a series of peak floods superimposed on a base flow which, in a normal year, begins about December and ends in June.

Some of the water from the Magela system infiltrates to deep aquifers associated with faults in the basement rock. Several major fault lines have been identified within the catchment. Other types of groundwater storage include porous limestone, shallow aquifers in weathered rock, and deposits of old sand in and along stream channels. Water tables oscillate annually and frequently intersect the surface during the wet season. In the vicinity of the Ranger One deposit, the annual fluctuation in the potentiometric surface is superimposed on a net gradient towards the north, which generally follows the surface contours.

1.2.1 Ranger One ore body

The Ranger One ore body (Figure 1) is shown in some more detail in Figure 2. The geology has recently been described by Hegge et al.[11]. The deposits are in altered microgneiss, schist and silicified carbonate near the base of the lower Cahill Formation. "The orebody can be divided into two major host rock types (Figure 2) - the upper mine sequence UMS and lower mine sequence LMS. The UMS is chloritised schist and microgneiss, whereas the LMS is silicified carbonate. These major rock types grade down-dip into their unaltered parent material. Both sequences are extensively brecciated in the ore zones and extensively intruded by chlorite veins. It is this chlorite which carries the majority of the mineralisation."[11]. The upper 25 to 30 m of the UMS is a zone of surface oxidation.

1.2.2 Jabiluka ore deposits

As with the Ranger One deposit, the uranium in Jabiluka One and Two ore bodies is hosted by the lower members of the Cahill Formation. Jabiluka One coincides with an erosional window through an unconformably overlying sandstone (Figure 3). The upper 20 m is a zone of weathering. To the east, Jabiluka Two is covered by between 20 and 200 m of sandstone. Host rocks are mainly chlorite and/or graphite schists and their brecciated equivalents. Mineralization consists principally of pitchblende, although minor amounts of coffinite and brannerite have been reported.

1.2.3 Nabarlek ore body

Hegge et al.[11] have provided a brief description of the geology of the Nabarlek region (Figure 1); the uranium mineralization consists of massive and disseminated pitchblende associated with a halo of secondary minerals; the ore body occurs within chloritic schists and is best developed where the adjacent country rocks are chloritic; hematite is a major constituent towards the centre of the zone of mineralization; the ore body is underlain by the Oenpelli dolerite sill which is locally about 200 m thick. A generalized geological cross-section[11] is shown in Figure 4 (insert).

The principal aquifers are within the fracture zones of the relatively impermeable crystalline rock mass. The groundwater generally occurs over a 20 m interval between 55 and 35 m. The top of the aquifer zone occurs at depths of 10 to 25 m below ground level. The aquifer is overlain by weathered material which, within the mine area, is often clayey and extends to depths of about 10 to 20 m. It is covered by less than 1 m of lateritic soil and sand. During the wet season, the groundwater flow is generally towards the east and controlled largely by topography. The flow direction changes towards the south-west during the day, and is possibly determined by the bed-rock fracture patterns[12].

1.2.4 Koongarra deposit

The uranium mineralization occurs in two distinct ore bodies separated by a barren gap. Both consist of primary zones containing uraninite veins within steeply dipping quartz-chlorite schists of the lower member of the Cahill Formation[13]. In the No. 1 ore body (Figure 5), which is the subject of the investigation, secondary mineralization is present in the weathered schists running almost from the surface to the base of the weathering at depths of 25 m and 30 m. The secondary mineralization in the weathered schists forms a tongue-like fan of ore grade material extending down-slope for about 80 m.

The groundwater hydrology in the area of the Koongarra deposits has been studied extensively by Australian Groundwater Consultants and McMahon, Burgess and Yeates[14]. Their data, interpreted by Snelling[16], are shown schematically in Figure 5B. The groundwater is believed to recharge along a major fault line and flow in a generally southerly direction away from the escarpment. The location of the sampling wells is shown in Figure 5A.

2. MATHEMATICAL MODELLING OF THE UPPER SEQUENCES OF THE ORE BODY

2.1 General Description of the Model

All comprehensive geochemical models involve both non site-specific and site-specific elements.

(a) Non site-specific element: Generalized equations can be written to describe the decay of $^{238}U(U_8)$, $^{234}U(U_4)$ and $^{230}Th(I)$ under open-system conditions.

(b) Site-specific element: Boundary conditions for the generating equations can only be set on the basis of a description of the salient features of the system to be modelled.

A detailed examination of the drill core, the observed uranium series fraction and the mineralogy led to the classification of the upper sequences of the Ranger One, Jabiluka One and Nabarlek ore deposits into four zones:

Zone I - zone of leaching; unsaturated in the dry season.

Zone II - permanently saturated within the weathered rock.

Zone III - a transition zone between the weathered and unweathered rock.

Zone IV - unweathered crystalline rock.

A general description of the zones is presented in Table 1. The $^{230}Th/^{234}U$ activity ratios show systematic variations (Figure 6A). Zone I exhibits substantial ^{230}Th excess. Zone II which is a zone of uranium deposition shows a tendency towards a ^{230}Th deficit. The weathering process in zone III leads to the mobilization of ^{234}U and hence to many samples with a $^{230}Th/^{234}U$ activity ratio exceeding one.

Detailed mineralogy has also been undertaken. The results have been reported in Table 4 of reference 1. A comparison of the predicted uranium geochemistry from mineralogical and isotope data is presented in Table 2. It is important to note that this four-zone classification does not apply to the secondary mineralization associated with the Koongarra ore body (see Section 5).

A schematic representation of the model is shown in Figure 6B. The dynamics of the system is determined not only by the groundwater flow characteristics, but also by the rate of advance of the weathering front W, which is assumed to balance approximately the rate of surface erosion E, and the time-averaged position of the water table over a very long period. If E and W were not roughly in balance, the thickness of the weathered zone, which has been developing since the Tertiary, would either be very small (E>W) or very large (W>E).

The aim of the model is to calculate the following parameters:

- the residence time t of uranium within each zone,
- the net rate of leaching (or accumulation) of uranium, and
- the activity ratio (AR) of the $^{234}U/^{238}U$ associated with leaching or deposition.

If t and the heights h_I, h_{II}, h_{III} above the boundaries of the respective zones I/II, II/III and III/IV are known, the rate of advance of the weathering W (= rate of erosion E) may be calculated from the average values of the quotients h_I/t, h_{II}/t or h_{III}/t.

In the calculation, it is necessary to define two independent sets of initial conditions:

- $(^{234}U/^{238}U)_0$, $(^{230}Th/^{234}U)_0$ and $(^{231}Pa/^{235}U)_0$. The values of the ARs for zone I, say, are assumed to be equal to those found in the upper region of zone II. The initial values for zones II and III are defined similarly.
- t_0. The initial time t_0 is defined as the time of the passage of the zone boundary.

2.2 Mathematical Formulation of the Model

In the original version of the model[2] it was assumed that leaching or deposition were linear functions of time. This arbitary restriction has been removed in the development discussed below. Following Hille[15], it is now assumed that leaching and deposition are first order processes, i.e. they are proportional to the concentration of accessible uranium in the ore. Although this is a satisfactory description for leaching, it means that the rate of deposition is related to a property of the substrate and therefore valid only if there is good correlation between the level of uranium in the ore and in the groundwater. It can be argued that, in the weathered region, the relevant property is the number of accessible sites on the amorphous component of the iron or aluminium. It is important to note that the formulation presented below, is identical to that given in the first Annual Report[2] for low leaching rates.

The generating equations can be written as follows:

$$U_8 = U_8(t_0)\left[\exp - (\lambda_8 + \xi)\right]t; \text{ and} \quad (1)$$

$$U_5 = U_5(t_0)\left[\exp - (\lambda_5 + \xi)\right]t \ . \quad (2)$$

Hence

$$-dU_4/dt = (\lambda_4 + R\xi)U_4 - \lambda_8 U_8 \quad , \tag{3}$$

$$-dI/dt = \lambda_i I - \lambda_4 U_4 \quad , \text{ and} \tag{4}$$

$$-dPa/dt = \lambda_p Pa - \lambda_5 U_5 \quad , \tag{5}$$

where $\lambda_8 U_8$, $\lambda_5 U_5$, $\lambda_4 U_4$, $\lambda_i I$ and $\lambda_p Pa$ are activities of ^{238}U, ^{235}U, ^{234}U, ^{230}Th and ^{231}Pa respectively; ξ is the rate of leaching (+ve) or deposition (-ve); R is the $^{234}U/^{238}U$ ratio of the leachate (or of the depositing material); t is the elapsed time; and $U_8(t_0)$, $U_5(t_0)$ are the levels of ^{238}U, ^{235}U at the initial time, t_0.

The following expressions were developed in Appendix A of Reference 1:

(a) Uranium-234

$$Su = Su(t_0) \exp (b-a)t + \frac{\lambda_4}{(b-a)} (\exp(b-a)t - 1) \quad . \tag{6}$$

(b) Thorium-230

$$Si \times D = Si(t_0) \exp(a - \lambda_i)t + \lambda_i(1 - \exp(a - \lambda_i)t)/(\lambda_i - a)$$

$$+ \lambda_i\lambda_4\left[(b - a) \exp (a - \lambda_i)t + (a - \lambda_i) \exp [-(b - a)] + \lambda_i - b\right]/$$

$$[(b - a)(a - \lambda_i)(b - \lambda_i) S(t_0)] \quad , \tag{7}$$

where $D = 1 + \lambda_4\left[1 - \exp[-(b - a)t]\right]/[(b - a) Su(t_0)]$.

(c) Protactinium-231

$$Sp = Sp(t_0) \exp (c-\lambda_p)t + \frac{\lambda_p}{c-\lambda_p} (\exp (c-\lambda_p)t - 1) \quad , \tag{8}$$

where $Su = {}^{234}U/{}^{238}U$, (9)

$Si = {}^{230}Th/{}^{234}U$, (10)

$Sp = {}^{231}Pa/{}^{235}U$, (11)

$Su(t_0)$, $Si(t_0)$ and $Sp(t_0)$ are the values at the defined zero time t ,

$$a = \lambda_4 + R\xi \ , \tag{12}$$

$$b = \lambda_8 + \xi \ , \text{ and} \tag{13}$$

$$c = \lambda_5 + \xi \ . \tag{14}$$

2.3 Output of the Model

The computational techniques outlined in the first Annual Report[2] require the following steps:

(i) Select an appropriate range of values for the variable parameters ξ and R, and the ARs $Su(t_0)$, $Si(t_0)$ and $Sp(t_0)$ at zero time.

(ii) Calculate the values $^{234}U/^{238}U$, $^{230}Th/^{234}U$ and $^{231}Pa/^{235}U$ and compare them with the measured values.

(iii) List those sets of parameters in which all observed and calculated ARs agree to within 10 per cent.

(iv) Select those sets of parameters which are internally self-consistent. The following criteria are used:

(a) mass balance: the total leaching rate should approximately balance the total deposition; and

(b) the assumed constancy of the rate of erosion E and the rate of advance of the weathering front W, i.e. $W = t/h_{III}$ (Figure 6B) should be approximately constant.

The computer program is listed in Appendix B.

Data from Jabiluka One, Ranger One and Nabarlek are listed in Tables 2 to 6(a) of Reference 4. By way of example, the calculations for drill hole DH 16, Jabiluka One are reproduced here in Table 3. The average values and ranges of the calculated rates of leaching (or deposition) and of the rates of surface erosion (or advance of the weathering front) are listed.

Because of the relatively short half-life of radium-226, an adaptation of the model is needed to calculate R_{geol}, its rate of leaching or deposition. It has been shown (Reference 2, Appendix B) that

$$\frac{\lambda_r Ra}{\lambda_i I} = 1 + \frac{R_{geol}}{\lambda_i I} \ , \tag{15}$$

where $\lambda_r Ra$ is the activity of radium-226 and $\lambda_i I$ is the activity of the parent $^{230}Th(I)$.

One of the advantages of developing full analytical expressions for the ARs is that the sensitivity of the computer values to the variable parameters can be readily assessed. An extreme example of the importance of a sensitivity analysis is shown in Figure 7. In this instance, the ARs $^{230}Th/^{234}U$, $^{231}Pa/^{235}U$ and $^{234}U/^{238}U$ are plotted as a function of the leaching (deposition) rate ξ when R is 0.50 and the elapsed time is 75,000 years. A discontinuity in $^{230}Th/^{234}U$ is observed at moderate values of ξ.

3. VALIDITY OF THE MODEL

Two approaches have been made to validate different aspects of the model. These are broadly classified as follows:

(a) An independent assessment of the assumptions of the model; in particular

- the four-zone classification,
- separation of leaching and depositional zones, and
- a comparison of the model predictions with independent evidence.

(b) Establishment of a mathematical correlation between this and other open-system models.

3.1 Independent Assessment of the Assumptions of the Model

3.1.1 Four-zone classification

As outlined in Section 2.1, there are three independent lines of evidence for the four-zone classification:

(a) *Mineralogical:* The drill core grades from an oxidized ferricrete or ferruginous zone near the surface through a mottled zone to a palid zone. Underlying the pallid zone is a transition region between weathered and unweathered rock, which grades into unweathered schists. Extensive mineralogical work on a number of cores has been undertaken[1,4].

(b) *Hydrological:* The upper zone I is unsaturated in the dry season and is characterized by a seasonally oscillating water table; zone II is fully weathered, but permanently saturated.

(c) *Isotopic:* A systematic variation of the $^{230}Th/^{234}U$ ARs is found which correlates with zonal classification determined by the mineralogy (Figure 6).

3.1.2 Separation of leaching and depositional zones

General evidence for the separation of zones of leaching and deposition has been obtained from the consistent trend of $^{230}Th/^{234}U$ ARs from three deposits (Figure 6A). Confirmation has recently been obtained from studies of the $^{230}Th/^{234}U$ and $^{234}U/^{236}U$ ARs in phases extracted sequentially from S1/146 core samples from the weathered profiles of Ranger One (Figures 8 and 9). Of particular interest are the data from the amorphous iron and ferrihydrite phases which provide increasing evidence that the uranium is in isotopic equilibrium with the groundwater. In the upper leaching zone I

there is an excess of thorium; $^{230}Th/^{234}U$ ARs vary from 1.4 to 4.7. Zone II, the zone of deposition, is deficient in ^{230}Th (ARs vary from 0.75 to 0.37). Not surprisingly, the $^{230}Th/^{234}U$ variability in the amorphous iron is more pronounced than in the whole rock samples (Figure 6A) as leaching processes are involved and the uranium in the crystalline iron and clay/quartz phases is less accessible to the groundwater.

3.1.3 Comparison with independent geomorphological evidence (erosion)

The calculated erosion rates at Ranger One and Nabarlek are 0.06 and 0.05 m per 1000 y with ranges of 0.02-0.18 and 0.01-0.08 m per 1000 y respectively. Data are summarized in Table 3.

Independent estimates of the erosion rate before mining commenced have been attempted by consideration of the sediment balance. The value found (0.1 mm/1000 y) in the Ranger area[3] is in acceptable agreement with the model. There are problems in relating the calculated erosion rates to the assumed stability of the landscape since the Tertiary period. However, it is noted that erosion is a local phenomenon, and that observations at a specific site over a relatively restricted period (<500 000 y) cannot necessarily be generalized over geological time. Estimates of erosion and deposition rates produced values that were consistent with those found from the model.

3.2 Mathematical Correlation with Other Open-system Models

An early attempt to develop an open-system model of aragonitic mollusc shells was made by Rosholt[16], because an excess of ^{231}Pa was observed in some samples. It was assumed (a) that the uranium is slowly assimilated by the shells over a relatively long period after deposition in marine sediments, and (b) that the ^{231}Pa and ^{230}Th are authigenic and none is leached from the shell. Analytical expressions for the ^{231}Pa, ^{230}Th, ^{234}U and ^{238}U in the shell sample were developed and rationalized with experimental values by adjusting the $^{234}U/^{238}U$ ratios associated with the uranium flux, and the uranium leached from the sample. In a later development of the model, Szabo and Rosholt[17] allowed for an initial assimilation of uranium and subsequent weathering, leading to the uptake of ^{230}Th and ^{231}Pa as well as ^{234}U.

Hille[15] proposed an approach in which the daughter products remain chemically stable but the uranium, which migrates into the shell shortly after the death of the organism, changes with time according to a first order law.

Of more direct relevance to the current work is the uranium trend dating model developed recently by Rosholt[18]. The aim of this model is to date the deposition of alluvial, aeolian, lacustrine and other deposits. The application of uranium series disequilibria to geochronology has recently been extensively reviewed[19].

3.2.1 Mathematical correlation between the current model and the uranium trend dating model (UTDM)

3.2.1.1 *Correlation between the UTDM flux factor and the leaching/deposition parameter*

The UTDM[18] is used to date the deposition of alluvial, aeolian, lacustrine and other materials. The principle depends on the fact that water, with a small amount of uranium and its daughter products, permeates the deposit. The flux of the mobile phase uranium is defined in terms of an empirical factor F_0 which is associated with an exponential decay constant λ_0. Time t is measured from the commencement of the movement of water through the system.

A relationship is developed between $(^{234}U\text{-}^{238}U)/^{238}U$ and $(^{238}U\text{-}^{230}Th)/^{238}U$ which defines the 'uranium trend line', the product $\lambda_0 t$, and related parameters involving the isotopic decay constants. A calibration from known deposits is required to separate λ_0 from t and hence to determine the age of the deposit.

When the model is applied to specific horizons, a uranium trend line is obtained by plotting $(^{234}U\text{-}^{238}U)/^{238}U$ (=Y) against $(^{238}U\text{-}^{230}Th)/^{238}U$ (=X). The slope of an isochron is presented in the form of a Bateman equation:

$$Y/X = \frac{C_1 \exp(-\lambda_0 t) + C_2 \exp(-\lambda_4 t)}{C_3 \exp -(\lambda_0 t) + C_4 \exp(-\lambda_4 t) + C_5 \exp(-\lambda_i t)}, \qquad (16)$$

where C_1, C_2, C_3 are constants, and λ_0, λ_4, λ_i are the decay constants associated with the uranium flux factor F_0, ^{234}U and ^{230}Th, respectively.

In Appendix C, it is shown that, on the basis of the present model,

$$Y/X = (Su - 1)/(Su - Si_8)$$

$$= \frac{n \exp(-\xi t) + m \exp(-(\lambda_4 - \lambda_8 + \xi R)t)}{s \exp(-\xi t) + p \exp(-(\lambda_4 - \lambda_8 + \xi R)t) + q \exp(-(\lambda_5 - \lambda_8)t)}, \qquad (17)$$

where n, m, s, p and q are parameters which are defined explicitly in Appendix A. and Si_8 is the $^{230}Th/^{238}U$ AR.

Equations (16) and (17) are clearly very similar, especially as λ_8 is small and can normally be neglected. In the present model, it is obvious that parameter ξ plays a role similar to that of λ_0 associated with F_0 in the uranium trend dating model.

3.2.1.2 *Development of a uranium trend line and a UTDM calibration curve from the current model*

The uranium trend line is defined by a small segment of one of the infinite set of curves defining the relationship between Y and X. The uranium trend technique is applied to the dating of soil horizons. It is tacitly assumed that the time taken to develop the horizon ΔT is small compared with the time T which has elapsed since it was formed. It can be reasonably assumed that they have followed the same uranium series evolution curve (dotted curve, Figure 7). Thus far, it is not necessary to make any assumptions concerning ξ and R. The intercept X_i is determined by

- the slope $\Delta Y/\Delta X$, and
- the absolute value of the coordinate (X_t, Y_t).

The differential δY is given by

$$\delta Y = (\partial Y/\partial t)\ \delta t + \left(\frac{\partial Y}{\partial \xi}\right)\ \delta \xi + \left(\frac{\partial Y}{\partial R}\right)\ \delta R \quad . \tag{18}$$

A similar expression can be written for δY.

Over the short time element δt, it is assumed that $\delta \xi = 0$ and $\delta R = 0$. Experimental evidence for the constancy of R is found from Koongarra data. The transport of the secondary mineralization down-gradient can be rationalized in terms of the Osmond and Cowart formulation (Chapter 6) assuming ^{234}U migrates more slowly than ^{238}U - an assumption that is consistent with the $^{234}U/^{238}U$ ARs observed in most samples of modern groundwater. If $\delta \xi$ and δR are neglected,

$$\delta Y = (\partial Y/\partial t)\ \delta t \quad ; \tag{19}$$

$$\delta X = (\partial X/\partial t)\ \delta t \quad . \tag{20}$$

Hence the slope $(\partial Y/\partial X)$ which determines the uranium trend line is the ratio of the time differentials of Y and X.

The intercept X_i may be calculated from

$$Y_t = (\partial Y/\partial X)\ X_t + X_i \quad . \tag{21}$$

In Appendix D, it is shown that

$$X_i = X_x - Y_x \frac{S\ \xi\ E_1 + p\ C_1\ E_2 + q\ C_2\ E_3}{m\ \xi\ E_1 + m\ C_1\ E_2} \quad , \tag{22}$$

The calculation procedure for the uranium trend model involves three steps:

(i) Establishment of the intercept X_i.

(ii) Determination of the uranium flux factor λ_o from X_i using a semi-empirical curve.

(iii) Calculation of the time t_o from λ_o and conventional decay constants using the Bateman equations.

In Section 3.2.1, it was shown that Rosholt's parameter λ_o (Equation (16)) correlates with the parameter ξ (Equation (17)) of this model. The variation of ξ with X_i, calculated from Equation (22) is shown in Figure 11. In Rosholt's model, a calibration curve is established between a parameter directly related to λ_o and log X_i from samples of known age (Reference 7, Figure 3). For unknown samples, the curve may be used to establish λ_o from a measured intercept on the uranium trend line. The age t may be calculated from the slope of the uranium trend line using Equation (16).

The analogue of Rosholt's calibration curve is the plot of ξ^{-1} v. log X_i. Difficulties arise because X_i and ξ can each assume positive, negative and zero values. Hence, the family of curves leading to the uranium trend calibration curve can only be plotted in sections. Some examples are shown in Figure 12. A calibration curve, such as that published by Rosholt, could be developed from the family of curves by highlighting values from samples of known age on the intercept (X_i) - $(1/\xi)$ curve.

Because the current model allows explicit expressions for the $^{234}U/^{238}U$ and $^{230}Th/^{234}U$ in terms of the leaching/deposition parameter ξ, the $^{234}U/^{238}U$ fractionation associated with leaching/deposition and the initial ARs at a defined zero, a more direct method for the dating of soils has been developed. The method is outlined in Section 3.3.

3.2.2 Mathematical correlation with Hille's open-system model [15]

Hille's model was developed for the dating of skulls and bones. He assumed, that (i) all products of radioactive decay, including ^{234}U, are immobile, (ii) the initial levels of ^{230}Th and ^{231}Pa are zero, and (iii) the rate of uptake of uranium shortly after the death of the animal is given by

$$^{234,235,238}U(t) = {}^{234,235,238}U(o)\ \exp(-At)\ , \qquad (23)$$

where A is a chemical decay constant.

Hille showed that

$$^{231}Pa/^{235}U = \lambda_p[1 - \exp(-(\lambda_p - A)t)]/(\lambda_p - A)\ , \text{ and} \qquad (24)$$

$$^{234}U/^{238}U = (^{234}U/^{238}U)_o\ \exp(-\lambda_4 t) + \lambda_4[1 - \exp(-(\lambda_4 - A)t)]/(\lambda_4 - A)\ . \qquad (25)$$

The equivalent expressions in the present model are

$$(^{231}Pa/^{235}U) = (^{231}Pa/^{235}U)_o \exp(c-\lambda_p)t + \\ + \lambda_p (\exp(c-\lambda_p)t-1)/(c-\lambda_p) \quad , \qquad (26)$$

and

$$(^{234}U/^{238}U) = (^{234}U/^{238}U) \exp(b-a)t + \\ + \lambda_4 (\exp(b-a)t - 1)/(b-a) \quad , \qquad (27)$$

where $a = \lambda_4 + \xi R$, (28)

$b = \lambda_8 + \xi$, and (29)

$c = \lambda_5 + \xi$. (30)

Hille's equation (24) is formally similar to our Equation (26) if, as was assumed by Hille, $(^{231}Pa/^{235}U)_o = 0$. Equation (25) can be compared with our equation (27) which, in contrast to Hille, reflects the fact that leaching and deposition of both ^{238}U and ^{234}U is permitted, albeit at different rates.

3.3 Application of the Model to Open-system Dating

3.3.1 Dating of soil profiles

An approach to the dating of soil profiles using the UTDM was outlined above. A different approach to the dating of soil profiles is possible with the current model, because explicit expressions have been developed for the variation of $^{234}U/^{238}U$ and $^{230}Th/^{234}U$ ARs with

- the leaching/deposition parameter ξ,
- the ratio R of the ^{234}U and ^{238}U leaching parameters,
- the initial ARs, and
- the elapsed time t since the development of the horizon.

Mathematically, the procedure involves matching the values of the isotope ratios calculated from Equations (6), (7) and (8) with the experimental values. The following steps are included:

(a) *Choose a realistic value of* R. The most appropriate value is the $^{234}U/^{238}U$ AR of modern groundwater associated with the profile. In Figure 13, three values (1.15, 1.25 and 1.40) have been used for illustrative purposes.

(b) *Choose initial values for the $^{234}U/^{238}U$ and $^{230}Th/^{234}U$ activity ratios.* In the absence of other information, the value of 1.00 may be used. It is thereby tacitly assumed that the material which was laid down as the soil horizon was originally in secular equilibrium; and that perturbations in the ARs occurred as a result of groundwater percolation.

(c) *By solving Equations (6) to (8), obtain a set of values for the leaching/deposition parameter ξ and the time t which are consistent with the initial conditions and the experimental data.* In Figure 13A, which illustrates uranium deposition, the observed values of $^{234}U/^{238}U$ and $^{230}Th/^{234}U$ are 1.10 and 0.80, respectively; and in Figure 13B which shows the leaching mechanism, they are 0.90 and 1.25. In both cases, an accuracy of two per cent in the measurements is assumed.

(d) *Define a ξ, t domain from repeat measurements on a number of samples in the soil profile.* The various curves should be superimposed to define a ξ, t domain which is consistent with the experimental data for the horizon.

The above analysis demonstrates that it is not possible to define a precise uranium/thorium age for an open system. The best that can be achieved is the definition of a domain of leaching/deposition and age parameters which are consistent with the experimental values. The precision with which the system can be described may be increased under the following conditions:

(a) *Accuracy of the measurements.* The more precise the measurements, the less is the range of values of ξ and t. This property is illustrated in Figure 14. For the parameters shown in the key, the range of values of ξ and time for measurement precisions of two and five per cent is shown. It would appear that, with a five per cent measurement precision, it is impossible to date open systems with a single measurement.

(b) *Additional data.* The introduction of additional measurements such as $^{231}Pa/^{234}U$ will define the system much more closely. Work is under way to quantify the effect.

(c) *Independent estimate of a parameter.* There is a functional relationship between ξ and t for a given set of boundary conditions and experimental data. Thus if one parameter, t, can be estimated independently, the other, ξ, can be calculated much more accurately. In some cases it is possible to date a soil horizon independently. Examples have been cited by Rosholt[18] Recently, Short (private communication) has made an

interesting suggestion that iron concretions within lateritic profiles may be closed systems. If their age can be attributed to the general soil horizon, it will be possible to estimate ξ, i.e. the extent to which the horizon has been susceptible to uranium leaching or deposition since its development.

3.3.2 Examples of open-system dating

3.3.2.1 *Comparison with data published by J N Rosholt and co-workers*

Virtually all the data have been reinterpreted using the current model. For simplicity, several examples only are presented.

The output of the model is shown as 'age - leaching' domains in Figure 15. In this calculation, it was assumed that, consistent with the UTDM, the initial values of $^{234}U/^{238}U$ and $^{230}Th/^{234}U$ ARs were unity, and that disequilibrium was induced by leaching. The result calculated by Rosholt is also shown, assuming that his parameter λ_0 is equated to our leaching parameter ξ. Evidence for this assignment is shown in Section 3.2.1.1. Insofar as Rosholt's calculation falls within, or close to the domains defined by this calculation. A more satisfactory comparison would only be possible if the domains were more precisely defined (see Section 3.3.1). In contrast to the UTDM, the current model allows variation in the ratio of the ^{234}U to ^{238}U leaching rates. Values were found to vary from 0.75-1.40.

3.3.2.2 *Dating of shells - comparison with Hille's model*

Hille[15] has recalculated the ages of mullusc samples from three terraces in Southern California using $^{234}U/^{238}U$, $^{230}Th/^{234}U$ and $^{231}Pa/^{235}U$ ARs measured by Szabo and Rosholt[17]. The data have once more been recalculated with this model. Details for the three samples collected from Terrace C are shown in Figure 16. The time-leaching domain is shown, together with the individual values, and the average value shown calculated by Hille. The agreement is clearly satisfactory.

Inserted on Figure 16 is a diagram showing the number of times a given range of 'ages' and of R values gave acceptable solutions, where R is the relative rate of ^{234}U to ^{238}U leaching. This parameter is implicitly assumed to be unity in Hille's treatment. It would appear, however, from data presented in this graph that the value of R is somewhat less than unity.

4. EXTENSION OF THE MODEL TO MULTIPHASE SYSTEMS

4.1 Formulation of the Multiphase Model

Experimental evidence has been presented for extensive $^{234}U/^{238}U$, $^{230}Th/^{234}U$ and $^{226}Ra/^{230}Th$ fractionation between the amorphous iron, crystalline iron and clay/quartz phases of the weathered ore body schists (Section 3.1.1). It would appear that

(i) the uranium of the amorphous, but not of the crystalline iron, is directly accessible to groundwater;

(ii) on the geological timescale, exchange occurs between the amorphous and crystalline iron;

(iii) the bulk of the uranium and thorium is associated with the iron phases, whereas an excess of radium accumulates in the clay/quartz phase; and

(iv) the recoil effect leads to an accumulation of the daughter element in the clay/quartz.

The model is shown schematically in Figure 17. It is important to extend the model to include the multiphase description of weathered schists for the following reasons:

(i) Without this extension, a detailed understanding of the migration of radionuclides through clays will not be possible.

(ii) The extended model will provide a rational basis for quantifying kinetic sorption effects and is therefore important in the assessment of the long-term predidiction of radionuclide transport.

The relevant differential equations are set out below:

(a) Uranium-238

$$\frac{d^{8}U_{a}}{dt} = -(\lambda_{8}+\xi_{a})\ {}^{8}U_{a} - \tau\ ({}^{8}U_{a} - {}^{8}U_{x}) \quad , \tag{31}$$

$$\frac{d^{8}U_{x}}{dt} = -\lambda_{8}\,{}^{8}U_{x} + \tau\ ({}^{8}U_{a} - {}^{8}U_{x}) \quad , \tag{32}$$

$$\frac{d^{8}U_{CQ}}{dt} = -(\lambda_{8} + \xi_{CQ})\ {}^{8}U_{CQ} \quad . \tag{33}$$

(b) Uranium-234

$$\frac{d^4U_a}{dt} = (1 - {}^{a}Re^{x} - {}^{a}Re^{CQ} - {}^{a}Re^{GW})\lambda_8\,{}^{8}U_a + {}^{x}Re^{a}\,\lambda_8\,{}^{8}U_x + {}^{CQ}Re^{a}\,\lambda_8\,{}^{8}U_{CQ} + \\ + {}^{GW}Re^{a}\,\lambda_8\,{}^{8}U_{GW} - (\lambda_4 + R\xi_a)\,{}^{4}U_a - \tau({}^{4}U_a - {}^{4}U_x) \quad , \tag{34}$$

$$\frac{d^4U_x}{dt} = (1 - {}^{x}Re^{a} - {}^{x}Re^{CQ} - {}^{x}Re^{GW})\,\lambda_8\,{}^{8}U_x + {}^{a}Re^{x}\lambda_8{}^{8}U_a + {}^{CW}Re^{x}\,\lambda_8\,{}^{8}U_{CQ} + \\ + {}^{GW}Re^{x}\,\lambda_8\,{}^{8}U_{GW} - \lambda_4\,{}^{4}U_x + \tau({}^{4}U_a - {}^{4}U_x) \quad , \tag{35}$$

$$\frac{d^4U_{CQ}}{dt} = (1 - {}^{CQ}Re^{a} - {}^{CQ}Re^{x} - {}^{CQ}Re^{GW})\,\lambda_8\,{}^{8}U_{CQ} + {}^{a}Re^{CQ}\lambda_8\,{}^{8}U_a + \\ + {}^{x}Re^{CQ}\,\lambda_8\,{}^{8}U_x + {}^{GW}Re^{CQ}\,\lambda_8\,{}^{8}U_{GW} - (\lambda_4 + R_{\xi CQ})\,{}^{4}U_{CQ} \quad . \tag{36}$$

(c) Thorium-230

$$\frac{dI_a}{dt} = (1 - {}^{a}Re^{x} - {}^{a}Re^{CQ} - {}^{a}Re^{GW})\,\lambda_4\,{}^{4}U_a + {}^{x}Re^{a}\,\lambda_4\,{}^{4}U_x + {}^{CQ}Re^{a}\,\lambda_4\,{}^{4}U_{CQ} + \\ + {}^{GW}Re^{a}\,\lambda_4\,{}^{4}U_{GW} - \lambda_i I_a - \tau(I_a - I_x) \quad , \tag{37}$$

$$\frac{dI_x}{dt} = (1 - {}^{x}Re^{a} - {}^{x}Re^{CQ} - {}^{x}Re^{GW})\,\lambda_4\,{}^{4}U_x + {}^{a}Re^{x}\,\lambda_4\,{}^{4}U_a + {}^{CQ}Re^{x}\,\lambda_4\,{}^{4}U_{CQ} + \\ + {}^{GW}Re^{x}\,\lambda_4\,{}^{4}U_{GW} - \lambda_i I_x + \tau(I_a - I_x) \quad , \text{ and} \tag{38}$$

$$\frac{dI_{CQ}}{dt} = (1 - {}^{CQ}Re^{a} - {}^{CQ}Re^{x} - {}^{CQ}Re^{GW})\,\lambda_4\,{}^{4}U_{CQ} + {}^{a}Re^{CQ}\,\lambda_4\,{}^{4}U_a + {}^{x}Re^{CQ}\,\lambda_4\,{}^{4}U_x + \\ + {}^{GW}Re^{CQ}\,\lambda_4\;U_{GW} - \lambda_i I_{CQ} \quad . \tag{39}$$

In these equations, the subscripts (or superscripts) a, x, CQ and GW refer to amorphous iron, crystalline iron, clay/quartz and groundwater, respectively; ${}^{a}Re^{x}$ is the parameter describing recoil from, for instance,

amorphous iron a to the crystalline x; and τ is the rate of exchange between amorphous and crystalline iron. The activities are expressed per gram of ore.

The physical basis for the equations is as follows:

Equation (31). This equation represents the rate of accumulation of ^{233}U in the amorphous iron phase. It comprises two components, represented by the two terms on the right hand side (RHS). The first term is the net effect of radiogenic decay and leaching (or deposition). The second term reflects the fact that the iron phases are not stable over geological time. Crystallization of the amorphous iron is balanced by the slow dissolution and reprecipitation of the crystalline iron minerals. This leads to an exchange of uranium between the phases which can be represented by a first order rate constant τ.

Equations (32) and (33). These equations refer to the crystalline iron and quartz phases and are analogous to Equation (31). In the former equation, there is no leaching term because it is assumed that the groundwater does not have appreciable access to the crystalline iron; in the latter there is, of course, no term describing the exchange between iron minerals.

Equation (34). This equation represents the rate of accumulation of ^{234}U in the amorphous iron phase. Uranium-234 differs from ^{238}U in having an authigenic (recoil) component in addition to a normal allogenic component. The first four terms on the RHS describe the recoil processes; the fifth term is the net effect of decay and deposition; and the sixth, which represents the effect of exchange between the amorphous and crystalline iron, is analogous to the second term of Equation (31).

Recoil is described by a parameter $^{p}Re^{q}$, which is independent of the daughter nuclide formed by α-decay. The superscripts p, q are the host phases of parent and daughter, respectively. Of course, daughters lodging in the same phase as the parents do not contribute to isotopic fractionation between phases. The first term on the RHS of Equation (34) is the net effect of the build-up of ^{234}U in the amorphous iron due to the decay of ^{238}U in the phase and the loss due to recoil out of the phase. The second term is the build-up of ^{234}U in the amorphous iron phase due to the recoil of ^{234}U in the amorphous iron phase due to the recoil of ^{238}U in the crystalline iron phase, and so on.

Equations (35) and (36). Equations (35) and (36) are analogous to Equation (34). As with Equations (32) and (33), there is no leaching term associated with the crystalline iron and no exchange term associated with the clay/quartz phase.

Equations (37) to (39), are analogous to Equations (34) to (36).

The set of ordinary differential equations will be solved numerically using the computer program 'CLUTCH', developed by B.E. Clancy[21]. There are, of course, many advantages in obtaining analytical solutions of the generating equations. Substantial simplification of the above expressions may be obtained under the following conditions:

(i) For any sample there is a fixed relationship between the levels of radionculides in different phases. Thus, for instance,

$$ {}^{8}U_{x} = {}^{8}f_{a}^{x} \; {}^{8}U_{a} \quad , \tag{40} $$

$$ {}^{8}U_{CQ} = {}^{8}f_{a}^{CQ} \; {}^{8}U_{a} \quad , \text{ and} \tag{41} $$

$$ {}^{8}U_{GW} = {}^{8}f_{a}^{GW} \; {}^{8}U_{a} \quad . \tag{42} $$

(ii) Since the recoil distance is small compared with the dimension of the mineral phase, the magnitude of the recoil parameter will be proportional to the surface area. Thus

$$ {}^{a}R^{x} = Re \; {}^{a}S^{x} \quad , \tag{43} $$

where ${}^{a}S^{x}$ is the area of contact between amorphous and crystalline iron,
and the recoil parameter Re is independent of the phase and the nuclide.

Under these conditions, it can be shown that

$$ d^{4}U_{a}/dt = {}^{8}\phi_{e}^{a} \lambda_{8} \; {}^{8}U_{a} - (\lambda_{4} + Re \; \xi_{a}) \; {}^{4}U_{a} - \tau({}^{4}U_{a} - {}^{4}U_{x}) \quad , \tag{44} $$

where

$$ {}^{8}\phi_{e}^{a} = 1 - Re \; ({}^{a}S^{x} + {}^{a}S^{CQ} + {}^{a}S^{GW} - {}^{x}S^{a}{}_{8}f_{a}^{x} - {}^{CQ}S^{a}{}_{8}f_{a}^{CQ} - {}^{GW}S^{a}{}_{8}f_{a}^{GW}) \; . \tag{45} $$

Since the individual iron minerals comprise only two to four per cent of the total mass, the dominating term in parenthesis is ${}^{a}S^{CQ}$. Hence Equation (45) may be simplified to

$$ \phi_{e}^{a} = 1 - Re \; \Theta_{a}(S) \quad . \tag{46} $$

where $\Theta_{a}(S)$ is a function of the contact surface area (Equations (43), (45), weighted by the uranium ratios (Equations (40) to (42)).

Similarly

$$d^4U_x/dt = {}^8\phi_e^x \lambda_8 {}^8U_x - \lambda_4 {}^4U_x + \tau({}^4U_a - {}^4U_x) \quad , \tag{47}$$

and

$$d^4U_{CQ}/dt = {}^8\phi_e^{CQ} \lambda_8 {}^8U_{CQ} - (\lambda_4 + Re\ \xi_{CQ}) {}^4U_{CQ} \quad , \tag{48}$$

where $${}^8\phi_e^x = 1 - Re\ e_x(S) \quad , \tag{49}$$

and $${}^8\phi_e^{CQ} = 1 + Re\ e_{CQ}(S) \quad . \tag{50}$$

Analogous expressions have been developed for thorium-230:

$$dI_a/dt = {}^4\phi_e^a \lambda_4 {}^4U_a - \lambda_i {}^4I_a - \tau(I_a - I_x) \quad , \tag{51}$$

$$dI_x/dt = {}^4\phi_e^x \lambda_4 {}^4U_x - \lambda_i {}^4I_x + \tau(I_a - I_x) \quad , \text{ and} \tag{52}$$

$$dI_{CQ}/dt = {}^4\phi_e^{CQ} \lambda_4 {}^4U_{CQ} - \lambda_i I_{CQ} \quad . \tag{53}$$

General solutions to these equations are presented in Appendix C.

It is hoped that the mathematical framework will facilitate estimates of the following parameters:

Re = the phase-independent, nuclide-independent recoil factor;

τ = the rate of exchange of amorphous and crystalline iron; and

ξ_a, ξ_{CQ} = the leaching parameters.

Since the nuclides in the crystalline iron are thought to be inaccessible to groundwater, there may be a means of assessing (through knowledge of the amorphous/crystalline iron exchange parameter τ) the time-dependence of distribution coefficients on clays.

4.2 Application to Experimental Data

The computational approach is similar to that outlined in Section 2.2. Parameter values are inserted systematically into the generating equations; the values chosen are those which produce calculated ARs matching the experimental values to within 10 per cent. Since there are more variables than the equations which can be set up using experimental information, the number of sets of parameters giving agreement between calculated and observed values is usually very large. One way around this problem is to examine parameters from a wider range of samples.

Drill core sample S1/146, Ranger One

The observed and calculated ARs are listed in Table 4. The number of independent parameters may be reduced by assuming the following:

(i) The $^{234}U/^{238}U$ activity ratio (R) associated with leaching is that found in the groundwater close to the deposit.

(ii) The timescales are consistent with those found for the whole samples, i.e. those deduced from the four-zone model. It should be recalled that the calculated time is the time since the passage of the zone boundary (associated with the advancing weathering front, Section 2.1).

(iii) Approximate values for $^{X}\emptyset^{Y}$, the probability that the α-recoil product from a parent in phase X will be located in phase Y, may be calculated by the procedures outlined in Section 4.3.1.

Although it is not possible to define precisely the other parameters, a number of generalizations can be made:

(i) Although leaching/deposition is assumed to occur from both the amorphous iron and the clay/quartz phases, the intrinsic rate associated with the amorphous iron is substantially greater. It will be noted that the units of L(D) in Table 4 are % U per 1000 years. If differences in the uranium levels were also taken into account, the ratios to leaching (amorphous iron/clay/quartz) would be even greater. This result is quite consistent with conclusions, from laboratory experiments, that the groundwater is in isotopic equilibrium with the amorphous iron.

(ii) The experimental and calculated ARs can only be made consistent if it is assumed that the $^{230}Th/^{234}U$ AR is in excess of two. Since the formation of goethite involves a crystallization process, discrimination between chemical elements is to be expected.

(iii) The results from this drill core suggest that the exchange constant associated with this process can be expressed as a half-life of between 30 000 and 500 000 years. The implications of this result for the mechanism of retardation are discussed in Section 4.3. It is conceded that the process may be described by a complete spectrum of half-lives, and that the value deduced in the model is an artefact using the thorium/uranium system to establish the constant. This problem will be studied more closely using short-lived isotopes.

Drill core - Koongarra

Analysis of data from a set of Koongarra drill core samples has recently been completed. Average values are listed in Table 5. Uranium-234/uranium-238 and $^{230}Th/^{234}U$ ARs normalized to those found in the ferrihydrate (amorphous iron) fraction are shown in parenthesis. In all cases:

AR (ferrihydrite, amorphous Fe)	<	AR (crystalline Fe-goethite)	<	AR (clay, quartz)

For comparison, the corresponding data for S1/146 Ranger One is also listed. The trends are similar except that in S1/146 drill core the $^{230}Th/^{234}U$ ARs in clay/quartz tend to be numerically less than those in the goethite phase.

It is also of interest that the average value of the $^{234}U/^{238}U$ ARs in the amorphous iron is similar to that of the Koongarra groundwater, where the average value for wells intersecting the deposit is 0.82 (Reference 4, Table 28).

4.3 Discussion of the Multiphase Model

4.3.1 Radionuclide transport between phases - the parameter $\emptyset_e$

The parameter $\emptyset_e$ provides the basis for a quantitative description of the uranium series fraction between different phases caused by α-recoil. From Equation (46),

$$\emptyset_e = 1 - Re\,\theta(S, p) \quad , \tag{54}$$

where Re is dependent only on the physics of the recoil process and θ is a function of the surface area of contact S, and the relative activities of the parent elements p at the surfaces. Particular attention is paid to the contact surface area because of the recoil distance (~200 Å) is short compared with the dimensions of many of the identifiable minerals.

The observed $^{234}U/^{238}U$ disequilibria in the clay/quartz phases is used to estimate $\emptyset_e$. This element of the system was chosen for the following reasons:

(a) In contrast to $^{230}Th/^{234}U$ couple, the weathering processes leading to the formation of clays would not be accompanied by fractionation.

(b) In contrast to the amorphous iron phase, $^{234}U/^{238}U$ is not in isotopic equilibrium with groundwater. Leaching or deposition from groundwater to clay/quartz is clearly a less significant process.

To verify these concepts, at least semi-quantitatively, a quasi steady state is assumed. From Equation (36),

$$\frac{dU^4_{CQ}}{dt} = 0 = (1 - {}^{CQ}Re^{ax} - {}^{CQ}Re^{GW})\,{}^8U_{CQ} + {}^{ax}Re^{CQ}\,{}^8U_{ax} - U^4_{CQ} \quad , \tag{55}$$

where amorphous and crystalline iron are grouped as one phase ax, the recoil from the groundwater to the clay/quartz phase is negligible, and the effect of leaching from the clay/quartz to the groundwater, i.e. ξ_{CQ} is neglected.

From Equation (55)

$$R_{CQ} - 1 = {}^{ax}Re^{CQ}\,\frac{{}^8U_{ax}}{{}^8U_{CQ}} - ({}^{CQ}Re^{ax} + {}^{CQ}Re^{GW}) \quad . \tag{56}$$

The variation of $(R_{CQ} - 1)$ with ${}^8U_{ax}/{}^8U_{CQ}$ is shown in Figure 18A. Although $R_{CQ} - 1$ increases regularly with the uranium ratio, the relationship is not linear.

The deviation can be explained in terms of systematic variations in the parameter ${}^{ax}Re^{CQ}$ from sample to sample. Since the recoil distance of the daughter produce ($\sim$ 200 Å) is small compared with the size of the mineral phases, it may be assumed that the recoil flux is proportional to the contact surface area ${}^{ax}S^{CQ}$.

$${}^{ax}Re^{CQ} = Re\ {}^{ax}S^{CQ} \quad . \tag{57}$$

Since the iron minerals are either in contact with groundwater or clay/quartz, the total contact area is

$${}^{ax}S_{(total)} = {}^{ax}S^{CQ} + {}^{ax}S^{GW} \quad . \tag{58}$$

The validity of the assumptions were tested by assuming that at low CQ, uranium (points 4, 6, 7 Figure 18) the contact surface area ${}^{ax}S^{CQ}$ (as a fraction of the total) increased with increasing ${}^8U_{CQ}$, i.e.

$${}^{ax}S^{CQ} = f({}^8U_{CQ}) \quad . \tag{59}$$

If the functional relationship is linear, it follows from (56) and (59) that

$$\frac{R_{CQ} - 1}{U_{CQ}} = \frac{A\,{}^8U_{ax}}{U_{CQ}} + B \quad , \tag{60}$$

where A and B are constants. The plot of $(R_{CQ} - 1)U_{CQ}$ against ${}^8U_{ax}/{}^8U_{CQ}$ is shown in Figure 18B. There is clearly a considerable improvement in the linearity.

Assuming that

$$^{ax}S^{CQ} = K\, U_{CQ} \quad \text{(i.e. a proportionality relationship)} \tag{61}$$

then

$$^{CQ}Re = Re\ ^{CQ}S^{ax}$$

$$= K'\, Re\, U_{CQ} \tag{62}$$

and similarly,

$$^{CQ}Re^{GW} = K''\, Re\, U_{CQ} \quad . \tag{63}$$

From Equations (56) and (60)-(63),

$$\frac{R_{CQ} - 1}{U_{CQ}} = K\, Re\, \frac{U_{ax}}{U_{CQ}} - Re\,(K' + K'') \quad . \tag{64}$$

The values of $^{ax}\emptyset^{CQ}$ calculated from the slope of the linear plot (Figure 18B) are listed in Table 6.

From Figure 18B it is seen that zero fractionation occurs ($R_{CQ} = 1$) when the uranium activity ratio U_{AX}/U_{CQ} is approximately two. Physically, this condition would occur when the concentration of the parent ^{238}U in the two phases close to the boundary were equal. Due to the inevitable spread of data a definitive conclusion on the distribution of uranium within the clay/quartz phase cannot be drawn.

Direct fission track and α-track evidence has shown that the level of uranium in quartz grains is very small. Thus the parameter $^{AX}Re^{CQ}$, the probability of net ^{234}U recoil from the iron into the clay/quartz phase at a given uranium concentration would be expected to decrease with increasing quartz content. This is because the higher the percentage quartz, the lower the percentage clay and the higher the concentration of uranium in the clay. The higher the clay U concentration, the smaller the U concentration gradient across the iron (AX)/clay interface and the lower the net recoil. The effect is shown in Figure 19.

On the basis of these considerations the *net* flux of radionuclides on clays may be represented as in Figure 20. The thicker the arrow, the more rapid is the process; the longer the arrow, the greater the net flux attributed to the process. Where applicable (e.g. for ^{234}U) the *net* flux due to α-recoil is shown by dotted lines. The mechanism accounts for the following:

- observed isotopic equilibrium between the U isotopes on ferrihydrate and the groundwater,
- results of laboratory experiments with ^{236}U,
- evidence for time-dependent sorption coefficients,

- observed ^{234}U enrichment in the clay/quartz and goethite phases relative to the amorphous iron, and

- observed excess of ^{228}Th over ^{232}Th in groundwater.

4.3.2 A mechanism for enhanced retardation on clays over long timescales

The mechanism shown schematically in Figure 20 provides a basis for assessing the effect of long timescales on retardation factors. As the time increases, the following processes become successively more significant:

- the reversible adsorption in accessible minerals,

- factors leading to time-dependent sorption coefficients, and

- exchange between ferrihydrate and goethite.

It should be noted that if a substantial component of the radionuclide were transported by colloids, and if the colloids were not retarded, the radionuclide concentration in groundwater would be substantially greater than that calculated from conventional retardation factors.

4.3.3 Transferability of information from the analogue to the repository site

An important measure of the usefulness of the analogue approach is the extent to which the information can be applied directly to repository sites. Uranium series nuclides are ubiquituous and can be measured at very low concentrations. Under normal circumstances, fractionation can be measured with sufficient precision on groundwater and host rock samples from the repository site. It should therefore be possible to assess

- the role of colloids in transport,

- kinetic effects associated with radium and thorium sorption, and

- the role of specific minerals, particularly iron in retardation.

It is equally important to realize that there are serious limitations in the interpretation of uranium series measurements at the repository site. Except for the parent ^{238}U and ^{232}Th, most nuclides within the decay series are largely authigenic, i.e. they were generated *in situ* by radioactive decay. In contrast, most radionuclides of interest in repository assessment are allogenic, i.e. they originated from elsewhere. Their distributions are therefore not affected by radioactive decay.

Use can be made of the multiphase model to calculate the distribution of the allogenic radionuclides through the host rock (assumed to be clays).

Three steps are required:

(i) Assume an initial distribution of the key element X. For instance, it could be assumed to be in equilibrium with the ferrihydrate phase but of low concentration elsewhere.

(ii) Estimate final distributions through the separable mineral phases. This could be done by relating the distribution of X to uranium, thorium or other chemical analogues. An enormous advantage of uranium ore bodies is that, in principle, it is possible to measure low levels of the fission products and trans-uranics of immediate interest.

(iii) Use Equations (31) to (33) to calculate the distribution of X through the various phases. The parameters τ and ξ_a, ξ_{CQ} (for uranium) can be calculated by analysis of the uranium series data with the multiphase model.

Having estimated the distribution of elements through the host rock, an assessment of the kinetic effects of sorption can be made. They may *either* be incorporated into transport codes, *or* provide a basis for calculating a conservative value of the distribution coefficients which may be used to estimate the upper bounds of radionuclide migration. These concepts are elaborated in Section 6.5.

5. KOONGARRA SECONDARY MINERALIZATION - MODELLING OF A ROLL FRONT

5.1 Uranium Series Fractionation within the Secondary Mineralization

A brief description of the geology and hydrology of the Koongarra deposit was presented in Section 2.3.4. This ore body differs from Ranger One, Jabiluka One and Nabarlek, which have been discussed in previous reports[1-3], in two important respects:

(i) Close to the escarpment, which is near to the fault boundary of the deposit (Figure 5B), there appears to be a net accretion of material rather than erosion.

(ii) A well-defined region of secondary mineralization has been formed by the deposition of uranium leached from the primary ore by groundwater which infiltrates principally in the region of the boundary fault. The schematic representation of groundwater flow patterns developed by Snelling[13] is shown in Figure 5B.

A systematic set of samples was collected from diamond drill holes (Figure 5). Uranium-234/uranium-238 and thorium-230/uranium-234 ARs were measured (Table 17 of Reference 1).

The data are in marked contrast to those observed at the Ranger One, Jabiluka One and Nabarlek deposits. The most obvious differences are in the $^{230}Th/^{234}U$ ratios. With the exception of Koongarra, large thorium excesses are observed at the surface. This is attributed to the selective leaching of uranium by the infiltrating rainwater. Below the leaching zone, a region of uranium deposition characterized by thorium-230 is identified in many cores.

The observed data can be explained in terms of the current view of the groundwater hydrology[13]. Precipitation infiltrates to substantial depths along the fault zone bounding the escarpment and migrates upward through the deposit (Figure 5). Any effect due to the solution of surface uranium by distributed precipitation is outweighed by the deposition of uranium dissolved by groundwater percolating through the ore body. A second important difference between Koongarra and the other ore bodies should be noted. Evidence was presented for the long-term surface erosion at Ranger One, Jabiluka One and Nabarlek which roughly balanced the rate of advance of the weathering front. At Koongarra, there is an appreciable accretion of material eroding from the neighbouring escarpment. Rather than a gradual but continuous exposure of the uranium deposit, there is an accumulation down-gradient of secondary mineralization. This is analogous to roll front deposition.

General discussion of the distribution of ^{238}U, ^{234}U and ^{230}Th in a redox frontal system has been presented by Osmond and Cowart[20] who defined five classifications of the relative $^{234}U/^{238}U$, $^{230}Th/^{238}U$ ARs on the assumption

that ^{234}U moves more rapidly than ^{238}U (see Figure 4 of Reference 20). This implies that $^{234}U/^{238}U$ ARs exceed unity, as is the normal case. However, it can be seen in Table 7 which has been extracted from Table 3 of Reference 23, that all but one sample of Koongarra groundwater are deficient in ^{234}U.

The qualitative ideas developed by Osmond and Cowart have been quantified in part by Lever. Under prescribed conditions, uranium retarded travel times have been calculated from analysis of the whole rock data using a transport equation. This value has been compared with an independent estimate of the same parameter using groundwater flow velocities and measured uranium sorption coefficients. By comparing the two independent estimates a basis exists, in principle, for assessing the assumptions underlying both on the basis of geochemical evidence. Details are presented in the following sections.

Ultimately it is hoped to refine this approach to the extent that it will be possible to assess the validity of appropriate transport codes for long-term prediction.

5.2 A Simple Migration Model

The simplest quantitative model includes the effects of transport by flowing groundwater and linear, equilibrium sorption, described by a constant retardation factor. Different isotopes of the same element can have different distributions between the various rock phases, arising from the effects of α-recoil. This is modelled by assigning to them different retardation factors, although we do not expect the differences to be large. The transport model is one-dimensional with a constant groundwater velocity u. Neither variations vertically nor variations along the migration path are as yet considered. In the chains we examine, it will not be necessary to consider two elements with the same mass number, so we write the concentration in the groundwater of the i^{th} member of the chain with mass number m_i as c_{m_i}, which satisfies the equation

$$R_{m_i} \frac{\partial c_{m_i}}{\partial t} + u \frac{\partial c_{m_i}}{\partial x} + R_{m_i} \lambda_{m_i} c_{m_i} = R_{m_{i-1}} \lambda_{m_{i-1}} c_{m_{i-1}}, \qquad (65)$$

where λ_{m_i} and R_{m_i} are the appropriate decay constant and retardation factor.

A model for the mobilization of the uranium as the rock is weathered is also required. We assume that this takes place comparatively rapidly, leading to a distribution of mobile ^{238}U across the ore body. So we solve an initial value problem with this distribution. Thereafter we assume that linear equilibrium sorption is appropriate. Obviously this treatment of the chemistry is very simplified. The kinetics of leaching and mobilization could be important, as could the kinetics in the depositional region as the distribution in the diferent rock phases develops as a result of α-recoil. In addition, the effects of non-linear sorption and solubility limitation could be significant. A method for addressing some of these will be described later.

Hydrodynamic dispersion has also been omitted from the model. We justify this on the grounds that the appropriate value of the dispersivity is difficult to estimate, and there is considerable uncertainty as to the initial extent and concentration of the uranium ore.

So general solutions to Equation (65) are developed. Then we attempt to deduce information about the migration rate of various members of the decay chains and the overall migration time from the experimental data. We concentrate on the ^{238}U decay chain, for which the important members are

$$^{238}U \xrightarrow{4.5\times10^{9}\text{yrs}} {}^{234}U \xrightarrow{2.5\times10^{5}\text{yrs}} {}^{230}Th \xrightarrow{8\times10^{4}\text{yrs}} {}^{226}Ra$$

$$\xrightarrow{1600\text{yrs}} {}^{222}Rn \xrightarrow{3.8\text{ days}} {}^{210}Pb \xrightarrow{19\text{ yrs}} {}^{206}Pb\ \text{(stable)}.$$

In addition, we discuss the $^{235}U \rightarrow {}^{207}Pb$ chain briefly later.

5.3 General Solutions

With the neglect of dispersion, the initial distribution of ^{238}U, $c^{o}_{238}(x)$, migrates with the retarded groundwater velocity:

$$c_{238}(x,t) = c^{o}_{238}\,(x - ut/R_{238})e^{-\lambda_{238}t}\,. \tag{66}$$

This leads to the most obvious estimate of the migration time

$$t_u = R_{238}\,L/u = \phi\,R_{238}\,L/q, \tag{67}$$

Where L is the migration distance, q is the Darcy velocity and ϕ is the porosity. The corresponding solution for c_{234} is

$$c_{234}(x,t) = e^{-\lambda_{234}t}\,c^{o}_{234}(x - \frac{ut}{R_{234}}) + e^{-\lambda_{238}t}\,\frac{R_{238}\,\lambda_{238}}{R_{234}}\,.$$

$$\int_{o}^{t} e^{-(\lambda_{234}-\lambda_{238})t'}\,c^{o}_{238}(x - \frac{ut}{R_{238}} - ut'(\frac{1}{R_{234}} - \frac{1}{R_{238}}))dt'\,, \tag{68}$$

and the general solution for daughter nuclides is

$$c_{m_i}(x,t) = e^{-\lambda_{m_i} t} c^{o}_{m_i}\left(x - \frac{ut}{R_{m_i}}\right) + e^{-\lambda_{m_i} t} \frac{R_{m_{i-1}} \lambda_{m_{i-1}}}{R_{m_i}},$$

$$\int_0^t e^{\lambda_{m_i} \bar{t}} c_{m_{i-1}}\left(x - \frac{u(t-\bar{t})}{R_{m_i}}, \bar{t}\right) d\bar{t} . \qquad (69)$$

The solution for the stable daughter m_n is obtained by setting $\lambda_{m_n} = 0$.

From these solutions, the activity a_{m_i} on the rock can be deduced using

$$a_{m_i} = \phi(R_{m_i} - 1)\lambda_{m_i} c_{m_i} . \qquad (70)$$

For most nuclides, $R_{m_i} >> 1$ and so $R_{m_i}-1$ will be replaced by R_{m_i}.

From these solutions, it is clear that in general it will be difficult to interpret activity ratios on the rock. However, we can progress after making some approximations. First, we note that, for the three chains which are potentially interesting (^{238}U, ^{235}U, ^{232}Th), the half-life of the parent is much longer than that of any of the daughters. Further, we assume that the timescale of interest is significantly longer than the half-life of any of the daughters. Then the solutions for the various intermediate daughters depend only on $c^{o}_{m_1}$ and $x-ut/R_{m_1}$, and they can be written as

$$c_{m_i}(x,t) = e^{-\lambda_{m_1} t} g_{m_i}(x - ut/R_{m_1}), \qquad (71)$$

where g_{m_i} are functions related to $c^{o}_{m_1}$.

For the case without flow this is termed secular equilibrium, and all the activity ratios are equal to 1. When there is flow, a pulse passes through the system keeping the same form, with the daughters moving either ahead of or behind the long-lived parent, depending on their relative mobilities. One interesting result can be obtained by substituting Equation (71) into Equation (65), which yields

$$u(1-\frac{R_{m_i}}{R_{238}})\, g'_{m_i} = R_{m_{i-1}}\, \lambda_{m_{i-1}}\, g_{m_{i-1}} - R_{m_i}\, \lambda_{m_i}\, g_{m_i} \quad . \tag{72}$$

This implies that, at a given time, the activity of the daughter is a maximum where the total activities of the parent and daughter are equal. Osmond and Cowart[20], in a qualitative study, observed that this was approximately true, and we have demonstrated the result for our simplified model. As a consequence, the maximum activity of the daughter is lower than that of the parent, and the activity of the daughter is more dispersed.

Finally, to obtain solutions that can be used to analyse observed rock ARs, we assumed that $c^o_{m_1}$ varies only slowly with distance. Then if we replace $c_{m_{i-1}}$ within the integrals in Equations (68) and (69) by Taylor series expansions about $x-ut/R_{m_1}$, the integrals can be evaluated as power series. The members of the chain are approximately in secular equilibrium, and we investigate the first perturbation to this equilibrium. The AR of successive decaying nuclides is given by

$$\frac{a_{m_i}}{a_{m_{i-1}}} = 1 - \frac{u(\frac{R_{m_1}}{R_{m_i}} - 1)}{R_{m_1}\, \lambda_{m_i}} \frac{1}{a_{m_1}} \frac{da_{m_1}}{dx} \quad . \tag{73}$$

The analogous solution for the stable daughter m_n, making the same approximations, can also be found as

$$c_{m_n} = \lambda_{m_1} \int_0^t \frac{R_{m_1}}{R_{m_n}}\, c^o_{m_1}\, (x - \frac{ut}{R_{m_n}} + ut''\, (\frac{1}{R_{m_n}} - \frac{1}{R_{m_1}}))dt''$$

$$- \sum_{k=1}^{n-1} \frac{\lambda_{m_1}\, (\frac{1}{R_{m_k}} - \frac{1}{R_{m_1}})R_{m_1}}{\lambda_{m_k}\, (\frac{1}{R_{m_n}} - \frac{1}{R_{m_1}})R_{m_n}} (c^o_{m_1}(x - \frac{ut}{R_{m_1}}) - c^o_{m_1}(x - \frac{ut}{R_{m_n}}))$$

$$+ c^o_{m_n}(x - \frac{ut}{R_{m_n}}) \quad . \tag{74}$$

In deriving Equation (74), it is assumed that the initial concentrations of the short-lived daughters do not contribute significantly. This will be valid if the initial ARs are around unity. Furthermore, we assume that t is much less than the half-life of the long-lived parent.

In the case where both the mobility of the intermediate daughters has no effect on the concentration of lead and the lead itself is immobile, Equation (74) reduces to the usual formula used in lead dating[21], with $1-\exp(-\lambda_{m_1} t)$ replaced by $\lambda_{m_1} t$.

5.4 Analysis of Rock ARs

There is a considerable body of data from Koongarra on the ARs on rock of ^{234}U to ^{238}U and ^{230}Th to ^{238}U. A qualitative method of analysis was proposed by Osmond and Cowart[20], and now we have made it more quantitative.

There are six possible cases, depending on the relative magnitudes of R_{238} R_{234} and R_{230}; however these are really three pairs, with the paired cases having relative rates of migration reversed. So in Figures 21-23, the activities of the three nuclides as a function of distance are plotted for three cases along with the corresponding plot of the ^{234}U to ^{238}U AR against ^{230}Th to ^{238}U AR. For each case, there is a region on the AR plot where we do not expect to find points (shown as forbidden zones). In addition, the approximate solutions based on Equation (73) are shown as straight lines passing through (1,1). Deviations from these lines arise from higher order terms in the series expansion, which have been neglected in Equation (73).

The gradient of the line is

$$G = \left(1 + \frac{(R_{238}/R_{230}-1)\,\lambda_{234}}{(R_{238}/R_{234}-1)\,\lambda_{230}}\right)^{-1} , \qquad (75)$$

which is independent of the local values of a_{238} and da_{238}/dx. So if the values of R_{238}/R_{234} and R_{238}/R_{230} are constant throughout the region and the assumptions made in developing Equation (73) are valid, then all the points should lie on or be close to a single straight line, and it should be possible to compare values from different streamlines throughout the weathered zone. By examining the value of G, we can see the three different cases. If ^{238}U is more mobile than both ^{234}U and ^{230}Th ($R_{238} < R_{234}$, $R_{238} < R_{230}$) then $0<G<1$ (Figure 21). In the other two cases ^{234}U moves more rapidly than ^{238}U ($R_{234} < R_{238}$). G is ∞ when

$$R_{234} = R^{\infty}_{234} = \left(1 - \left(\frac{R_{238}}{R_{230}} - 1\right)\frac{\lambda_{234}}{\lambda_{230}}\right)^{-1} R_{238} . \qquad (76)$$

The cases with $R_{234} < R^{\infty}_{234}$ ($G > 1$) and $R^{\infty}_{234} < R_{234} < R_{238}$ ($G<0$) are shown in Figures 22 and 23. Osmond and Cowart describe these as "fast" and "slow" systems respectively.

At Koongarra, it is found experimentally that, except in the region where ^{238}U, ^{234}U and ^{230}Th are close to equilibrium, the ARs on drill core sample of ^{234}U to ^{238}U and ^{230}Th to ^{234}U are either both greater than one (on the upstream side of the deposit) or both less than one (on the downstream side). This is consistent with the picture shown in Figure 21, with $R_{238} < R_{234}$, R_{230}. However, it is not the same as the results of Osmond and Cowart, who found that for their case ^{234}U moved more rapidly than ^{238}U. The points obtained from samples from various drill holes are shown in Figure 24, along with the best linear fit to them. It is thought that ^{230}Th is much less mobile than ^{238}U and ^{234}U, and with the assumption that $R_{230} = \infty$, the retardation factor of ^{234}U is estimated to be 1.2 times that for ^{238}U. The region that is inaccessible if ^{230}Th is immobile is also shown on the figure.

Obviously there is considerable scatter on the points in Figure 24. However, it is clear that the vast majority of the points lie in the zones corresponding to $R_{238} < R_{234}, R_{230}$. The scatter could arise from

(i) variations in composition from sample to sample,

(ii) oversimplifications in the model which mean it is inappropriate to compare samples on different streamlines, and

(iii) experimental error.

However, this simple type of analysis is very appealing because it enables the data that is currently available to be used simply. It will become clearer whether or not it is appropriate if further data are obtained.

Equation (73) can also be used to estimate the migration time if the gradient of ^{238}U activity is estimated from drill core samples. The estimate is

$$t_u = \frac{R_{238}L}{u} = \frac{(\frac{R_{238}}{R_{m_1}} - 1)}{(1 - \frac{a_{m_1}}{a_{m_{i-1}}})\lambda_{m_1}} \frac{L}{a_{238}} \frac{da_{238}}{dx} . \qquad (77)$$

5.5 Estimates of the Migration Time

In the previous Sub-sections we have developed two methods of estimating the time that the uranium has been migrating. First, one can be found from Equation (67) based on laboratory and field estimates of distribution coefficients and numerical estimates of the groundwater velocities. Alternatively, Equation (77) gives an estimate based on the spatial gradient of ^{238}U activity, and the disequilibrium between ^{234}U and ^{238}U or ^{230}Th and ^{234}U. These are examined in turn.

In order to use Equation (67), estimates of the migration distance L, the Darcy velocity q, the porosity ϕ, the rock density ρ and the distribution coefficient K_{238} for ^{238}U are required. Then R_{238} is calculated from

$$R_{238} = 1 + \rho K_{238} (1-\phi)/\phi \quad . \tag{78}$$

The estimates of the first four are

$$L = 50 \text{ m} ,$$

$$q = 2 - 10 \text{ m yr}^{-1} [25] ,$$

$$\phi = 0.2 - 0.5 ,$$

$$\rho = 2.5 \text{ gm ml}^{-1} \quad . \tag{79}$$

It is harder to get an accurate estimate of K_{238}. Laboratory experiments on ^{236}U suggest that K_{236} starts from around 10^3 ml gm^{-1} at pH = 4.5, rises to a maximum possibly as high as 1.6×10^4 at pH = 7.0, and then falls again to around 200 at pH = 8.0 (although there is a large variation in values at this pH). Uranium-236 is not naturally occurring, it is newly added for the laboratory sorption experiments and so it is only sorbed to very accessible minerals. Uranium-238 in the field has had time to become associated with less accessible minerals. The best available estimates suggest that 25 per cent of ^{238}U is sorbed to accessible minerals, so the range of K_{238} considered is

$$K_{238} = 8 \times 10^2 - 6.3 \times 10^4 \text{ ml gm}^{-1} \quad . \tag{80}$$

It is also possible to obtain field estimates of K_{238} using concentrations of ^{238}U in bore hole groundwater and from drill core samples. Values from three bore holes across the region of secondary mineralization are around

$$K_{238} = 2 \times 10^4 \text{ ml gm}^{-1} \quad . \tag{81}$$

Substitution of Equations (79) and (80) into (78) and (67) yields a migration time based on laboratory sorption value in the range

$$t_u = 5 \times 10^3 - 3 \times 10^6 \text{ yrs} \quad , \tag{82}$$

whereas the range based on the field estimate Equation (81) is

$$t_u = 1.2 \times 10^5 - 10^6 \text{ yrs} \quad . \tag{83}$$

To estimate the migration time with Equation (77) using the disequilibrium data, we need to find $\zeta = L a_{238}^{-1} da_{238}/dx$. Unfortunately, there are relatively few good disequilibrium values in the main body of the secondary mineralization. One from DDH 3 has $\zeta = 0.5$, $^{230}Th/^{234}U$ AR = 0.91 and

$^{234}U/^{238}U$ AR = 0.96. If we assume again that ^{230}Th is immobile and that $R_{234}/R_{238} = 1.2$, then these respectively give

$$t_u = 2.4 \times 10^6 \text{ and } 3 \times 10^6 \text{ y} \quad . \tag{84}$$

However, it should be stressed that this is based on only a little data, in which there is considerable uncertainty. Further data are required to confirm that this is an appropriate interpretation.

An examination of Equations (82), (83) and (84) shows that if the lower groundwater velocities and higher sorption values are appropriate, then a consistent picture may be appearing with a uranium migration time around $1\text{-}3 \times 10^6$ y.

5.6 Analysis of Lead Data

There is a small amount of data on the concentration of various lead isotopes in the region of secondary mineralization. If the lead and the intermediate daughters are effectively immobile, and the uranium is mobile and migrating as a step function, then the time since the uranium arrived can be calculated from

$$\left(\frac{c_{m_n}}{c_{204}}\right)_{obs} = \left(\frac{c_{m_n}}{c_{204}}\right)_{init} + \left(\frac{c_{m_1}}{c_{204}}\right)_{obs} \left(e^{\lambda_{m_1} t_{m_1}} - 1\right), \tag{85}$$

where c_{204} is the concentration of ^{204}Pb, which does not arise from radioactive decay and so is primordial, and t_{m_1} is the time associated with the decay of parent m_1.

The results from five samples are given in Table 8 using the data for ^{206}Pb (from ^{238}U) and ^{207}Pb (from ^{235}U). The first three of the samples come from the region where there would have been primary ore before weathering and the other two come from the region that would originally have been outside the ore body. This is reflected in the time estimates. The first three are in the 10^8 - 10^9 y range, whereas the last two range from $2\text{-}5 \times 10^7$ y. The latter range is however considerably higher than the estimates quoted earlier (Equations (82)-(84)). As the absolute lead levels are low for these two samples, this suggests that the discrepancy does not arise from an element being very mobile. The alternative is that either lead or an intermediate daughter from both the ^{238}U and ^{235}U chains are slightly mobile, possibly as a colloid. Then some of the lead with the long time signature from the primary ore body is present, increasing the estimates.

The approximately linear solution (Equation (74)) can be used to estimate if any of the intermediate daughters could either have a significant disequilibrium associated with them or if they could move a sizeable distance during their lifetime. Most of the intermediate daughters have such a short half-life that even if they are mobile, they decay before they have migrated

any distance. The nuclide with the largest half-life is ^{226}Ra (1622 y), and the best estimates of the distribution coefficient suggest that it is rather more mobile than uranium. For the conditions envisaged above (low flow, high uranium sorption) along with the best estimates of radium distribution coefficients, it seems possible that the ^{226}Ra to ^{230}Th AR could be significantly different from 1, but that ^{226}Ra will not move a substantial distance ahead of the ^{238}U.

5.7 Application of Laplace Transform Techniques

All the analysis developed so far in this section has assumed that the linear solution (Equation (73)), appropriate for slowly varying input functions is valid. If this approximation is not valid or if additional phenomena are to be included, such as hydrodynamic dispersion, kinetic or non-linear effects, then a different solution technique has to be adopted.

We have developed a partly analytical, partly numerical solution based on Laplace transforms. This technique has been applied to a number of problems in transport by groundwater[25-27]. The model is not restricted to slowly varying input functions, and it allows linear, kinetic effects to be included with the rock described as two phases. The first comes into equilibrium with the groundwater rapidly, and its effect is modelled by a simple retardation factor, corresponding to sorption values measured in the laboratory. The second part only comes into equilibrium with the groundwater on a longer timescale, and so is described by two parameters: a sorption capacity K'_{m_i} and a relaxation time $\xi^{-1}_{m_i}$. Hydrodynamic dispersion is not included in the present analysis, but it can be incorporated in a straightforward manner. However, models with non-linear sorption cannot be solved using this technique.

The equations for the ith member of the chain are

$$R_{m_i} \frac{\partial c_{m_i}}{\partial t} + \phi^{-1} \frac{\partial s_{m_i}}{\partial t} + u \frac{\partial c_{m_i}}{\partial x} + R_{m_i} \lambda_{m_i} c_{m_i} + \phi^{-1} \lambda_{m_i} s_{m_i} =$$

$$R_{m_{i-1}} \lambda_{m_{i-1}} c_{m_{i-1}} + \phi^{-1} \lambda_{m_{i-1}} s_{m_{i-1}} , \qquad (86)$$

$$\frac{\partial s_{m_i}}{\partial t} + \lambda_{m_i} s_{m_i} = \xi_{m_i} (K'_{m_i} c_{m_i} - s_{m_i}) + \lambda_{m_{i-1}} s_{m_{i-1}} , \qquad (87)$$

where s_{m_i} is the quantity sorbed per unit volume on the second phase of the rock. We solve these equations as a boundary value problem with the values of c_{m_i} at $x = 0$ specified as a function of time. We assume that $c_{m_i} = s_{m_i} = 0$ at $t = 0$ for $x > 0$. The solution can be simply modified to solve the initial value problem instead.

The Laplace transform of c_{m_i} is defined as

$$\bar{c}_{m_i}(p) = \int_0^\infty e^{-pt} c_{m_i}(t)dt \ . \tag{88}$$

Equations (86) and (87) when transformed become

$$u \frac{\partial \bar{c}_{m_i}}{\partial x} + R_{m_i}(p + \lambda_{m_i})\bar{c}_{m_i} + \phi^{-1}(p+\lambda_{m_i})\bar{s}_{m_i} = R_{m_{i-1}} \lambda_{m_{i-1}} \bar{c}_{m_{i-1}} + \phi^{-1}\lambda_{m_{i-1}} \bar{s}_{m_{i-1}}, \tag{89}$$

and

$$(p+\lambda_{m_i})\bar{s}_{m_i} = \xi_{m_i}(K'_{m_i} \bar{c}_{m_i} - \bar{s}_{m_i}) + \lambda_{m_{i-1}} \bar{s}_{m_{i-1}} . \tag{90}$$

If we write

$$\alpha_i = (p + \lambda_{m_i})\left(R_{m_i} + \frac{\phi^{-1}\xi_{m_i} K'_{m_i}}{p + \lambda_{m_i} + \xi_{m_i}}\right) , \quad \beta_i = R_{m_{i-1}} \lambda_{m_{i-1}} ,$$

$$\gamma_i = \frac{\phi^{-1}\xi_{m_i} \lambda_{m_{i-1}}}{p + \lambda_{m_i} + \xi_{m_i}} , \quad \delta_i = \frac{\xi_{m_i} K'_{m_i}}{p+\lambda_{m_i} + \xi_{m_i}} , \quad \varepsilon_i = \frac{\lambda_{m_{i-1}}}{p+\lambda_{m_i} + \xi_{m_i}} , \tag{91}$$

then Equations (89) and (90) can be solved to give

$$\bar{c}_{m_i} = \sum_{k<j<i} \theta_{ijk} \exp\left(-\frac{\alpha_j x}{u}\right) {}_o\bar{c}_{m_k} \tag{92}$$

and

$$\bar{\varepsilon}_{m_i} = \sum_{k<j<i} \phi_{ijk} \exp\left(-\frac{\alpha_j x}{u}\right) {}_o\bar{c}_{m_k} , \tag{93}$$

where ${}_o\bar{c}_{m_k}$ is the Laplace transform of the boundary value at x = 0, and θ_{ijk} and ϕ_{ijk} are given iteratively by

$$\theta_{iii} = 1 ,$$

$$\sum_{\substack{j \\ i \neq k}} \theta_{ijk} = 0 ,$$

$$(\alpha_i - \alpha_j)\, \theta_{ijk} = \beta_i\, \theta_{i-1jk} + \gamma_i\, \phi_{i-1jk} ,$$

$$\phi_{ijk} = \delta_i\, \theta_{ijk} + \varepsilon_i\, \phi_{i-1jk} . \tag{94}$$

We have now obtained analytical solutions to the transformed equations. These are inverted numerically using the algorithm due to Talbot. For the case of no dispersion, it is helpful to note that the θ_{ijk} and ϕ_{ijk} in Equations (92) and (93) represent the arrival of the nuclide i resulting from the decay of source k travelling at the retarded velocity u/R_{m_i} (modified slightly by kinetic effects). No nuclide can arrive before the retarded travel time $R_{m_i}\, x/u$, and this can be exploited in the inversion by multiplying the transform by $\exp(R_{m_j}\, x/u)$ and noting that the transform of a function satisfies

$$\overline{f(t-t_o)H(t-t_o)} = \exp(-pt_o)\ \overline{f(t)H(t)} , \tag{95}$$

where H(t) is the Heaviside step function.

The numerical inversion has been checked by comparison with the analytical solution for a step function input. It has then been used to examine the solution for two general pulse inputs $t^n e^{-\zeta t}$ and $t^{-\frac{1}{2}}\exp(-(x-vt)^2/4Dt$. An example with $R_{238} < R_{234} < R_{230}$ is found for the first of these inputs in Figure 25. Both the plot of activities of ^{238}U, ^{234}U and ^{230}Th against migration distance and the plot of the $^{234}U/^{238}U$ AR against the $^{230}Th/^{238}U$ AR are shown. The features considered in the discussion of Figure 21 are clear. The activity ratios are moved away from secular equilibrium because the pulse cannot be regarded as being slowly varying.

5.8 Concluding Remarks

In this Section we have developed simple models, which explore ways in which data that is currently available can be used. These models give estimates of the time that migration has been taking place. However, a number of simplifications are made in them:

(i) The rock is treated as a single phase which is in equilibrium with the groundwater.

(ii) Hydrodynamic dispersion is omitted.

(iii) Transport by colloids is not considered.

(iv) The models are one-dimensional, vertical variation is neglected, and all parameters are assumed to be constant in space and time.

All these aspects should be considered further in future, focussing in particular on the following areas:

(i) Is it adequate to treat the mobilization and leaching as a process that takes place over a short time as the primary ore body is weathered?

(ii) The investigation should be continued into the importance of the different timescales on which different rock phases come into equilibrium with the groundwater.

(iii) Consideration should be given to the inclusion of colloids in the model, in particular to modelling the transfer of nuclides between groundwater, colloid and rock and to the timescale on which it occurs.

(iv) Currently there is considerable scatter on the AR plots. Further data, particularly from the region of secondary mineralization where there was no primary ore, would be extremely helpful in deciding whether the analysis by the current model is adequate and whether additional features are required (which may or may not be amenable to a simple extension of the analysis).

(v) Further lead data in the same region and also downstream of the whole body would also be of great interest.

6. APPLICATION OF THE MODEL TO THE DEVELOPMENT AND REFINEMENT OF THE ANALOGUE

6.1 Calculation of Source Terms

One of the major advantages of uranium ore bodies as analogues of waste repoisitories is the existence of extremely low, yet measurable levels of some of the transuranics (e.g. ^{239}Pu, ^{237}Np) and fission products (e.g. ^{129}I, ^{99}Tc). Incorporation of these elements into the analogue involves the estimation of

- source terms, and
- retardation factors.

The magnitude of the source term depends on

- the rate of production,
- the rate of release to the groundwater.

The current modelling program is designed to quantify the rate of mobilization of elements generated within the uranium ore. The rate of release to the groundwater is the sum of the following terms:

(i) the rate of leaching from the unweathered rock;

(ii) the rate of mobilization accompanying weathering; and

(iii) the rate of leaching from the weathered zone.

The method of calculation depends on whether it is appropriate to use

- the four-zone model (Section 2), or
- the roll front model (Section 5).

Four-zone Model

This model, which has been applied to data from Ranger One and Nabarlek, involves the assumption that uranium and other radionuclides are mobilized by weathering. The rate of release Rw (term (ii) above) is given by

$$Rw = W\, Tu_x \quad , \tag{96}$$

where W is the rate of advance of the weathering front (Section 2.1 and Table 3), and Tu_x is the average concentration in the crystalline rock undergoing weathering.

Estimates of W can be made (Section 2.3) and hence Rw calculated. Most of the elements released from the crystalline rocks are re-adsorbed on the clays, iron minerals and other products of weathering. Only a fraction enters the groundwater system.

Radionuclide transport at Koongarra

A roll front model has been applied to the evolution of secondary mineralization at Koongarra. The aim of the model is to understand the evolution of secondary mineralization. As explained in Section 5.2, the approach is to rationalize observed uranium series disequilibria in terms of the values of the following parameters averaged over geological time:

- linear adsorption coefficients,
- groundwater velocity, and
- retardation factors.

The contribution of a radionuclide released from the source rock is a boundary condition. From the model, it is possible to calculate the residence time of uranium within the zone of secondary mineralization. It is therefore possible to calculate the rate of build-up of authigenic fission products and transuranics. The observed levels will be the net result of

- input from the source rock,
- build-up within the secondary mineralization, and
- groundwater leaching.

6.2 Interpretation of Laboratory Data in Terms of Time-dependent Retardation Factors

Extensive evidence is accumulating that adsorption of actinides is dominated by accessible iron and manganese oxides. In the samples studied, iron minerals dominate. On laboratory timescales, amorphous ferrihydrite is the only significant locus of adsorption for uranium; there is negligible adsorption on goethite or on the clay/quartz phases.

The substantial levels of uranium in the crystalline iron phases of weathered ore result from a combination of solid state diffusion or incorporation during the process of crystallization:

$$U_{aq} \underset{\text{rapid}}{\rightleftharpoons} U(\text{ferrihydrite}) \underset{\text{slow}}{\rightleftharpoons} U(\text{goethite}) \qquad (97)$$

In the multiphase model, it is assumed that the latter process dominates. Estimates have been made of the mean time τ associated with the exchange between the crystalline and amorphous iron. Preliminary estimates of τ for samples at Ranger One and Koongarra are shown in Table 5. From a knowledge of τ it is possible to assess kinetic effects associated with uranium sorption.

6.3 Separation of Authigenic and Allogenic Components of Uranium Series Elements

A substantial proportion of actinides in groundwater down-gradient of the uranium deposits are allogenic and hence are good analogues of radionuclides leached from breached repositories. However, for a full evaluation of this analogue, it is necessary to study not only the groundwater, but also the host rocks. Because of the very long residence times of uranium, both in the crystalline rock and in the associated weathered sequences, the daughter products are essentially all authigenic.

An allogenic element is transported by groundwater, adsorbed on the accessible ferrihydrite and gradually incorporated into the associated goethite during the crystallization process. Authigenic elements on the other hand are formed by decay.

A model, incorporating the features described in Section 4, is needed to separate the two effects and interpret the data in terms of radionuclide transport over a particular timescale.

6.4 Transferability of Information from the Analogue to the Repository Site

To maximise the usefulness of natural analogues of repository systems, it is necessary to assess problems associated with the transfer of information from the study area to the proposed site. Analogue study will yield two classes of information:

(i) *Generic.* Examples include

- evidence for the time-dependence of distribution coefficients,
- evidence for the effect of α-recoil on distribution coefficients,
- evidence for α-recoil induced transport between mineral phases,
- evidence for the transport of uraniun and thorium in groundwater colloids, and
- evidence for different roles of ferrihydrite, goethite and clay/quartz phases in the adsorption of radium and the actinides.

(ii) *Site-specific.* The second class of properties includes

- the petrology and mineralogy of the host rocks,
- the local and regional hydrology, and
- radionuclide distribution coefficients.

The problem of transferring information is essentially that of interpreting the generic effects evaluated in the analogue study in terms of the specific properties of the repository site. The problem is tractable if the following assumptions are made:

(i) Uranium and thorium series elements can be measured accurately at the repository site.

(ii) The transport properties of radionuclides can be described sufficiently accurately by interaction with accessible minerals.

(iii) Adsorption effects involving two or more separable mineral phases can be described mathematically. An appropriate model incorporating the above generic effects is needed.

6.5 Validation of Geochemical Transport Codes

Ultimately, evidence by proponents of particular repository systems, which demonstrate compliance with regulations on the limits to radiation dose affecting populations in the distant future, must be mathematical. It is therefore important to examine the validity of established geochemical codes for long-term prediction. An approach to this problem using natural analogues is outlined in Section 5. Attempts to verify the SWIFT code from data collected at the Koongarra deposit will be reported separately.

7. REFERENCES

1. P.L. Airey, D. Roman, C. Golian, S. Short, T. Nightingale, T. Payne, R.T. Lowson and P. Duerden, "Radionuclide Migration around Uranium Ore Bodies - Analogues of Radioactive Waste Repositories", USNRC Contract NRC-04-81-172, Annual Report 1983-84, AAEC Report C45 (1985).

2. P.L. Airey, D. Roman, C. Golian, S. Short, T. Nightingale, R.T. Lowson and G.E. Calf, "Radionuclide Migration around Uranium Ore Bodies - Analogues of Radioactive Waste Repositories", USNRC Contract NRC-04-81-172, Annual Report 1981-82, AAEC Report C29 (1982).

3. P.L. Airey, P. Duerden, D. Roman, C. Golian, T. Nightingale, T. Payne, B.G. Davey and D. Gray, "Radionuclide Migration around Uranium Ore Bodies - Analogues of Radioactive Waste Repositories", USNRC Contract NRC-04-81-172, Annual Report 1984-85, in preparation.

4. P.L. Airey, D. Roman, C. Golian, S. Short, T. Nightingale, R.T. Lowson and G.E. Calf, "Radionuclide Migration around Uranium Ore Bodies - Analogues of Radioactive Waste Repositores", USNRC Contract NRC-04-81-172, Annual Report 1982-83, AAEC Report C40 (1984) (NUREG/CR-391, Vol. 1).

5. P.L. Airey, P. Duerden, D. Roman, C. Golian, T. Nightingale, T. Payne et al., "Koongarra Ore Body: A Natural Analogue of Radionuclide Migration in the Far Field of HLW Repositories". Presented at the Natural Analogue Working Group Meeting, Brussels, 5-7 November 1985 (1985).

6. P.L. Airey and C. Golian, "Open System Uranium Series Modelling", in Proceedings of OSS Workshop on the Measurement of Long-lived Environmental Isotopes, Sydney, 29 April-1 May (1985).

7. M. Reeves and R.M. Cranwell, User Manual for the Sandia Waste-Isolation Flow and Transport Model (SWIFT). Release 4.81, Sandia Report SAND 81-2516, NUREG/CR-2324 (1981).

8. Ranger Uranium Environmental Inquiry, Second Report (Presiding Commissioner, Mr Justice R.W. Fox), (Australian Government Publishing Service, Canberra), Chap. 5, p.51, 1977.

9. R.S. Needham, I.H. Crick and P.G. Stuart-Smith, "Regional Geology of the Pine Creek Geosyncline", in Proceedings of IAEA International Symposium Uranium in the Pine Creek Geosyncline, Sydney, 4-8 June 1979, Ed. J. Ferguson and A.B. Goleby (IAEA, Vienna, 1980), p. 1.

10. R.S. Needham and M.J. Roarty, "An Overview of Metallic Mineralization in the Pine Creek Geosyncline", in Proceedings of IAEA International Symposium Uranium in the Pine Creek Geosyncline, Sydney, 4-8 June 1979, Ed. J. Ferguson and A.B. Goleby (IAEA, Vienna, 1980), p. 157.

11. M.R. Hegge, D.V. Mosher, G.S. Eupene and P.S. Anthony, "Geologic Setting of the East Alligator Uranium Deposits and Prospects, in Proceedings of IAEA International Symposium Uranium in the Pine Creek Geosyncline, Sydney, 4-8 June 1979, Ed. J. Ferguson and A.B. Goleby (IAEA, Vienna, 1980), p. 259.

12. J.A. Grounds, "Groundwater Monitoring Procedures and Evaluation at Nabarlek, NT", in Proceedings of Aust. Water and Wastewater Association International Specialist Conference on Water Regime in Relation to Milling, Mining and Waste Treatment including Rehabilitation with Emphasis on Uranium Mining, Darwin, Paper 16, 1983.

13. A.A. Snelling, "Uraninite and its Alteration Products, Koongarra Uranium Deposit", in Proceedings of IAEA International Symposium Uranium in the Pine Creek Geosyncline, Sydney, 4-8 June 1979, Ed. J. Ferguson and A.B. Goleby (IAEA, Vienna, 1980), p.487.

14. Australian Groundwater Consultants Pty Ltd and McMahon, Burgess & Yeates, "Report on Investigation of Groundwater and the Design of Water Management and Tailings Retention Systems for the Koongarra Project", Koongarra Project. Draft Environmental Impact Statement (Noranda Australia Ltd, Melbourne, 1978, Appendix XI.

15. P. Hille, "An Open System Model for Uranium Series Dating", Earth Planet. Sci. Lett., 42, 138-143, 1979.

16. J.N. Rosholt, "Open System Model for Uranium Series Dating of Pleistocene Samples", in Proceedings of Symposium on Radioactive Dating Methods and Low-level Counting, Monaco, 1967, (IAEA, Vienna), pp. 299-311.

17. B. Szabo and J.N. Rosholt, "Uranium Series Dating of Pleistocene Molluscan Shells from Southern California - An Open System Model", J. Geophys. Res., 74, 3253-60, 1969.

18. J.N. Rosholt, "Uranium Trend Dating of Quaternary Sediments", U.S. Geological Survey Open File Report 80-1087, 1980.

19. M. Ivanovich, "Uranium Series Disequilibria Applications in Geochronology", Chap. 3, in Uranium Series Disequilibrium. Applications to Environmental Problems, Ed. M. Ivanovich and R.S. Harmon Clarendon Press, Oxford, pp. 56-57, 1982.

20. J.K. Osmond and J.B. Cowart, "Uranium Series Disequilibrium in Groundwater and Core Composite Samples from the San Juan Basin and Copper Mountain Research Sites", US Department of Energy, Grand Junction, Colorado, Contract 50-51-5065, Sub-contract 78-167-E, Report GJBX 364(81), 1981.

21. B.E. Clancy, "CLUTCH - An Ordinary Differential Equation Solver for Initial Value Problems", AAEC Report E575, 1984.

22. P.L. Airey, D. Roman, C. Golian, S. Short, T. Nightingale, R.T. Lowson, G.E. Calf, B.G. Davey and D. Gray, "Radionuclide Migration around Uranium Ore Bodies - Analogues of Radioactive Waste Repositories", USNRC Contract NRC-04-81-172, Quarterly Report No. 10, AAEC Report C44, 1984.

23. B.R. Doe, "Lead Isotopes", Springer-Verlag, 1970.

24. F. Kalf, Australian Groundwater Consultants, Private Communication, 1985.

25. J.A. Barker, "Laplace Transform Solutions for Solute Transport in Fissured Aquifers", Adv. Water Resour. 5, 98-104, 1982.

26. D.P. Hodgkinson and D.A. Lever, "Interpretation of a Field Experiment on the Transport of Sorbed and Non-sorbed Tracers through a Fracture in Crystalline Rock", Radioact. Waste Manage. Nucl. Fuel Cycle, 4, 129-156, 1983.

27. D.P. Hodgkinson, D.A. Lever and T.H. England, "Mathematical Modelling of Radionuclide Transport through Fractured Rock using Numerical Inversion of Laplace Transforms: Application to INTRACOIN level 3", Ann. Nucl. Energy, 11, 111-122, 1984.

28. J.N. Rosholt, C.A. Bush, W.J. Carr, D.L. Hoover, W.C. Swadley and J.R. Dooley, J.R., "Uranium-Trend Dating of Quaternary Deposits in the Nevada Test Site Area, Nevada and California", US Geological Survey, Lakewood, Colorado, Open-File Report 85-540 (1985).

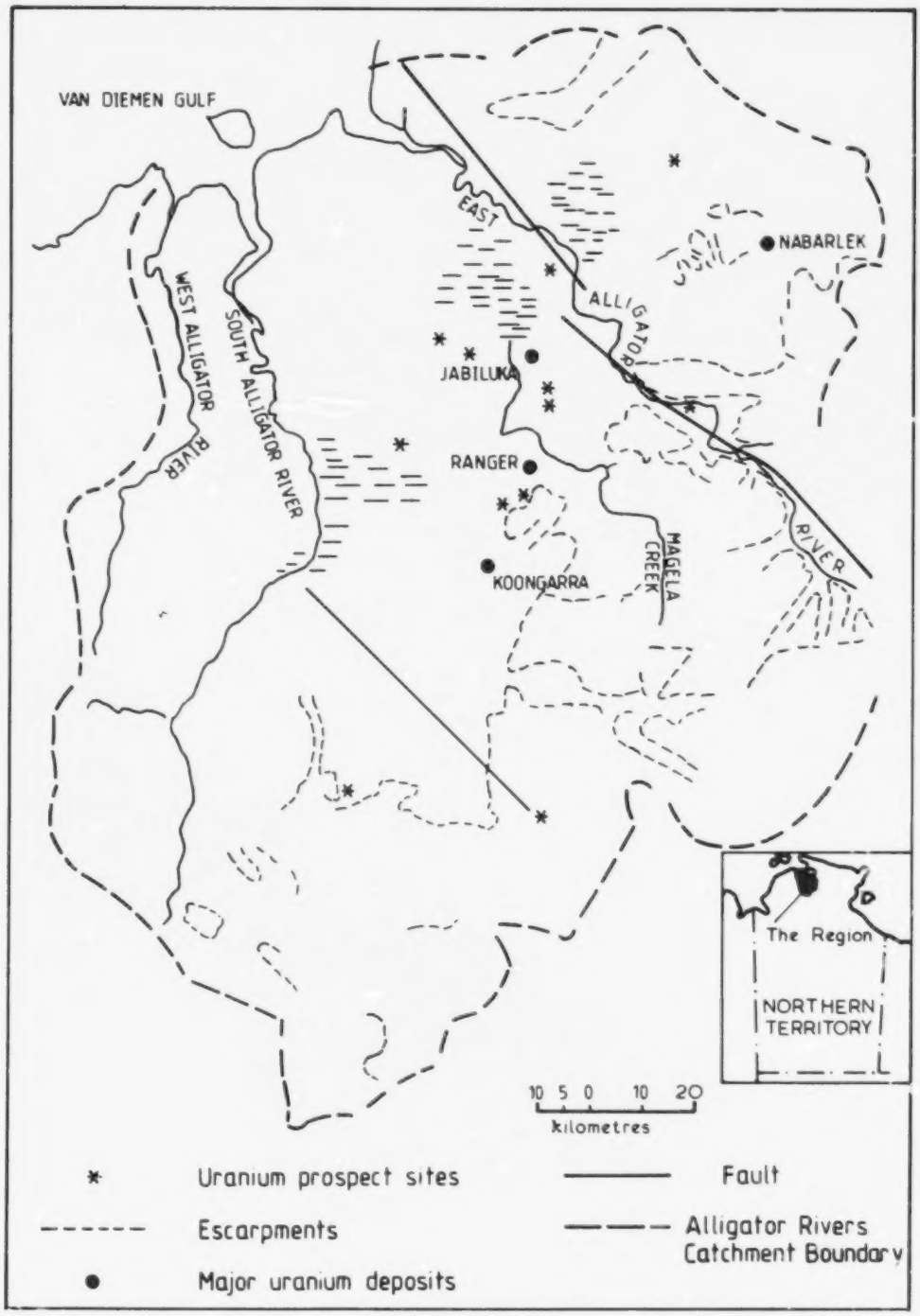

FIGURE 1 The location of the principal uranium ore bodies and prospects in the Alligator Rivers area of the Northern Territory of Australia. (Map 9, Reference 8.)

BEST COPY AVAILABLE

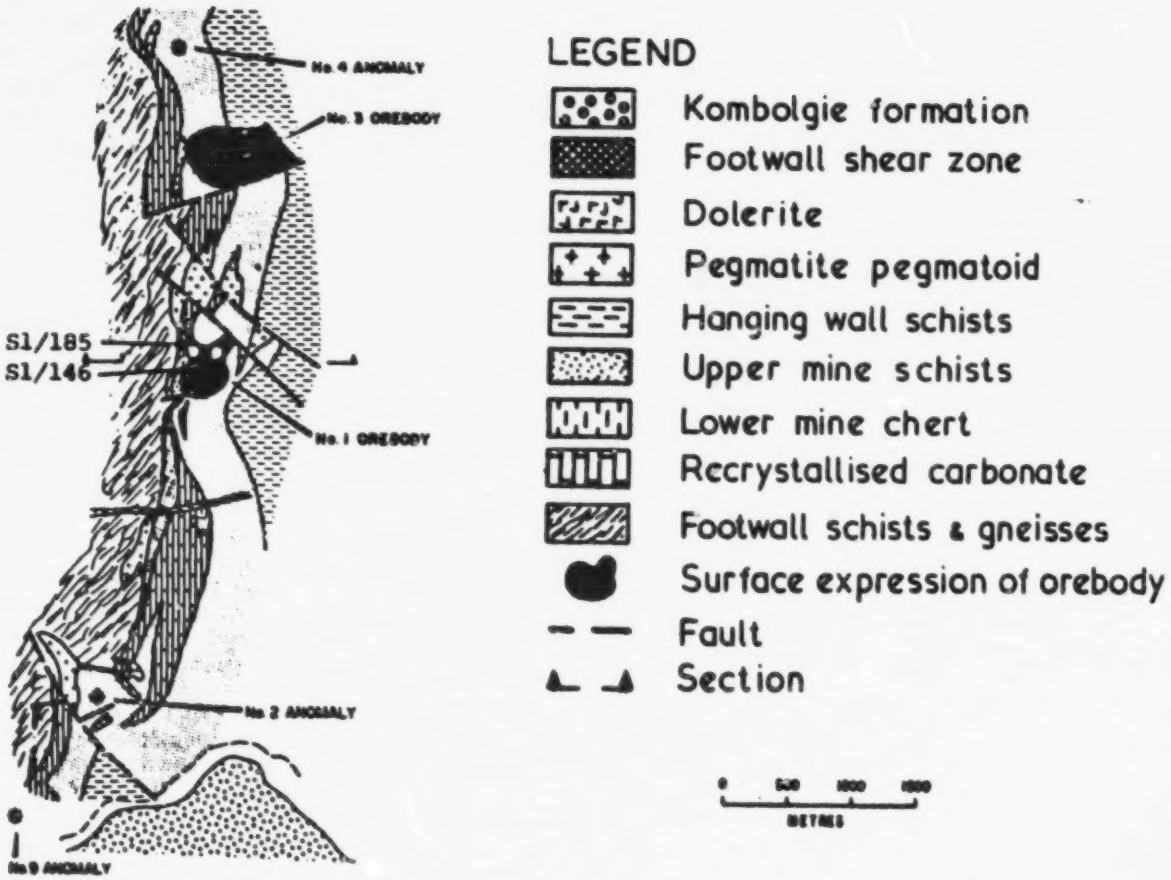

FIGURE 2 Generalized geologic plan of the Ranger One ore bodies and prospects (from Figures 4 and 5 of Reference 11). The location is shown in Figure 1.

BEST COPY AVAILABLE

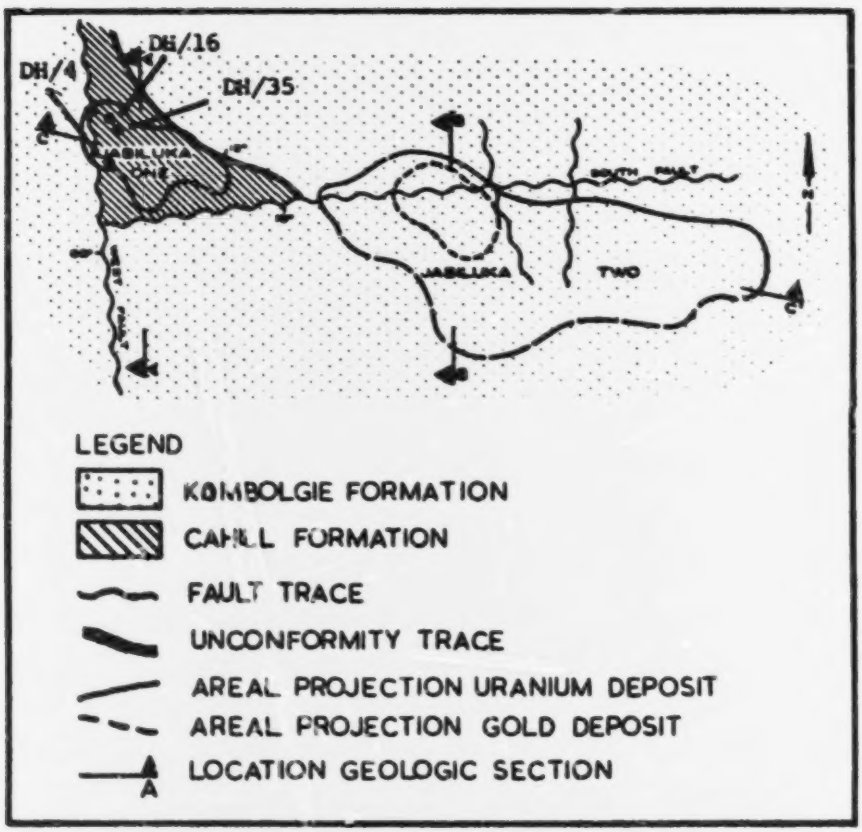

FIGURE 3 Generalized geologic plan and cross-sections of the Jabiluka One and Two ore bodies (from Figures 10 and 11 of Reference 11).

BEST COPY AVAILABLE

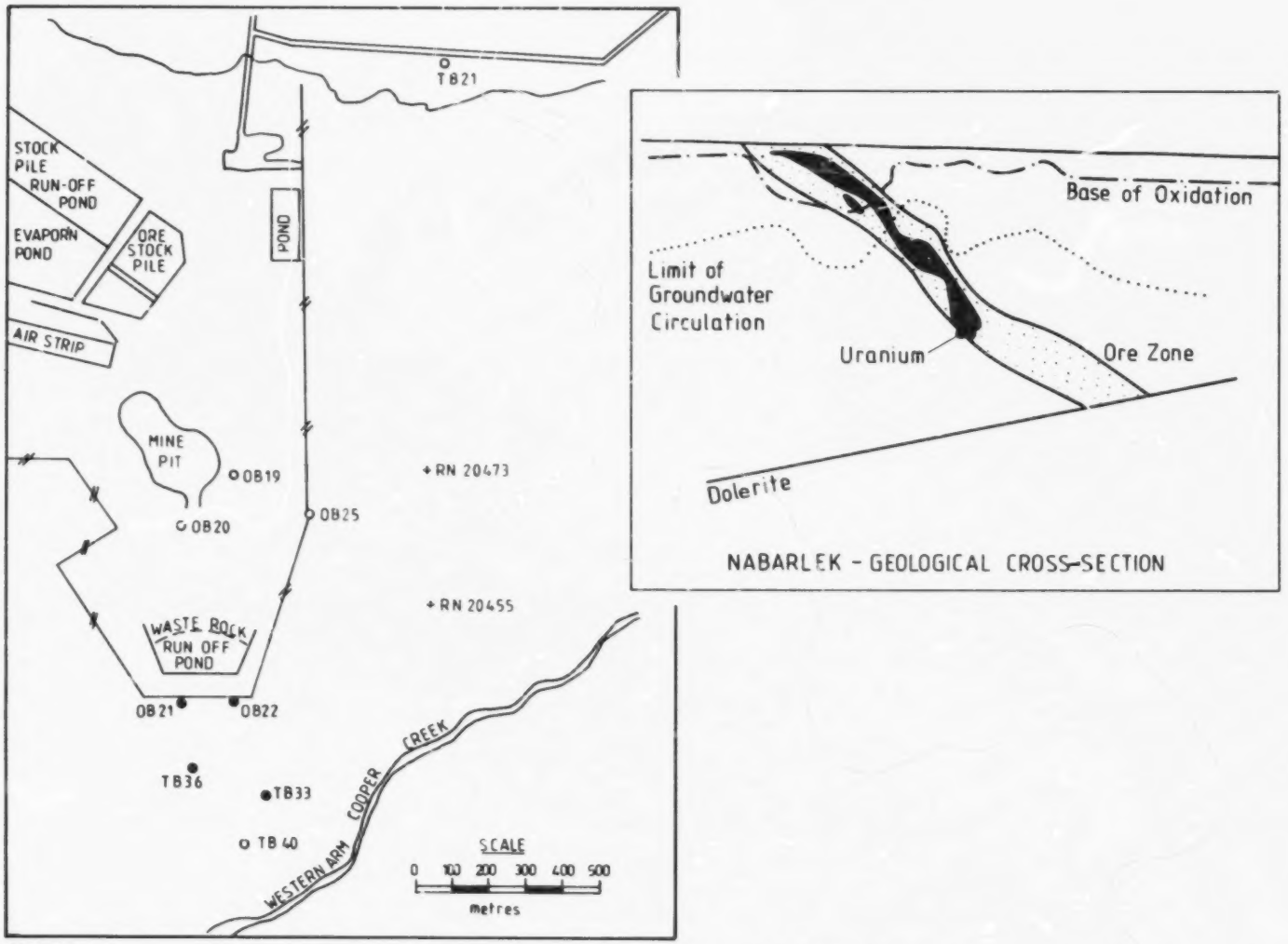

FIGURE 4 Location of the sampling wells at Nabarlek. Insert: General geological cross-section.

BEST COPY AVAILABLE

54

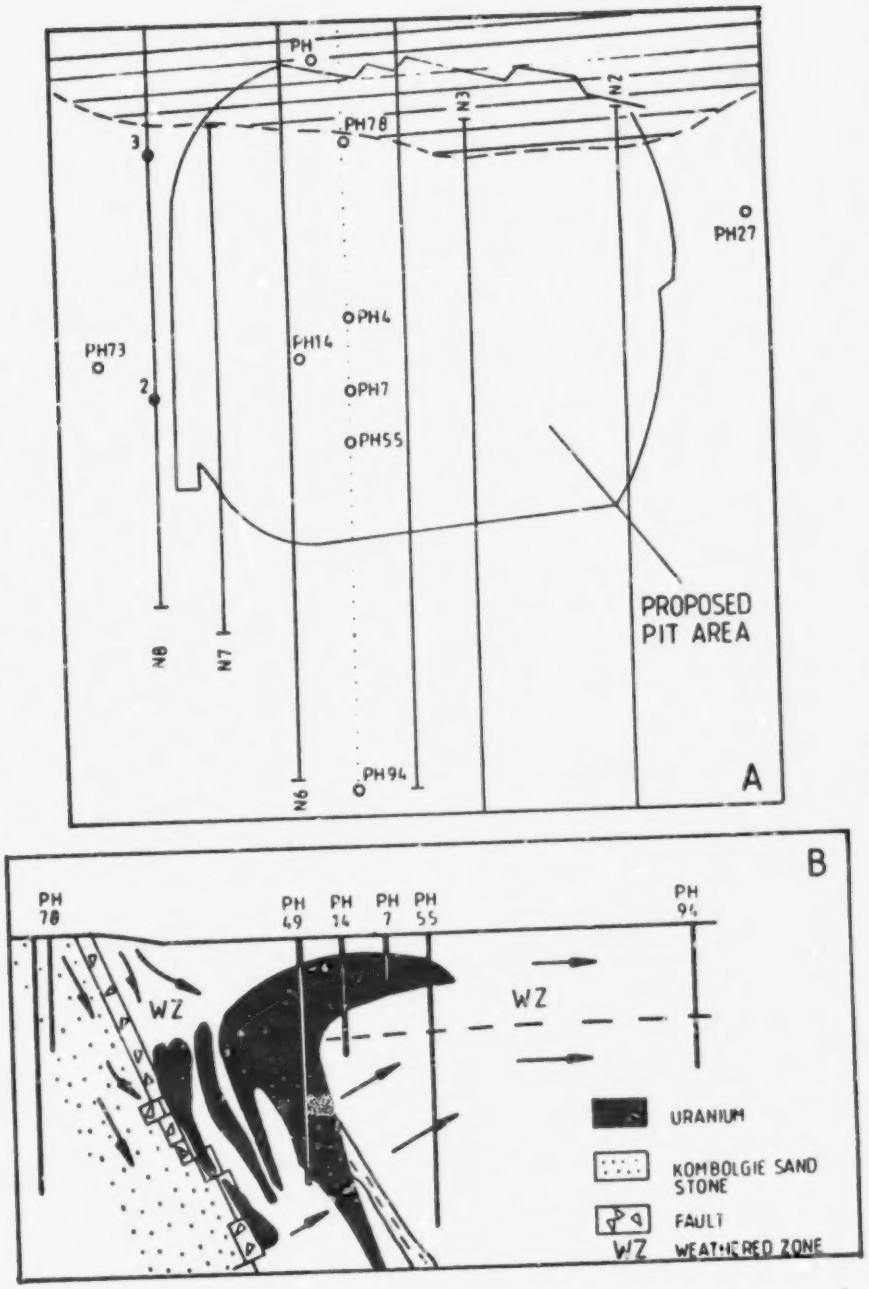

FIGURE 5 A. Location of the sampling wells at the Koongarra deposit.

B. A section between wells PH 78 and PH 94 showing the location of a major fault, the extent of the uranium deposits, the boundary of surface oxidation and the groundwater flow paths (adapted from Figure 1, Reference 9).

BEST COPY AVAILABLE

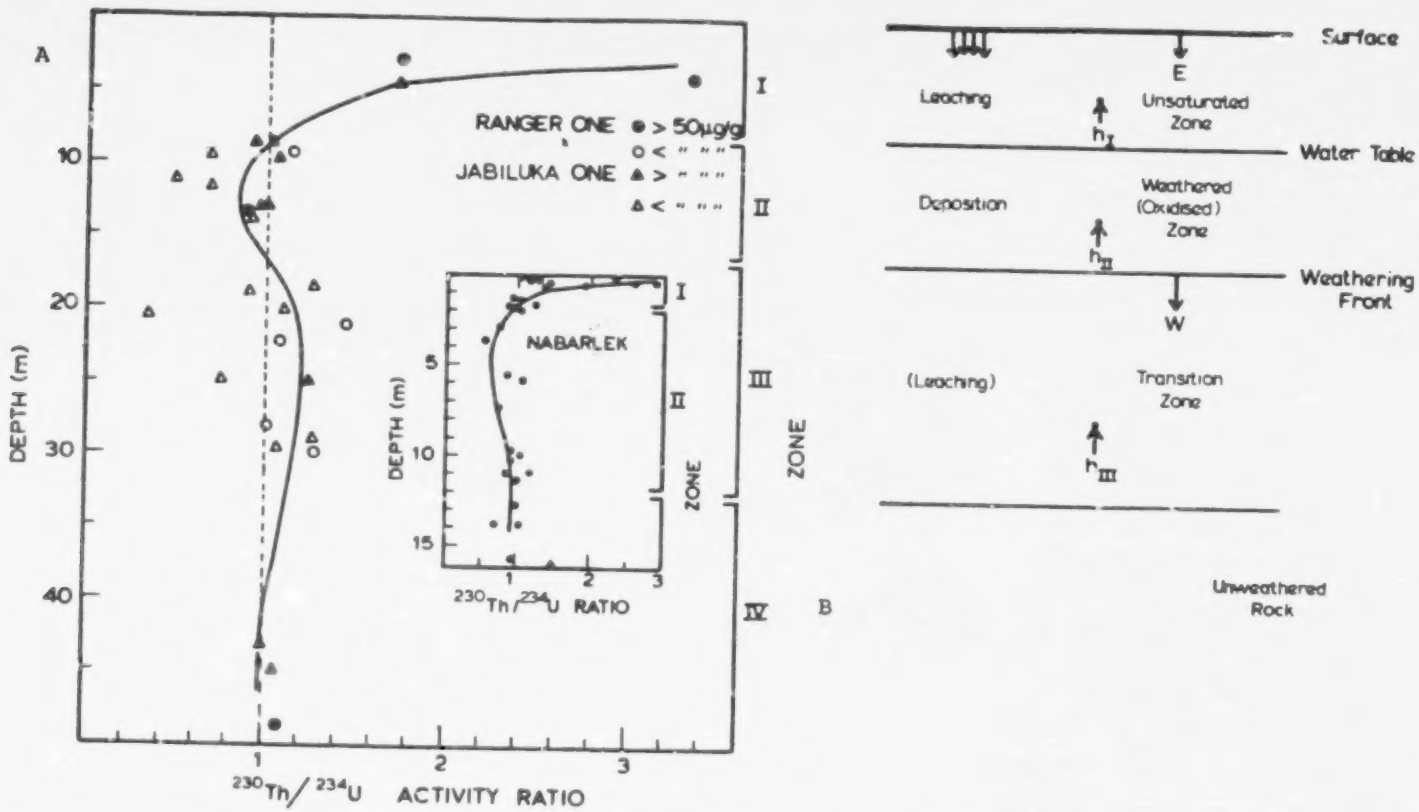

FIGURE 6 A. Composite illustration of the variation with depth of the $^{230}Th/^{234}U$ activity ratios from the Ranger One, Jabiluka One and Nabarlek (insert) ore bodies. A zonal classification based both on the activity ratio variation and systematic changes in the mineralogy (Table 1) is shown.

B. Schematic representation of the four-zone model. E and W are the rates of surface erosion and advance of the weathering front; h is the position of the sample above the zonal interface.

BEST COPY AVAILABLE

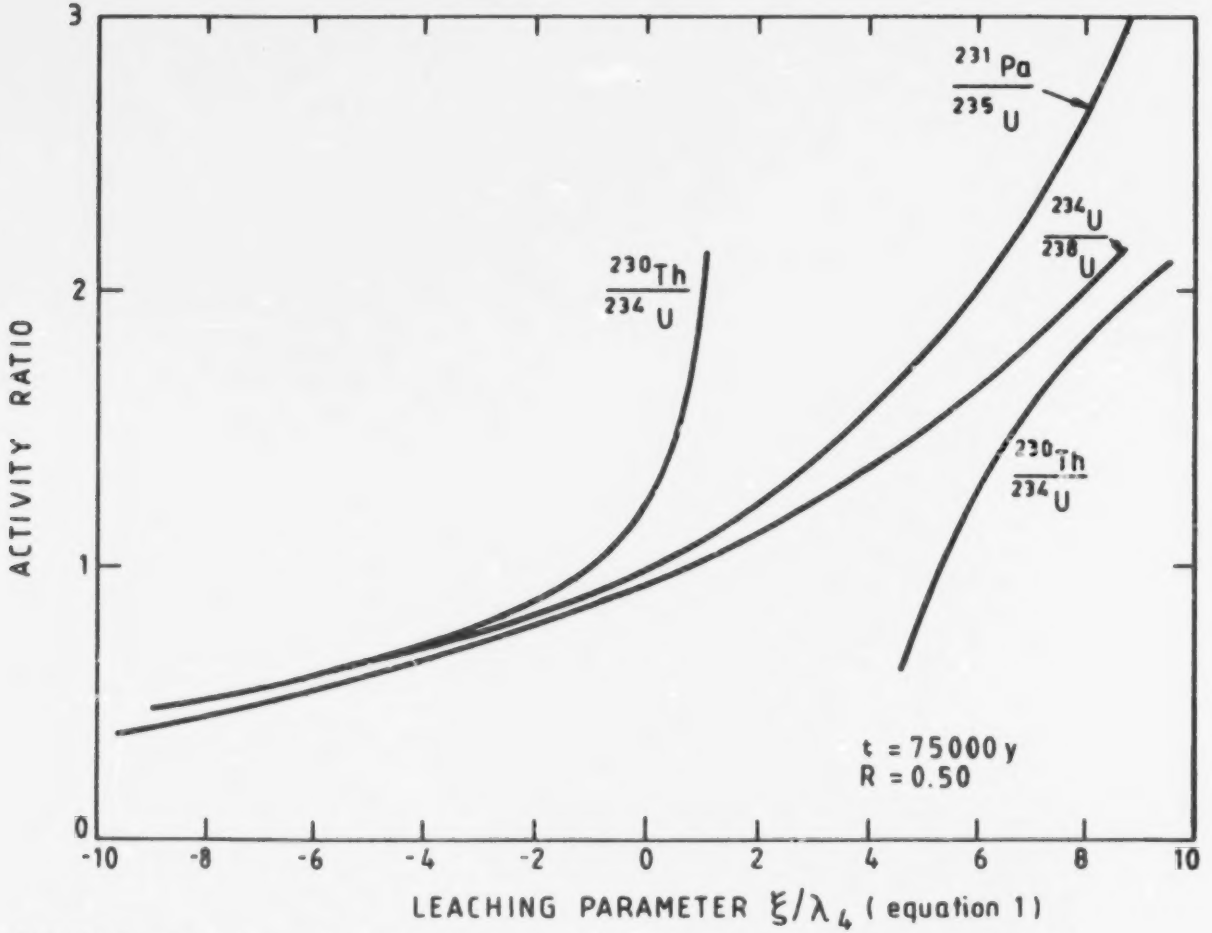

FIGURE 7 Variation of the isotope ratios with the erosion parameter ξ/λ_4 (Equation (3)). Positive values indicate leaching, negative values, deposition. In the calculation, a value of 0.5 is assumed for the $^{234}U/^{238}U$ ratios and 75 000 y for the time.

BEST COPY AVAILABLE

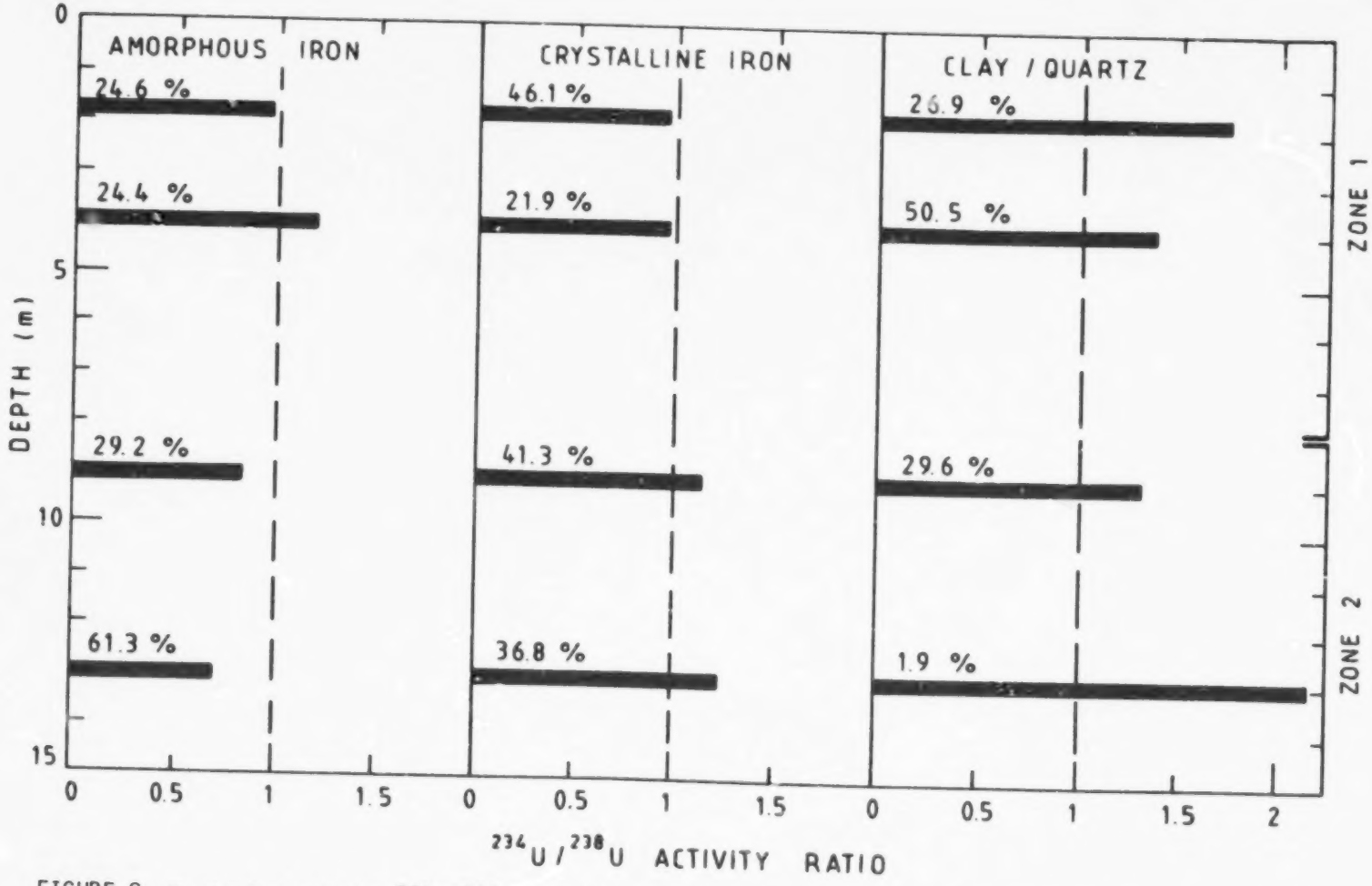

FIGURE 8 Variation of the $^{234}U/^{238}U$ ARs in selectively extracted phases from samples from the S1/146 core of the Ranger One ore body. (a) Amorphous iron, (b) crystlline iron, (c) clay and quartz phases.

BEST COPY AVAILABLE

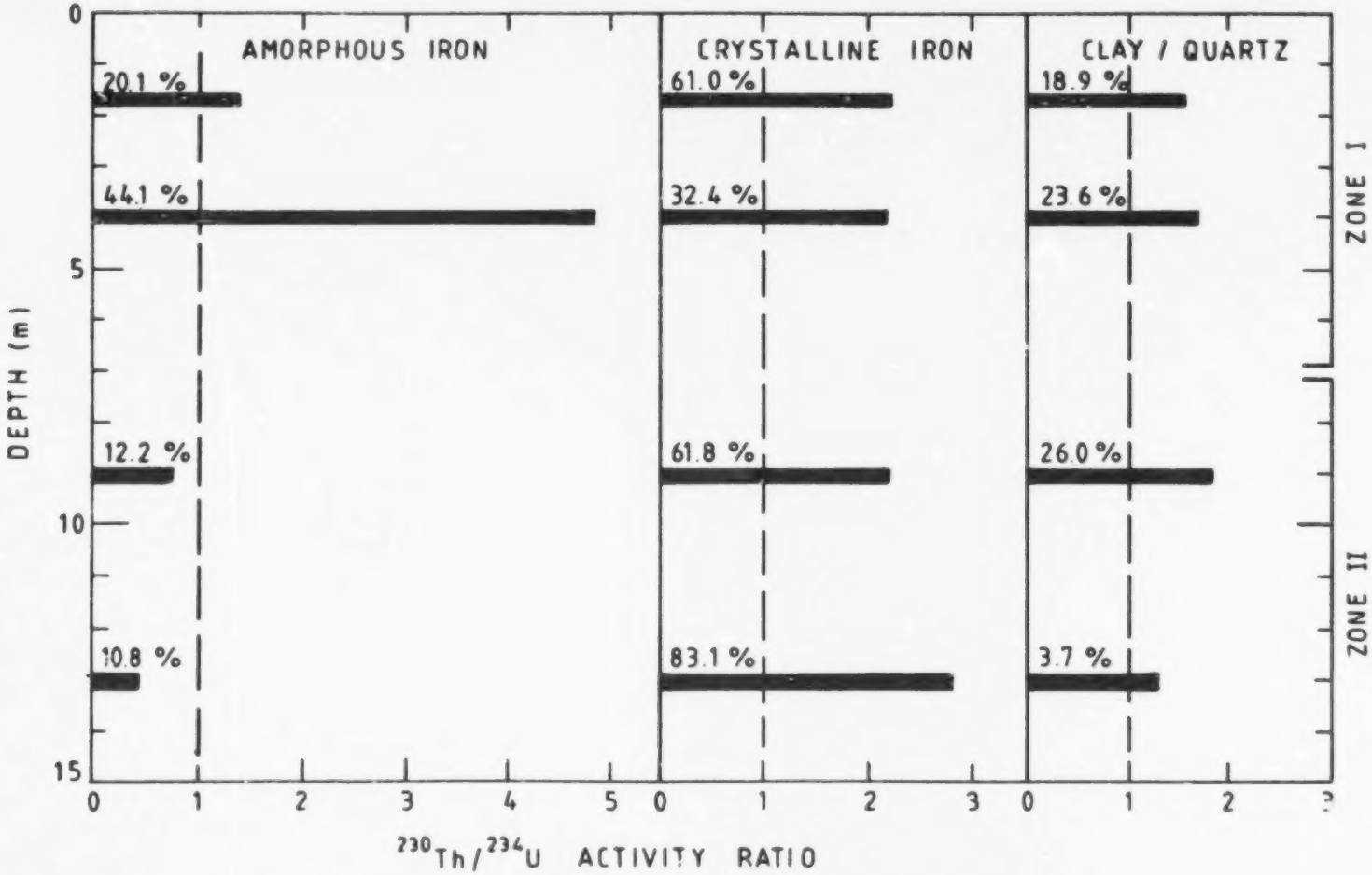

FIGURE 9 Variation of the $^{230}Th/^{234}U$ ARs in selectively extracted phases from samples from the S1/146 core of the Ranger One ore body. (a) Amorphous iron, (b) crystalline iron, (c) clay and quartz phases.

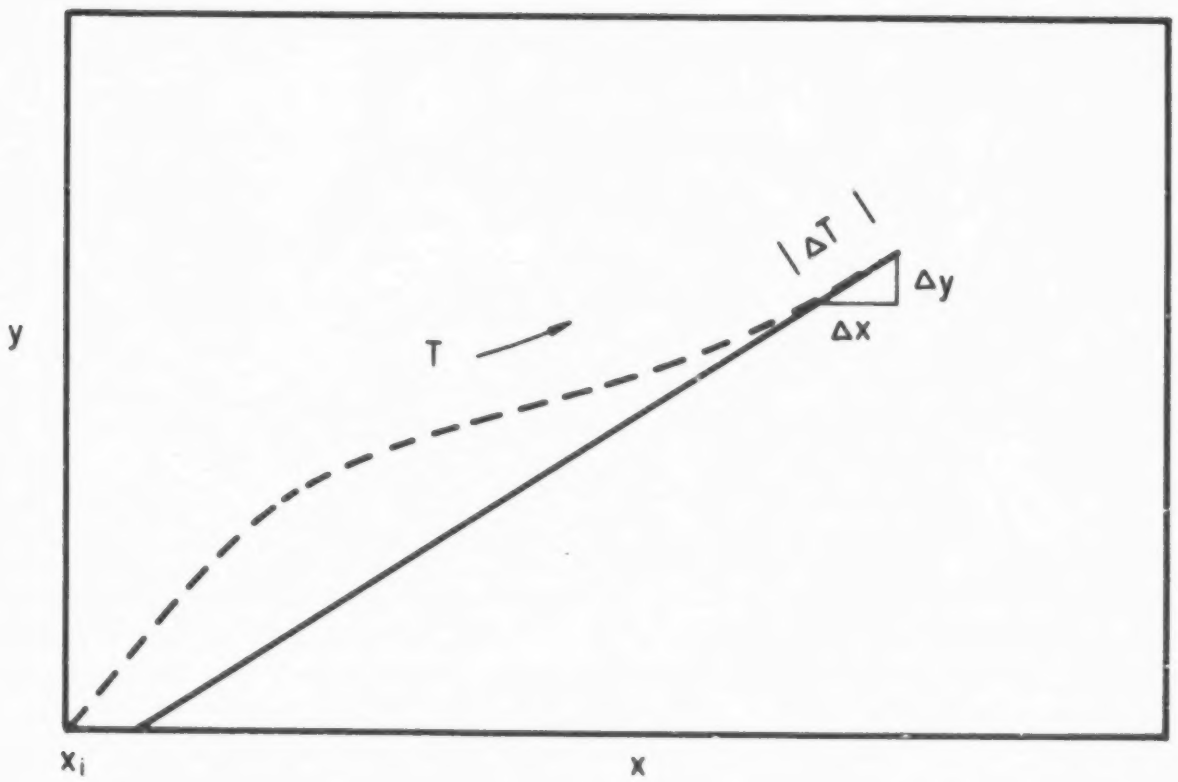

FIGURE 10 Schematic representation of the variation of X ($=(^{238}U-^{230}Th)/^{238}U$) and Y ($=(^{238}U-^{234}U)/^{234}U$) since the development of the soil horizon. ΔT was the period taken to form the horizon which occurred at time T before present.

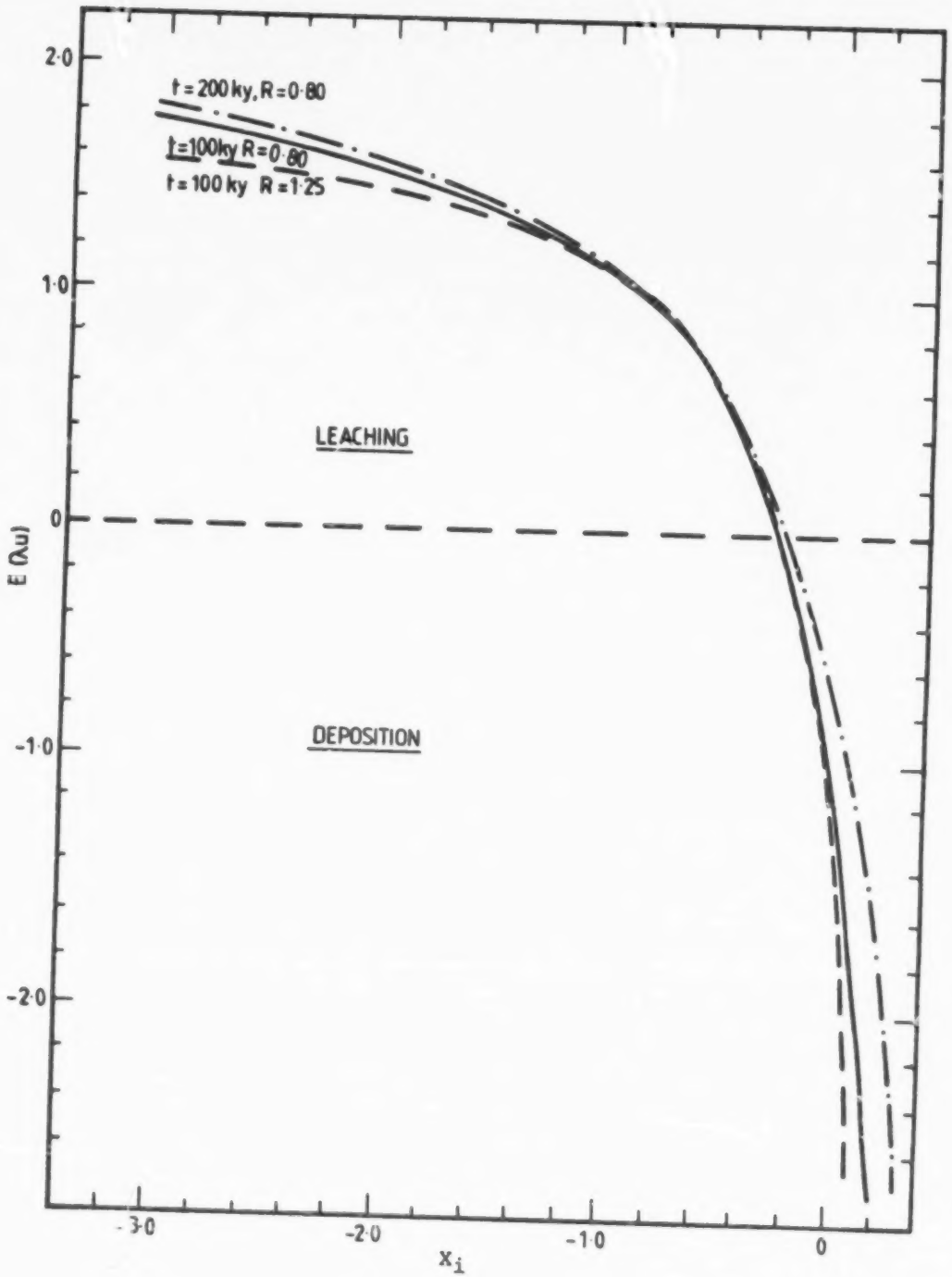

FIGURE 11 Variation of the leaching parameter ξ with the intercept X_i for conditions of leaching and deposition.

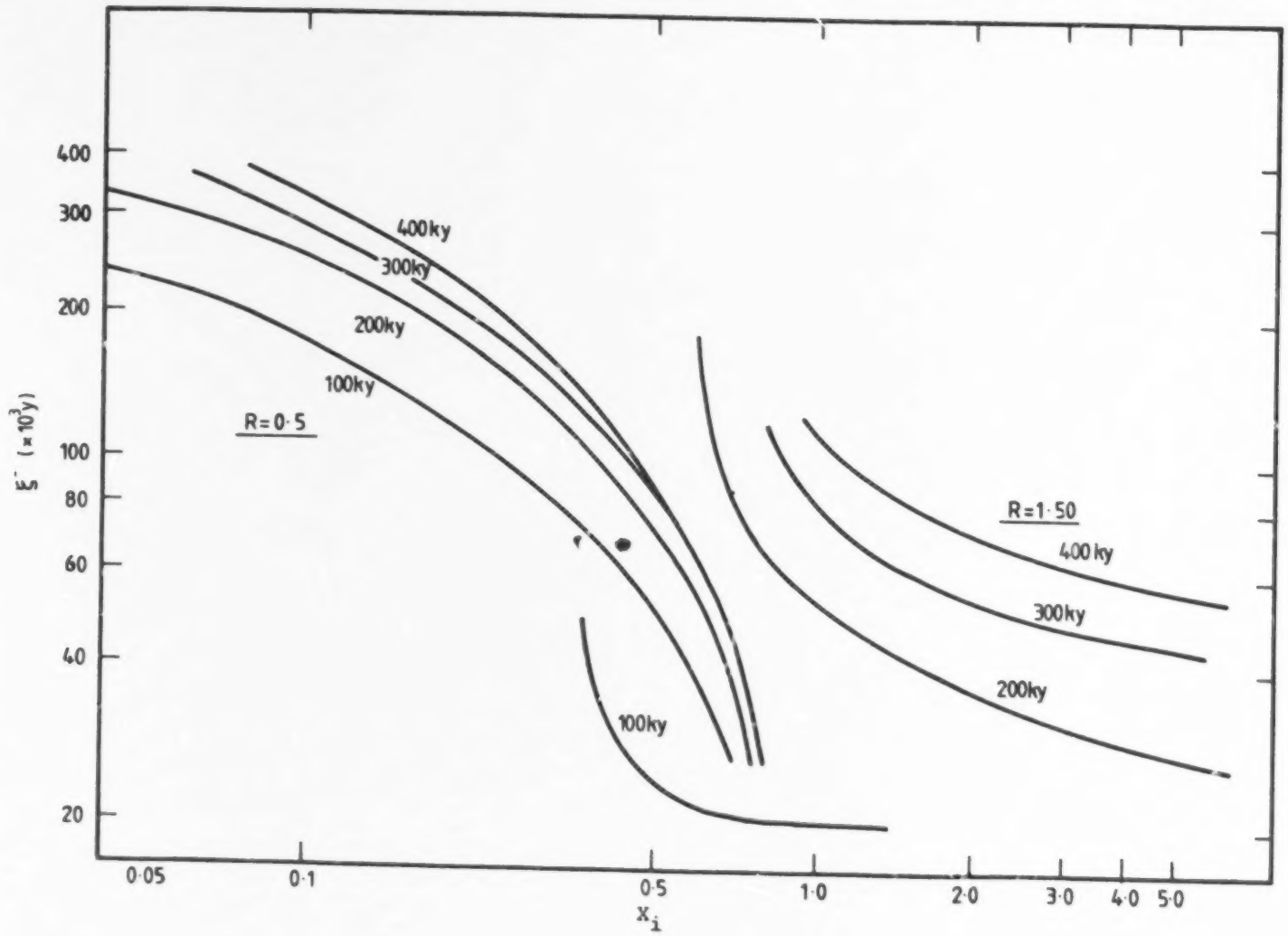

FIGURE 12 Variation of the reciprocal of the leaching parameter ξ^{-1} with the intercept X_i for different ages and selected values of the parameter R (equation (3)).

BEST COPY AVAILABLE

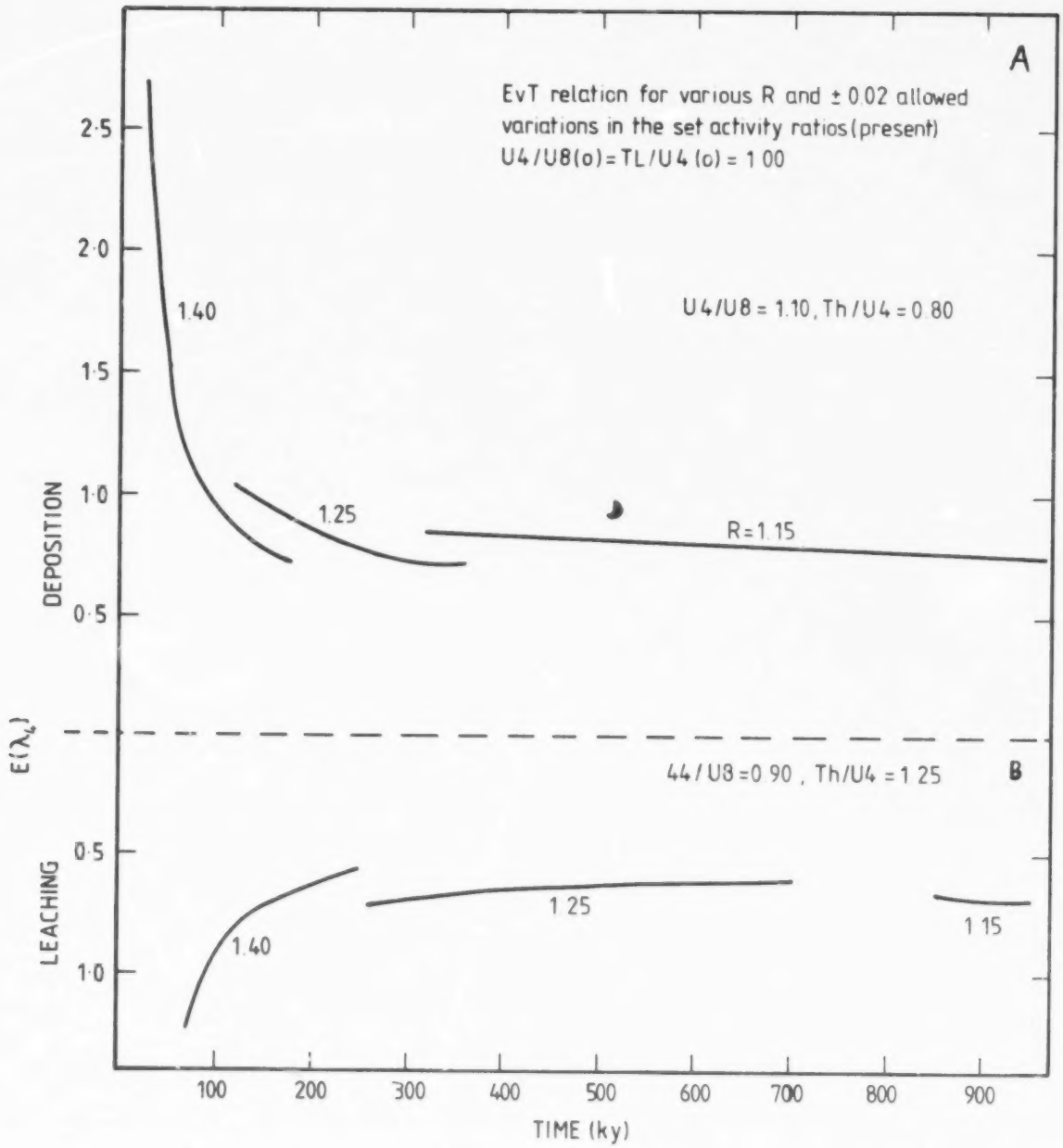

FIGURE 13 The range of validity of the leaching (or deposition) parameter ξ/time variation for $^{234}U/^{238}U$ and $^{230}Th/^{234}U$ ratios shown in the key. Measurement accuracies of ±0.02 are assumed. Three values of the parameter R (equation (3)) have been used. Figure 13A applies to leaching, and 13B to deposition. The normalized leaching parameter is used. One normalized unit is equivalent to 2.8×10^{-6} y^{-1} or 0.28% per 1000 y.

BEST COPY AVAILABLE

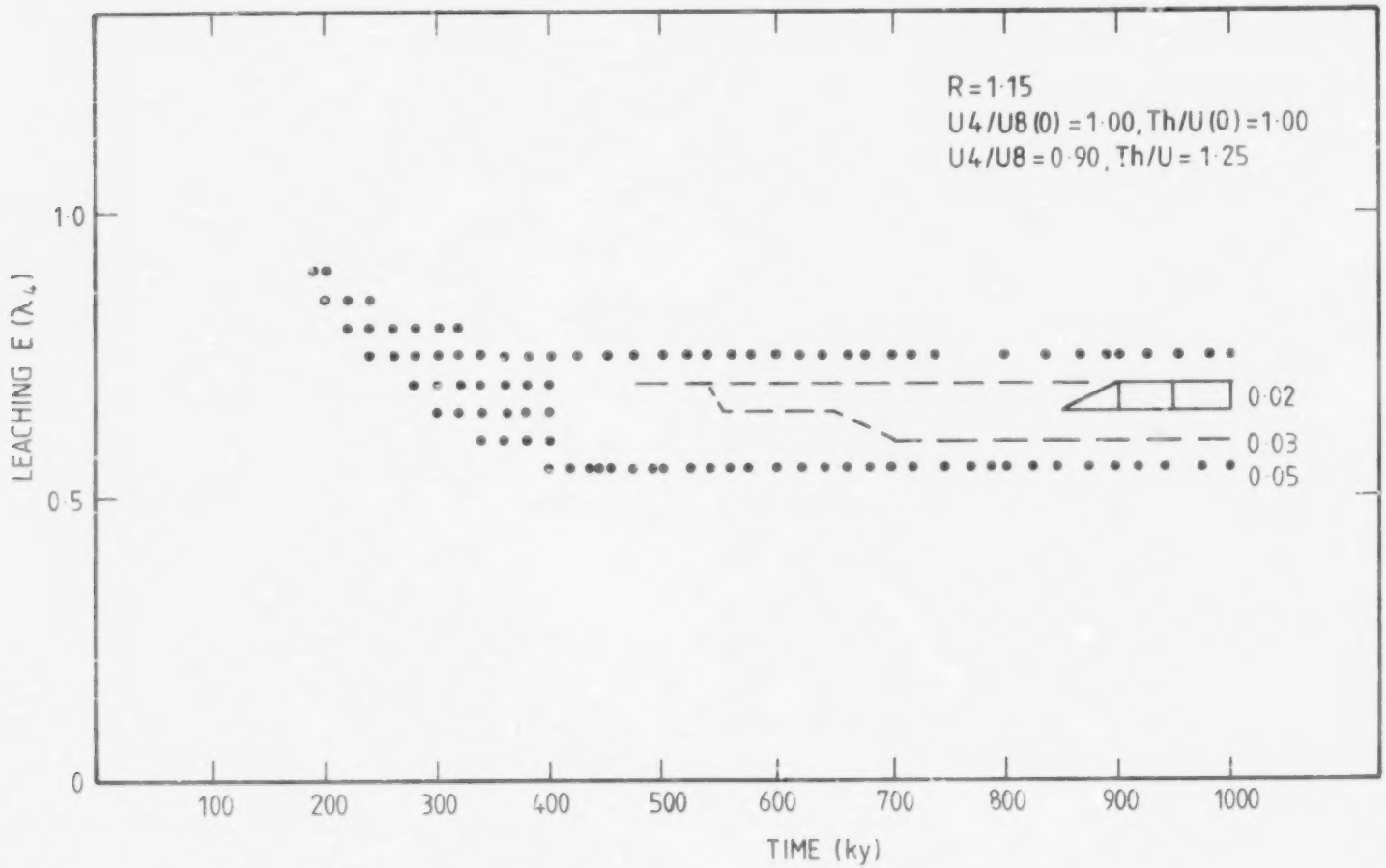

FIGURE 14 The domain of validity of the leaching parameter ξ/time relationship for $^{234}U/^{238}U$ = 0.90 and $^{230}Th/^{234}U$ = 1.25 assuming isotopic equilibrium at zero time. A value of R (equation (3)) of 1.15 has been chosen. The effect of measurement uncertainties of 0.02, 0.03 and 0.05 on the range of parameter values is shown. The normalized leaching parameter is used. One normalized unit is equivalent to 2.8×10^{-6} y^{-1} or 0.28% per 1000 y.

BEST COPY AVAILABLE

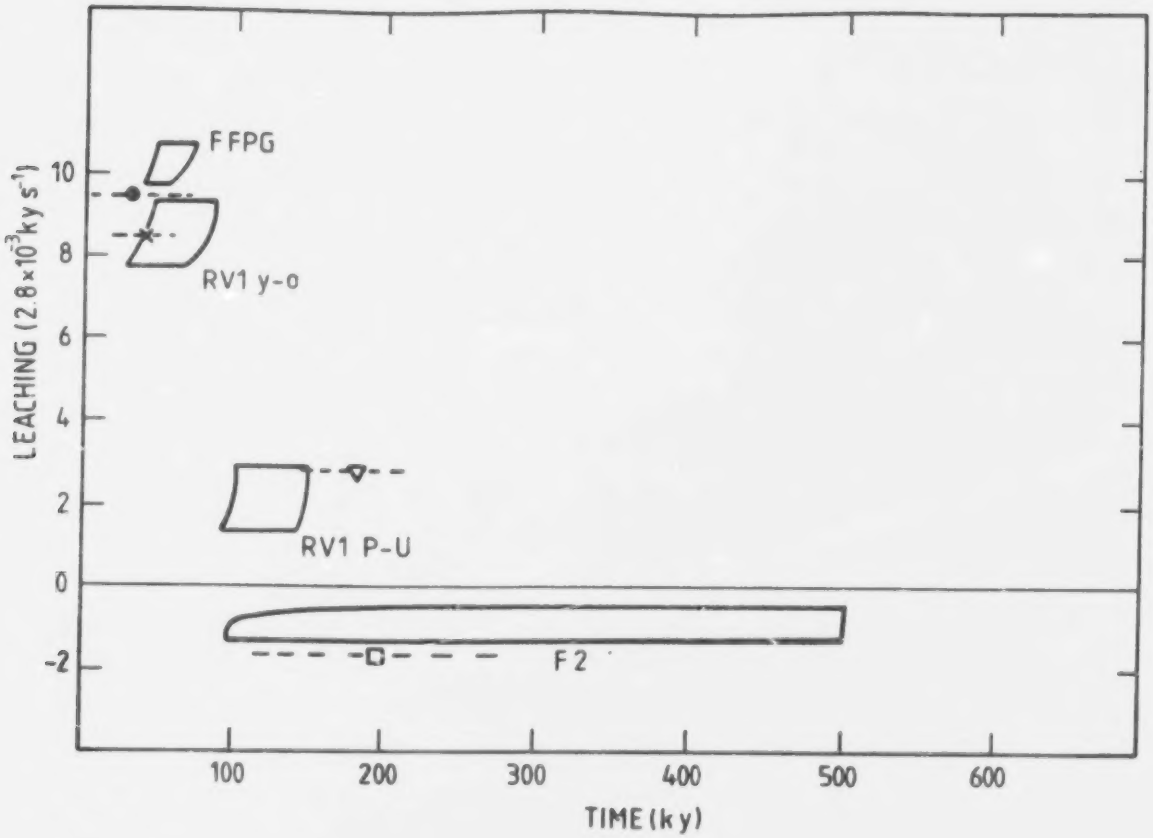

FIGURE 15 Comparison of interpretation of data for Quaternary deposits in Nevada [27].

Time - leaching domains - current model.
Time ranges and parameter t_o (assuming its equation to leaching parameter) - Rosholt's results.

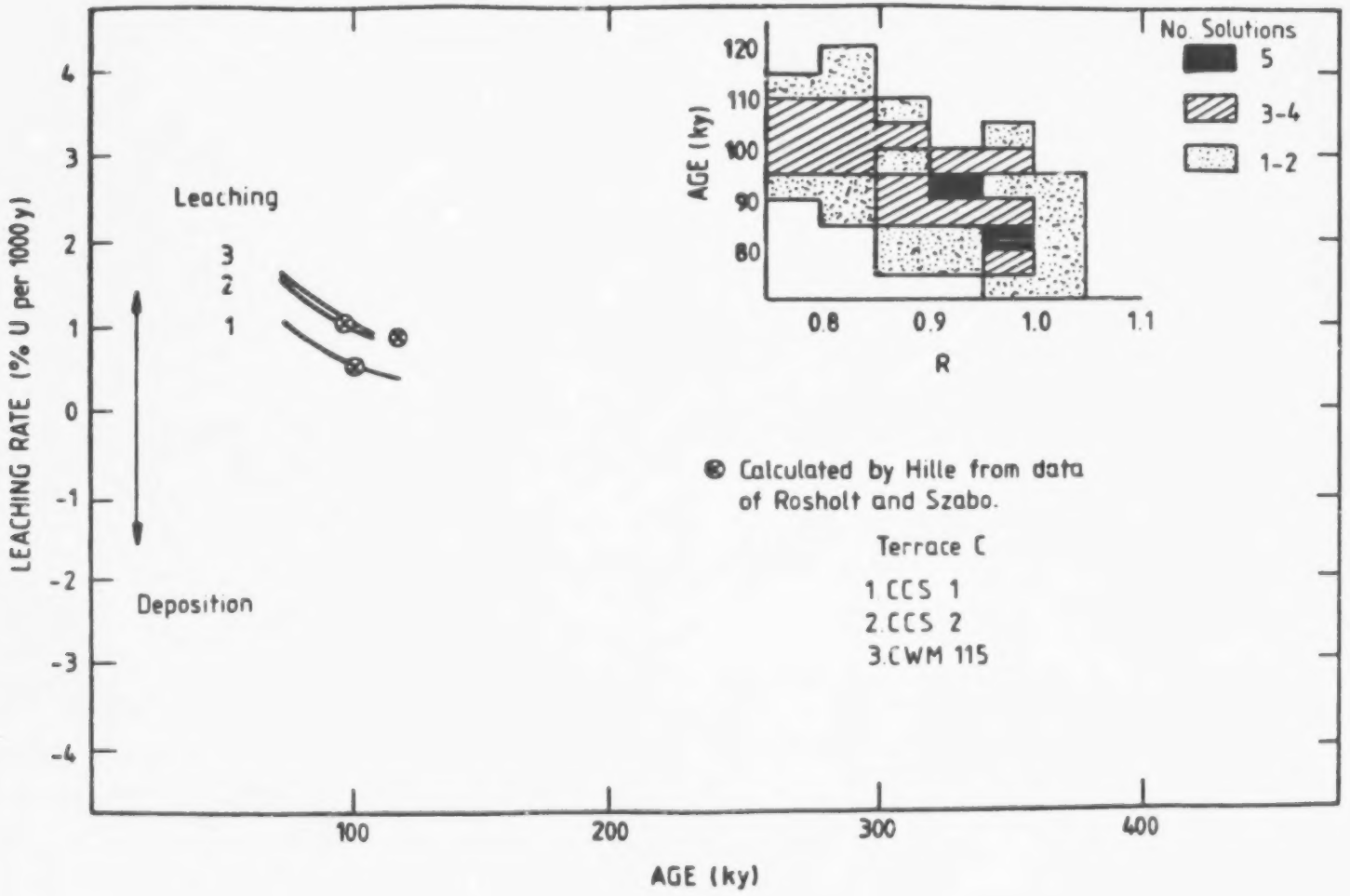

FIGURE 16 Dating of shells (data of Rosholt and Szabo[17]). Comparison of Hille's[15] model results and time-leaching domains obtained using the current model. Insert: Number of solution of transport equations obtained by varying parameter R.

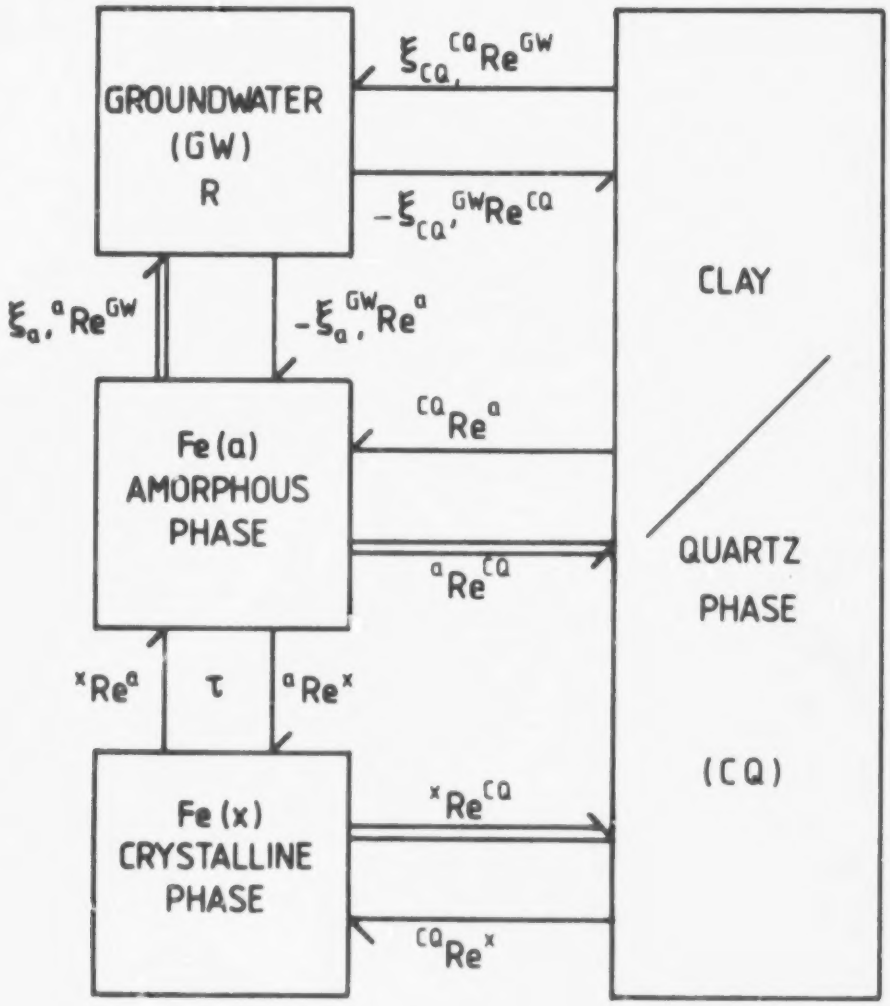

FIGURE 17 Schematic diagram of the microscopic four-phase model of uranium series nuclide geochemistry on the weathered surfaces of crystalline rocks. Leaching/adsorption coefficient is denoted by ξ, where the subscript denotes the two phases, Fe amorphous or clay/quartz, interacting with groundwater; Re denotes recoil loss of daughter nuclides from one phase to another where the left hand superscript represents the source phase and right hand superscript the sink phase; R is the $^{234}U/^{238}U$ activity ratio in groundwater; and τ is the phase change rate constant between the two Fe phases.

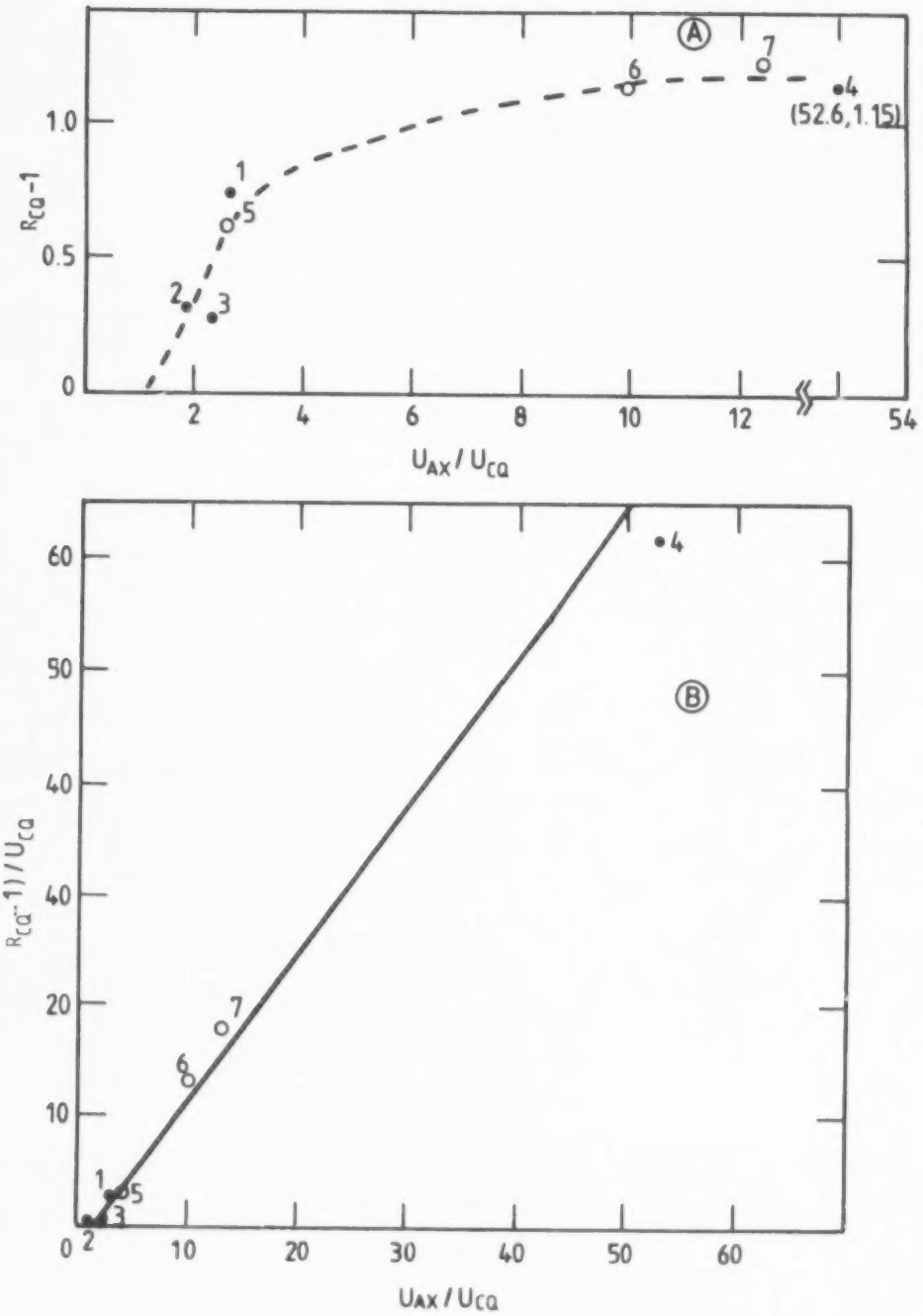

FIGURE 18A Variation of the $^{234}U/^{238}U$ excess in clay/quartz (R_{tCQ} - 1) (Equation (56), with the ratio of uranium on the iron phases to that on clay/quartz (U_{AX}/U_{CQ}).

18B Variation of the parameter R_{tCQ} - 1)/U_{CQ} with the uranium ratio U_{AX}/U_{CQ}.

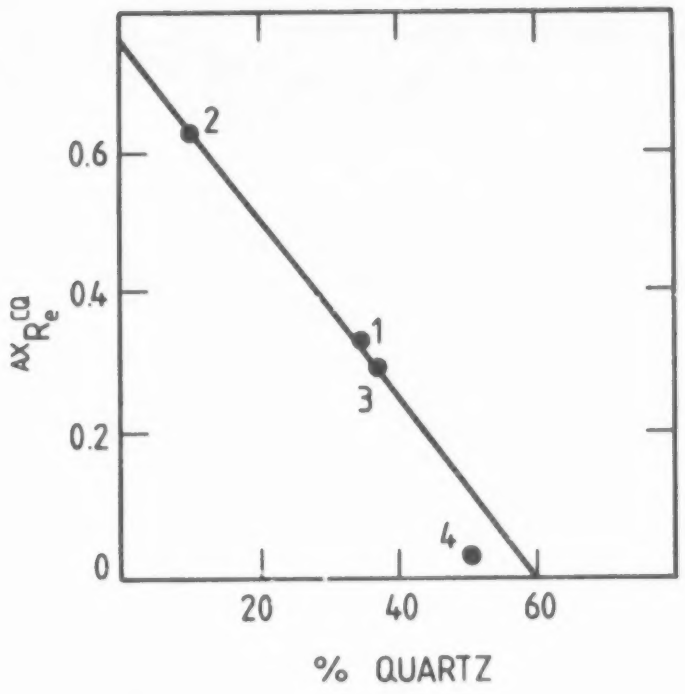

FIGURE 19 Variation of $^{AX}Re^{CQ}$ (Equation (55)), the probability that the product of α-recoil from a parent originating in the iron phases AX will be found in the clay/quartz phases CQ.

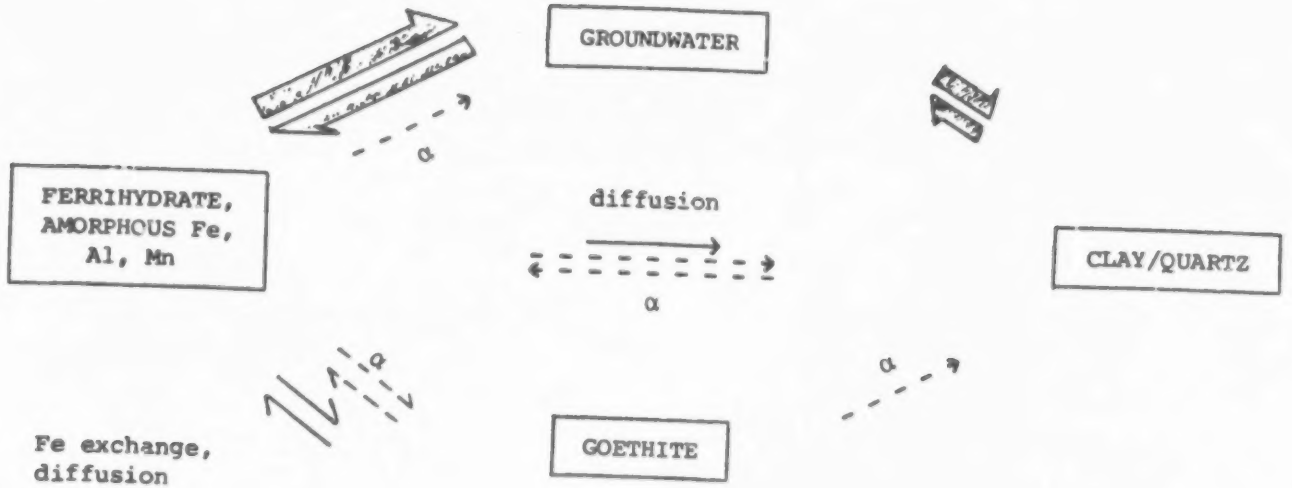

FIGURE 20 The flux of uranium between specified separable phases within the weathered ore.

BEST COPY AVAILABLE

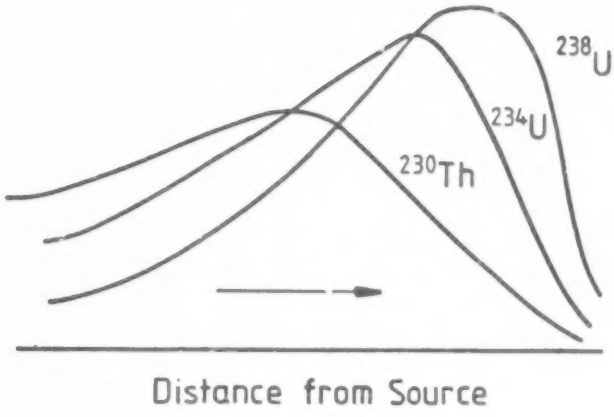

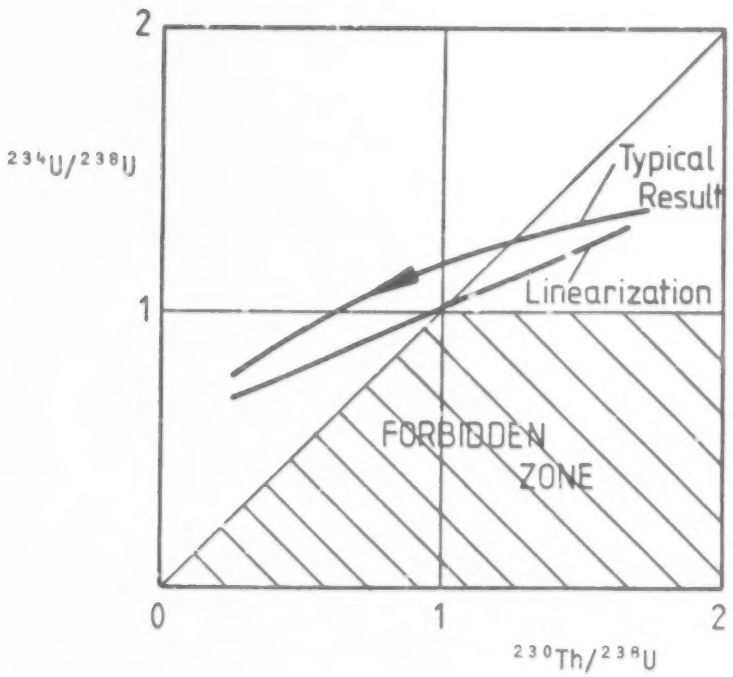

FIGURE 21 Schematic plot of the distribution of activity of ^{238}U, ^{234}U and ^{230}Th in the region of secondary mineralization and corresponding plot of the $^{234}U/^{238}U$ against $^{230}Th/^{238}U$ activity ratios for the case $R_{238} < R_{234}$ and $R_{238} < R_{230}$.

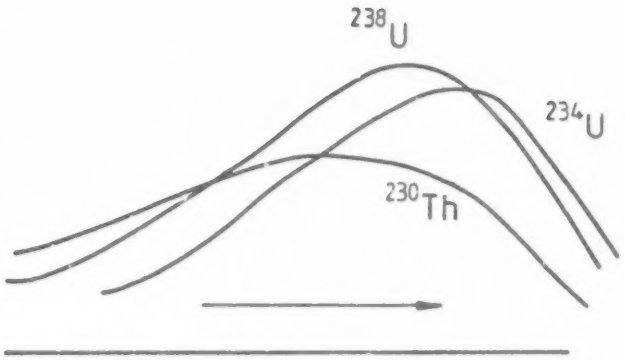

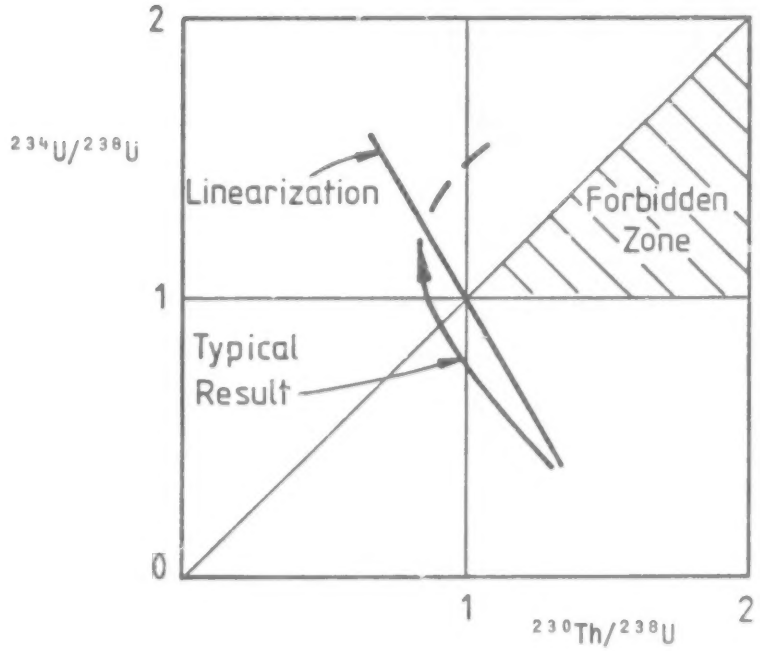

FIGURE 22 Schematic plot of the distribution of activity of ^{238}U, ^{234}U and ^{230}Th in the region of secondary mineralization and corresponding plot of the $^{234}U/^{238}U$ against $^{230}Th/^{238}U$ activity ratios for the case $R_{234} < R^{\infty}_{234}$ and $R_{238} < R_{238}$ ("fast" system).

BEST COPY AVAILABLE

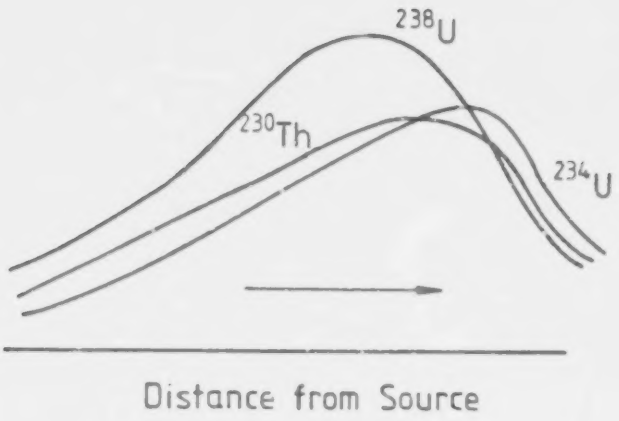

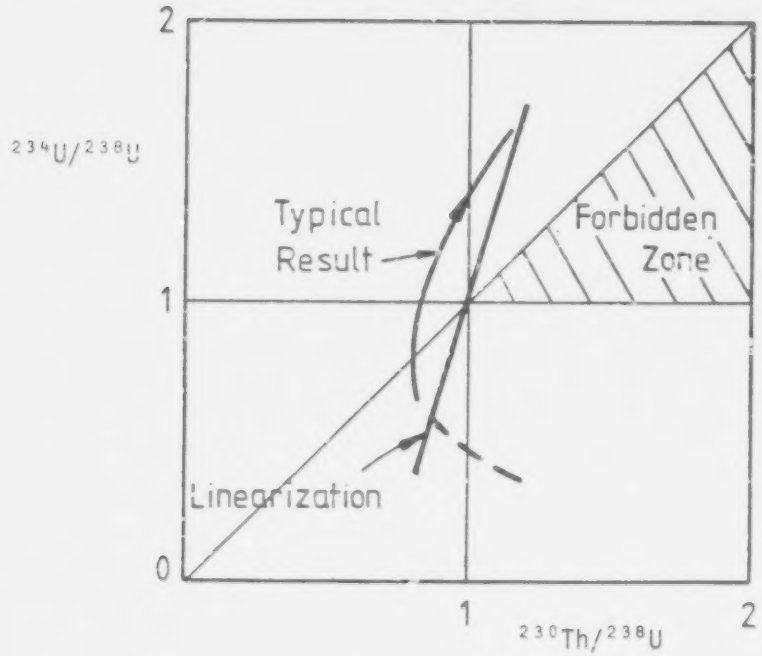

FIGURE 23 Schematic plot of the distribution of activity of ^{238}U, ^{234}U and ^{230}Th in the region of secondary mineralization and corresponding plot of the $^{234}U/^{238}U$ against $^{230}Th/^{238}U$ activity ratios for the case $R_{234} < R_{234} < R_{238} < R_{230}$ ("slow" system).

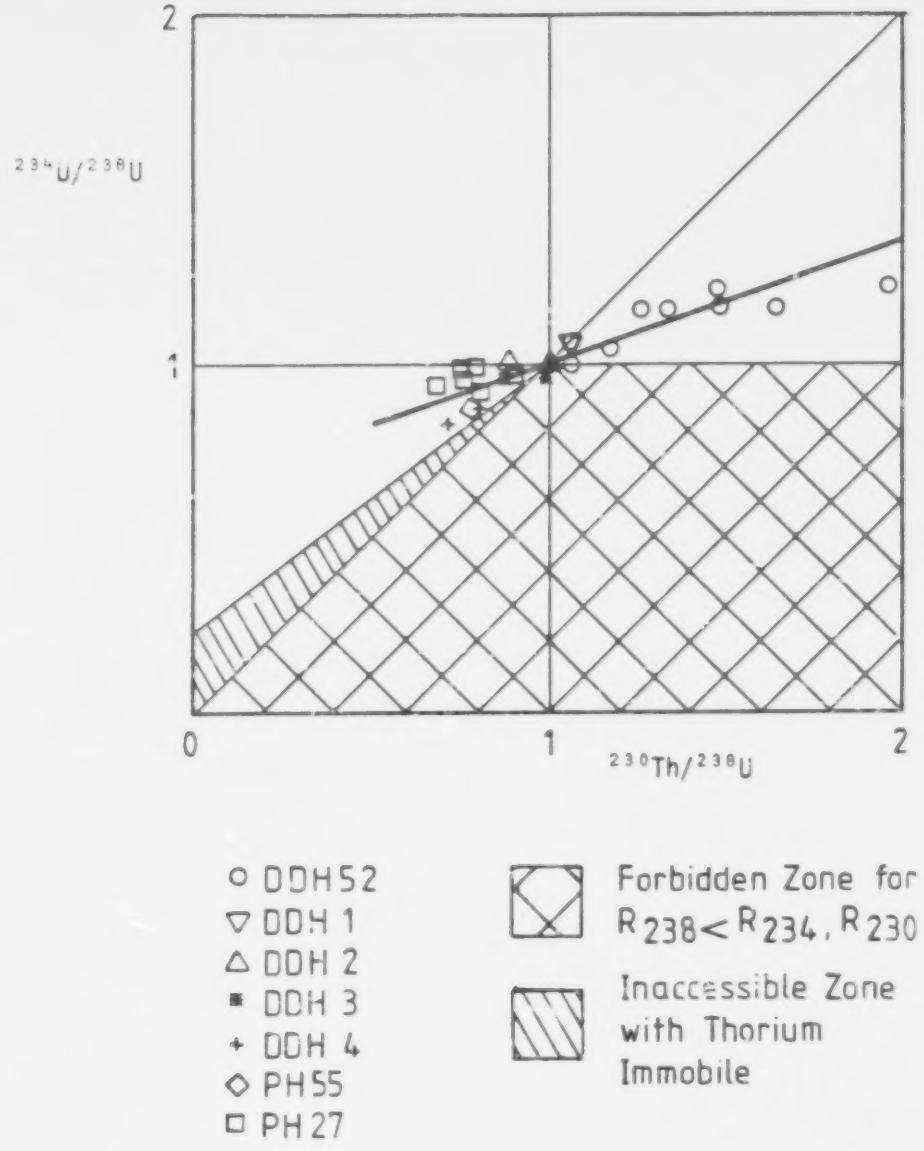

FIGURE 24 Plot of $^{234}U/^{238}U$ and $^{230}Th/^{238}U$ activity ratios found at Koongarra showing best linear fit ($R_{234} = 1.2\ R_{238}$, $R_{230} = \infty$).

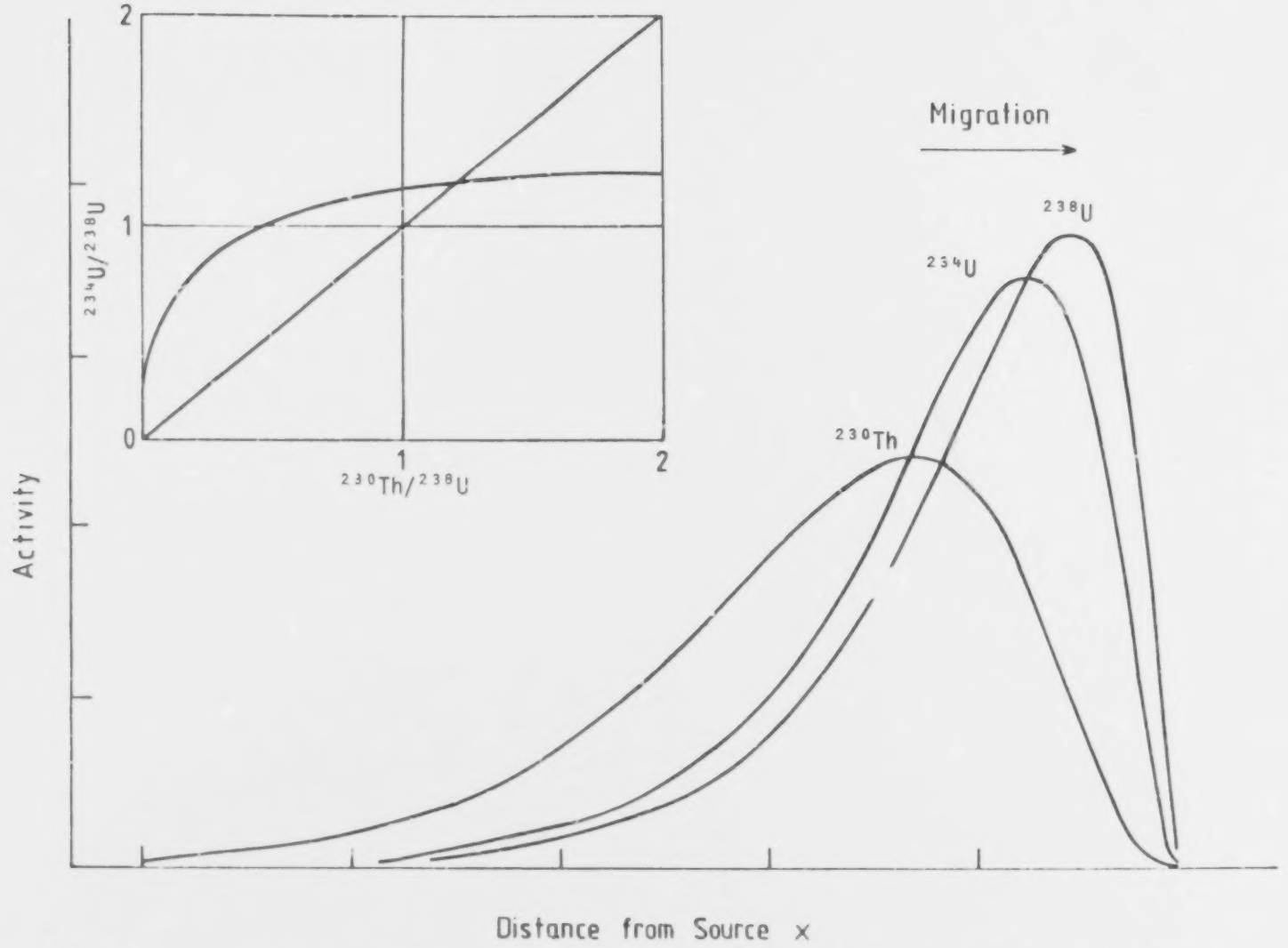

FIGURE 25 Example of numerical application of Laplace transform technique to the case of a pulse input ${}_{o}C_{238}(t) = t\, e^{-\zeta t}$, showing the corresponding activity ratio plot.

BEST COPY AVAILABLE

TABLE 1

FOUR-ZONE MODEL OF THE UPPER SEQUENCES OF THE ORE BODIES

Zone	Hydrology	Mineralogy	Comments
I	Unsaturated in the dry season; oscillating table	Oxidized ferricrete or ferruginous zone grading into a mottled zone	Uranium leaching
II	Permanently saturated	Generally corresponds to the pallid zone	Some U deposition
III	Saturated	Transition zone between weathered and unweathered rock; oxidized material; evidence of layering inherited from Cahill formation; in lower region weathering away from pre-existing cracks and fissures observed	Region of some U leaching
IV	Saturated	Unweathered rock from Cahill formation	

BEST COPY AVAILABLE

TABLE 2

RANGER: COMPARISON OF PREDICTED URANIUM GEOCHEMISTRY

FROM MINERALOGICAL AND ISOTOPE DATA

Mineralogical Data			Isotope Data	
Depth (m)	Horizon(s)	Predicted Uranium Geochemistry	Depth (m)	Predicted Uranium Geochemistry
0 - 5	A, B_1	leaching	0 - 8	leaching
5 - 13	B_2	may be deposition	8 - 15	deposition
13 - 25	C	leaching	15 - 30	leaching
25 -	D	?	30 --	variable

BEST COPY AVAILABLE

TABLE 3

DRILL CORE SAMPLES - MODEL PARAMETERS

Ore Body	Zone	Depth Range (m)	Uranium Leaching (L) or Deposition (D) Rate (% per 1000 y)[1]		Radium Leaching (L) or Deposition (D) Rate (% per 1000 y)[1][2]		Erosion Rate (E), Advance Weathering Front (W) (m per 1000 y)	
			Mean	Range	Mean	Range	Mean	Range
Ranger One	I	0- 8±1	0.7 (L)	0.03 (D)-1.5 (L)	18 (D)	67 (D)- 19 (L)		
	II	8-17±1	0.3 (D)[3]		1[3]		0.06	0.02-0.18[4]
	III	17-30±5	0.2 (D)	0.3 (D)-0.6 (L)	0.16 (D)	5 (D)- 30 (L)		
Jabiluka One	I	0- 8±1	0.3 (L)	0.3 (D)-1.5 (L)	3 (L)	3 (D)- 8 (L)		
	II	8-17±1	0.4 (D)	0.3 (D)-2.0 (L)	384 (D)	2546 (D)- 6 (L)	0.1	0.03-0.25
	III	17-30±5	0	0.3 (D)-0.3 (L)	308 (D)	12 (D)-1061 (D)		
Nabarlek	I	0-1.7	1.8 (L)	1.2 (L)-2.5 (L)			0.05	0.01-0.08
	II	1.7-10	0.2 (D)	0 -0.3 (D)				

NOTES:

(1) These values do not represent the net loss (or gain) of uranium or radium to the deposit; rather they show the rate of localized redistribution through the vertical profile.

(2) The calculated value is an instantaneous rate averaged over 1000 y to allow comparison with geochemical timescales. Large values reflect localized effects and are clearly artefacts of the calculation procedure.

(3) One estimate only available.

(4) One value (0.96 m per 1000 y) from eight omitted.

BEST COPY AVAILABLE

TABLE 4

URANIUM SERIES FRACTIONATION IN SEPARABLE PHASES FROM DRILL CORE S1/146, RANGER ONE

Depth (m) (1)	Phase	$^{234}U/^{238}U$		$^{230}Th/^{234}U$		Time x 10^3 y	Leaching (L) Deposition (D) % U per 1000 y	R	τ (2) (Half-life x 10^3 y)
		Obs.	Calc.	Obs.	Calc.				
2.7	A	0.98	0.97	1.31	1.32		0.8-1.5		
	C	0.99	0.99	2.15	1.99	20		0.9	50
	Cl/Q	1.78	1.71	1.56	1.55		0.2		
4.0	A	1.14	1.12	4.74	4.52		0.8-1.5		
	C	0.96	0.93	1.92	2.01	60		0.8	35
	Cl/Q	1.32	1.40	1.73	1.64		0.2		
9.1	A	0.80	0.89	0.75	0.83		0.5-1.5		
	C	1.08	0.88	2.17	2.14	80		0.3	500
	Cl/Q	1.27	1.33	1.85	1.72		0.2		
13.1	A	0.67	0.58	0.37	0.34				
	C	1.21	0.93	2.85	2.29	80		0.8	500
	Cl/Q	2.15	2.05	1.26	1.18		0.1		

(1) A = amorphous iron, C = crystalline iron, Cl = clay, Q = quartz.
(2) Rate of first order A $\rightleftharpoons$ C exchange expressed as a half-life.

TABLE 5

COMPARISON OF URANIUM SERIES FRACTIONATION ON KOONGARRA AND RANGER ONE (S1/146) DRILL CORE

Phase		U (%)		$^{234}U/^{238}U$		$^{230}Th/^{234}U$	
Reagent (1)	Mineralogy (Major)	Koongarra	S1/146 Ranger One	Koongarra	S1/146 Ranger One	Koongarra	S1/146 Ranger One
TAO	ferrihydrate amorphous Fe, Al, Mn	31±10	35±15	0.75±0.1 (1)	0.90±0.2 (1)	0.61±0.5 (1)	0.81±0.4 (2) (1)
DCB	goethite	54±7	36±9	1.09±0.12 (1.45)	1.06±0.1 (1.17)	1.23±0.13 (2.01)	2.27±0.4 (2.8)
Dissolution	clay/quartz	15±9	27±17	1.7±0.5 (2.26)	1.63±0.4 (1.81)	1.4±0.2 (2.30)	1.6±0.2 (2.0)

(1) TAO: Tamms acid oxalate reagent; DCB: dithionate/citrate/bicarbonate reagent; Dissolution: $HNO_3/HF/HClO_4$ digestion + Na_2O_2 fussion (ref [4], chapter 6).

(2) One sample excluded (activity ratio 4.74); if included an average value of 1.7±1.7 would be obtained.

TABLE 6

EXPERIMENTAL VERIFICATION OF THE MULTIPHASE MODEL

No.	Sample	^{238}U ($\mu g\ g^{-1}$)	$^{238}U_{(CQ)}$ %	R_{CQ} (1)	$R_{CQ}-1$	$\frac{R_{CQ}-1}{U_{CQ}}$ (2)	$\frac{U_{AX}}{U_{CQ}}$ (3)	% Quartz	$AX_{Re}CQ$
1	S1/146 (2.7 m)	47.2	26.9	1.78	0.78	2.89	2.70	35	0.36
2	S1/146 (4.0 m)	84.3	50.5	1.32	0.32	0.63	0.98	10	0.68
3	S1/146 (9.1 m)	35.6	29.6	1.27	0.27	0.91	2.38	30	0.41
4	S1/146 (13.1 m)	352.0	1.9	2.15	1.15	60.5	52.6	50	0.03
5	DDH 52 (1.7 m)	385.0	23.3	1.62	0.62	2.66	3.33		0.32
6	DDH 52 (15 m)	390.0	9.1	2.17	1.17	12.8	10.0		0.12
7	DDH 52 (35 m)	228.0	7.45	2.22	1.22	16.3	12.5		0.10

NOTES

(1) R_{CQ} is the $^{234}U/^{238}U$ activity ratio in the clay/quartz phase.

(2) U_{CQ} is the level of ^{238}U in the clay/quartz phase.

(3) U_{AX} is the level of ^{238}U in the amorphous (+ ferrihydrate) iron phase A and the goethite phase X.

TABLE 7

KOONGARRA GROUNDWATER - ISOTOPIC DATA

Well No.	[U] ($\mu g\ L^{-1}$)	$^{234}U/^{238}U$	$^{230}Th/^{234}U$
PH 78	0.41±0.02	0.76±0.07	<0.06
PH 27	1.30±0.03	1.02±0.03	0.05±0.01
PH 73	4.34±0.14	0.78±0.03	
PH 49	55.8±1.7	0.99±0.09	
PH 14	29.1±1.4	0.74±0.04	0.55±0.10
PH 7	62.3±1.1	0.65±0.02	<0.0025
PH 55	14.9±0.04	0.74±0.04	0.05±0.01
PH 94	1.66±0.07	0.82±0.06	
KTD 1	0.9±0.5	> 1	0.7±0.07
KD 1	0.085±0.006	1.42±0.20	

* Samples broken in transit.

TABLE 8

ESTIMATES OF MIGRATION TIME FROM ANALYSIS OF LEAD DATA

Sample	$(\frac{C_{206}}{C_{204}})_{obs}$	$(\frac{C_{207}}{C_{204}})_{obs}$	$(\frac{C_{206}+C_{207}+C_{208}}{C_{204}})_{obs}$	C_{Pb} (ppm)	C_U (ppm)	$(\frac{C_{238}}{C_{204}})_{obs}$ (1)	t_{235} (2) (yrs)	t_{238} (2) (yrs)
DDH52/22	2438	183	2678	80	1970	6.55×10^4	3.1×10^8	2.4×10^8
DDH52/54	6846	474	7395	112	213	1.40×10^4	1.8×10^9	2.6×10^9
DDH1/41	5720	371	6290	19	17	5.59×10^3	2.3×10^9	4.6×10^9
DDH2/22	388	46	503	5	864	8.65×10^4	4.9×10^7	2.8×10^7
DDH3/21	125	25	198	5	1060	4.19×10^4	3.3×10^7	1.7×10^7

(1) This is estimated from preceding quantities.

(2) The values used to calculate these are

$$\lambda_{235} = 1.54 \times 10^{-10} \text{ yr}^{-1}$$

$$\lambda_{238} = 9.71 \times 10^{-10} \text{ yr}^{-1}$$

$$(C_{238}/C_{235})_{obs} = 137.8$$

$$(C_{206}/C_{204})_{init} = 14$$

$$(C_{207}/C_{204})_{init} = 15$$

BEST COPY AVAILABLE

83

APPENDIX A

SOLUTION OF THE URANIUM TRANSPORT EQUATIONS

In Section 2.2, it was shown that, assuming leaching (or deposition) is a first order process, the uranium transport equations are

Uranium-238:

$$U_8 = U_8(t_o) \exp[-(\lambda_8 + \xi)]t \ , \tag{A1}$$

Uranium-235:

$$U_5 = U_5(t_o) \exp[-(\lambda_5 + \xi)]t \ , \tag{A2}$$

Uranium-234:

$$-dU_4/dt = (\lambda_4 + R\xi)U_4 - \lambda_8 U_8 \ , \tag{A3}$$

Thorium-230:

$$-dI/dt = \lambda_i I - \lambda_4 U_4 \ , \text{ and} \tag{A4}$$

Protactinium-231:

$$-dPa/dt = \lambda_p Pa - \lambda_5 U_5 \ , \tag{A5}$$

where $\lambda_8 U_8$, $\lambda_5 U_5$, $\lambda_4 U_4$, $\lambda_i I$ and $\lambda_\rho Pa$ are activities of ^{238}U, ^{235}U, ^{234}U ^{230}Th and ^{231}Pa respectively; ξ is the rate of leaching (+ve) or deposition (-ve); R is the $^{234}U/^{238}U$ ratio of the leachate (or of the depositing material); t is the elapsed time; and $U_8(t_o)$, $U_5(t_o)$ are the levels of ^{238}U, ^{235}U at the initial time t_o.

A1. URANIUM-234

Substituting equation (A1) into (A3),

$$-dU_4/dt = aU_4 - \lambda_8 U_8(t_o) \exp(-bt) \ , \tag{A6}$$

where $a = \lambda_4 + R\xi$, (A7)

and $b = \lambda_8 + \xi$.

From equation (A6), it may be shown that

$$U_4 = U_4(t_o) \exp(-at) + \frac{\lambda_8}{(b-a)} U_8(t_o) (\exp(-at) - \exp(-bt)) \ . \tag{A9}$$

The activity ratio

$$Su = \frac{\lambda_4 U_4}{\lambda_8 U_8} = \lambda_4 U_4 / \lambda_8 U_8(t_0) \exp(-bt) \ . \qquad \text{(A10)}$$

Substituting (A10) into (A9),

$$Su = Su(t_0) \exp (b-a)\ t + \frac{\lambda_4}{(b-a)} (\exp (b-a)t - 1) \ , \qquad \text{(A11)}$$

where $Su(t_0)$ is the activity ratio at the initial time t_0.

A2. THORIUM-230

From equations (A4), (A7), (A8) and (A10),

$$-dI/dt = \lambda_i I - \lambda_4 U_4(t_0) \exp (-at)$$

$$+ \frac{\lambda_4 \lambda_8}{(b-a)} U_8(t_0) (\exp (-at) - \exp (-bt)) \ . \qquad \text{(A12)}$$

The solution of (A12), which can be most readily checked by back substitution is

$$I = I_0 \exp (-\lambda_i t) + \frac{\lambda_4}{(\lambda_i - a)} U (t_0) [\exp(-at) - \exp(-\lambda_i t)]$$

$$+ \frac{\lambda_4 \lambda_8 \ U(t_0)}{(b-a)(\lambda_i - a)(\lambda_i \ b)} [(b-a) \exp (-\lambda_i t)$$

$$+ (\lambda_i - b) \exp (-at) - (\lambda_i - a) \exp (-bt)] \ . \qquad \text{(A13)}$$

The activity ratio

$$Si = \lambda_i I / \lambda_4 U_4 \ . \qquad \text{(A14)}$$

Substituting (A14) into (A13),

$$Si \times D = Si(t_0) \exp(a - \lambda_i)t + \lambda_i(1 - \exp(a - \lambda_i)t)/(\lambda_i - a)$$

$$+ \lambda_i \lambda_4 [(b - a) \exp((a - \lambda_i)t + (a - \lambda_i) \exp[-(b - a)]t + \lambda_i - b]/$$

$$[(b - a)(a - \lambda_i)(b - \lambda_i) S(t_0)] \qquad \text{(A15)}$$

where $D = 1 + \lambda_4(1 - \exp[-(b-a)]t)/(b-a)/Su(t_0)$.

A3. PROTACTINIUM-231

From equations (A2) and (A5),

$$-dPa/dt = \lambda_p Pa - \lambda_s U_s(t_o) \exp(-ct) , \quad (A16)$$

where $c = \lambda_s + \xi$. (A17)

From Equation (A16),

$$Pa = Pa(t_o) \exp(-\lambda_p t) + \frac{\lambda_s U_s(t_o)}{c-\lambda_p}(\exp(-\lambda_p t) - \exp(-ct)) . \quad (A18)$$

The activity ratio

$$Sp = \lambda_p Pa/\lambda_s U_s , \quad (A19)$$

hence, from (A18) and (A19),

$$Sp = Sp(t_o) \exp(c-\lambda_p)t + \frac{\lambda_p}{(c-\lambda_p)} (\exp(c-\lambda_p)t - 1) . \quad (A20)$$

APPENDIX B

COMPUTER PROGRAM - MAIN MODEL

```
0060        DIMENSION NAME(2)
0070        IC=73
0080 C
0090 C    GENERAL MODEL OF URANIUM TRANSPORT IN GROUNDWATER
0100 C
0110 C    PARAMETERS
0120 C    SUO, SIO, SPO = INITIAL ACT. RATIOS OF U4/U8,TH/U4,
0130 C    PA/U5
0140 C    AR234,AR230,AR231 = EXPERIMENTAL DATA - U4/U8,
0150 C    TH/U4,PA/U5
0160 C    E = LEACHING/DEPOSITION RATE IN [C4] UNITS
0170 C    R = EFFECTIVE L/D RATIO OF U4 TO U8
0180 C    T = TIME IN [KY]
0190 C
0200 C   INITIAL CODITIONS
0210 C
0220        CALL SCAN(2,1,IC,SUO,1)
0230        CALL SCAN(2,1,IC,SIO,1)
0240        CALL SCAN(2,1,IC,SPO,1)
0250        C4=0.693/248
0260        C8=0.693/4510000
0270        CI=0.693/75.2
0280        C5=0.693/710000
0290        CP=0.693/32.5
0300        ALE1=0.02
0310        ALE2=0.02
0320        ALE3=0.02
0330 C
0340 C   EXPERIMENTAL DATA
0350 C
0360        DO 60 I=1,5
0370        READ(1,10)NAME
0380     10 FORMAT(2A4)
0390        WRITE(3,11)NAME
0400     11 FORMAT(1H ,2A4,//)
0410        CALL SCAN(2,1,IC,AR234,1)
0420        CALL SCAN(2,1,IC,AR230,1)
0430        CALL SCAN(2,1,IC,AR231,1)
0440        WRITE(3,2)AR234,AR230,AR231,ALE1,ALE2,ALE3,SUO,SIO,SPO
0450      2 FORMAT(1H ,3X,11H234U/238U= ,F4.2,5X,12H230TH/234U= ,F4.2,
0460       14X,12HPA231/235U= ,F4.2,4X,/,4X,5HALE1=,F4.2,5X,5HALE2=,F4.2,
0470       25X,5HALE3=,F4.2,//,4X,4HSUO=,F4.2,5X,4HSIO=,F4.2,5X,
0480       34HSPO=,F4.2)
0490        WRITE(3,3)
0500      3 FORMAT(1H ,2X,4HTIME,13X,1HR,7X,13HLEACH +/- VAR)
0510     19 EMI=1000.0
0520        EMA=-1000.0
0530 C
```


BEST COPY AVAILABLE

```
0540 C    CALCULATION OF SU AND SP VALUES
0550 C
0560        DO 60 J1=1,31
0570        T=(J1+0.01)**2
0580        DO 60 J3=1,10
0590        R=0.40+0.15*J3
0600        DO 50 J2=1,150
0610        E=-15.05+0.2*J2
0620        E=E*C4
0630        A1=C8+E*(1-R)-C4
0640        EX1=EXP(A1*T)
0650        SU=SU0*EX1+C4*(EX1-1)/A1
0660        IF(SU.EQ.0.0) GO TO 50
0670        DSU=(SU-AR234)/SU
0680        DSU=ABS(DSU)
0690        IF(DSU.GE.ALE1) GO TO 50
0700        B5=C5-CP+E
0710        EX5=EXP(B5*T)
0720        SP=SP0*EX5+CP*(EX5-1)/B5
0730        IF(SP.EQ.0.0) GO TO 50
0740        DSP=(SP-AR231)/SP
0750        DSP=ABS(DSP)
0760        IF(DSP.GE.ALE3) GO TO 50
0770 C
0780 C    CALCULATION OF SI
0790 C
0800        A2=C4+R*E-CI
0810        A3=C8+E-CI
0820        B1=CI/(CI-C4-R*E)
0830        B2=CI*C4/A1/A2/A3
0840        B3=C4/A1
0850        EX2=EXP(A2*T)
0860        EX3=1/EX1
0870        SI2=B2*(A1*EX2+A2*EX3-A3)/SU0
0880        SI3=1+B3*(1-EX3)/SU0
0890        IF(SI3.EQ.0.0) GO TO 50
0900        SI1=SI0*EX2+B1*(1-EX2)
0910        SI=(SI1+SI2)/SI3
0920        IF(SI.EQ.0.0) GO TO 50
0930        DSI=(SI-AR230)/SI
0940        DSI=ABS(DSI)
0950        IF(DSI.GE.ALE2) GO TO 50
0960        E=E/C4
0970 C
0980 C    CALCULATION OF MEAN L/D RATE
0990 C
1000        IF(EMI.GE.E)EMI=E
1010        IF(EMA.LE.E)EMA=E
1020        E=E*C4
1030     50 CONTINUE
1040        EAV=(EMI+EMA)/2
1050        EBL=(EMA-EMI)/2
1060        IF(EMI.EQ.1000.0) GO TO 60
1070        WRITE(3,6)T,R,EAV,EBL
1080      6 FORMAT(1H ,2X,F5.0,10X,F4.2,5X,F5.2,3X,F5.2)
1090     60 CONTINUE
1100        STOP
1110        END
```


BEST COPY AVAILABLE

APPENDIX C

CORRELATION BETWEEN THE PRESENT MODEL AND THE URANIUM TREND DATING MODEL

Slope of the Uranium Trend Line

The uranium trend dating model involves interpretation of the plots of $(^{234}U\text{-}^{238}U)/^{238}U$ (=Y) against $(^{234}U\text{-}^{230}Th)/^{238}U$ (=X). The slope Y/X is presented in the form of the Bateman equation

$$Y/X = \frac{C_1 \exp(-\lambda_o t) + C_2 \exp(-\lambda_4 t)}{C_3 \exp(-\lambda_o t) + C_4 \exp(-\lambda_4 t) + C_5 \exp(-\lambda_i t)} \quad , \qquad (C1)$$

where C_1, C_2, C_3, C_4, C_5 are constant; and λ_4, λ_i and λ_o are decay constants associated with ^{234}U, ^{230}Th and the uranium flux factor F_o.

From the present model (Equations (6) and (7), Section 2.2)

$$Y/X = (Su - 1)/(Su - Si_8)$$

$$= \frac{Su(o)\ E_1 + \lambda_4(E_1-1)/A - 1}{(Su(o)E_1 + \lambda_4(E_1-1)/A - Si_8(t_o)E - \lambda_i\ Su(t_o)(E_1-E_2)/C - \lambda_i\ \lambda_4(AE_2 - BE_1 - C)/ABC} \qquad (C2)$$

where $a = \lambda_4 + R\xi$, $b = \lambda_8 + \xi$, $A = b - a$, $B = b - \lambda_i$, $C = \lambda_i - a$, $E_1 = \exp(b-a)t$, $E = \exp(b -)t$.[1] and Su and Si_8 are the $^{234}U/^{238}U$ and $^{230}Th/^{238}U$ ARs.

Equation (A2) may be expressed in the form

$$Y/X = (m\ E_1 + n)/(p\ E_1 + qE_2 + s) \quad , \qquad (C3)$$

where $m = Su(o) + \lambda_4/A$, $n = \lambda_4/A - 1$, $p = Su(o)(1 - \lambda_i/C) + \lambda_4(1 + \lambda_i/C)/A$, $q = \lambda_i(Su(o) - \lambda_4/B)/C - Si_8(o)$, and $s = \lambda_4(1 + \lambda_i/B)/A$.

Hence $$Y/X = (m\ G_1G_2 + n)/(p\ G_1G_2 + q\ G_oG_3 + s) \quad , \qquad (C4)$$

where $E_1 = G_1G_2$, $E_2 = G_oG_3$, $G_o = \exp(\xi t)$, $G_1 = \exp(\xi(1 - R)t)$, $G_2 = \exp(\lambda_8 - \lambda_i)t$, $G_3 = \exp((\lambda_8 - \lambda_i)t)$.

After dividing by G_o, rearranging and back-substitution.

$$Y/X = \frac{n \exp(-\xi t) + m \exp[-(\lambda_4 - \lambda_8 + \xi R)]t}{s \exp(-\xi t) + p \exp[-(\lambda_4 - \lambda_8 + \xi R)]t + q \exp[-(\lambda_i - \lambda_8)]t} \quad . \qquad (C5)$$

APPENDIX D

ALGEBRAIC EXPRESSION FOR THE INTERCEPT OF THE URANIUM TREND LINE

From Equation (21) of Section 3, the intercept x_i is given by:

$$x_i = x_t - y_t/(\delta y/\delta x) \quad , \tag{D1}$$

where $$\delta y/\delta x \cong (dy/dt)/(dx/dt) \quad , \tag{D2}$$

where x_t and y_t are the $(^{238}U\text{-}^{230}Th)/^{238}U$ and $(^{234}U\text{-}^{238}U)/^{238}U$ ARs at time t. From Equations (6) and (7) of Section 2.2

$$y = n \exp(-\xi t) + m \exp[-(\lambda_4 - \lambda_8 + \xi R)] \quad , \tag{D3}$$

$$x = s \exp(-\xi t) + p \exp[-(\lambda_4 - \lambda_8 + \xi R)]t + q \exp[-(\lambda_i - \lambda_8)]t. \tag{D4}$$

where n, m, s, p and q are defined by Equation (C3).

From Equation (D3),

$$dy/dt = -n \xi \exp(-\xi t) - m (\lambda_4 - \lambda_8 + \xi R)\exp[-(\lambda_4 - \lambda_8 + \xi R)]t \quad , \tag{D5}$$

$$dx/dt = -s \xi \exp(-\xi t) - p (\lambda_4 - \lambda_8 + \xi R)\exp[-(\lambda_4 - \lambda_8 + \xi R)]t - q (\lambda_i - \lambda_8)\exp[-(\lambda_i - \lambda_8)]t \quad . \tag{D6}$$

Hence

$$dy/dx = \frac{n \xi E_1 + mC_1 E_2}{s \xi E_1 + pC_1 E_2 + qC_2 E_3} \quad , \tag{D7}$$

where $E_1 = \exp(-\xi t)$ $\qquad C_1 = \lambda_4 - \lambda_8 + \xi R$

$E_2 = \exp[-(\lambda_4 - \lambda_8 + \xi R)]t$ $\qquad C_2 = \lambda_i - \lambda_8$.

$E_i = \exp[-(\lambda_i - \lambda_8)]t$

The intercept x_i is obtained by substituting Equation (D7) into equation (D1).

APPENDIX E

ANALYTICAL SOLUTIONS OF THE SIMULTANEOUS DIFFERENTIAL EQUATIONS DESCRIBING THE DISTRIBUTION OF ^{238}U, ^{234}U AND ^{230}Th IN AMORPHOUS AND CRYSTALLINE IRON

E1. URANIUM-238

The distribution of uranium-238 through the amorphous and crystalline iron may be described by Equations (E1) and (E2) which are identical to Equations (31) and (32) of Section 4.1. The symbols are defined following Equation (39)

$$\begin{cases} \dfrac{d^8U_a}{dt} = -(\lambda_8 + \xi_a)\ {}^8U_a - \tau\ ({}^8U_a - {}^8U_x) \ , & \text{(E1)} \\ \dfrac{d^8U_x}{dt} = -\lambda_8\ {}^8U_x + \tau\ ({}^8U_a - {}^8U_x) \ . & \text{(E2)} \end{cases}$$

Solution

$$= h_1 e^{x_1 t} + h_2 e^{x_2 t} \ , \qquad \text{(E3)}$$

$$= \frac{x_1 - a}{\tau} h_1 e^{x_1 t} + \frac{x_2 - a}{\tau} h_2 e^{x_2 t} \ , \qquad \text{(E4)}$$

where $$a = -(\tau + \xi + \lambda_8) \ , \qquad \text{(E5)}$$

$$x_{1/2} = -(\tau + \lambda_8 + \frac{\xi}{2}) \pm \tfrac{1}{2}\sqrt{\xi^2 + 4\tau^2} \ , \qquad \text{(E6)}$$

$$h_1 = -\frac{x_2\ {}^8U_{a(o)} - {}^8E_{a(o)}}{x_1 - x_2} \ , \qquad \text{(E7)}$$

$$h_2 = \frac{x_1\ {}^8U_{a(o)} - {}^8E_{a(o)}}{x_1 - x_2} \ , \qquad \text{(E8)}$$

$${}^8E_a = a\ {}^8U_{a(o)} + \tau\ {}^8U_{x(o)} \ . \qquad \text{(E9)}$$

The level of uranium in the clay/quartz (CQ) phase is represented by Equation (33) of Section 4, or

$$\frac{d^8U_{CQ}}{dt} = -(\lambda_8 + \xi_{CQ})\ {}^8U_{CQ} \quad , \tag{E10}$$

the solution of which is

$${}^8U_{CQ} = {}^8U_{CQ}(0)\ \exp\ (-(\lambda_8 + \xi_{CQ})t) \quad , \tag{E11}$$

where ξ_{CQ} is the rate of leaching of uranium-238 from the clay/quartz phase.

E2. URANIUM-234

The equations describing the distribution of uranium-234 in the amorphous and crystalline iron are set out as Equations (44) and (47) of Section 4.

$$\begin{cases} \dfrac{d^8U_a}{dt} = {}^8\phi_e^a\ \lambda_8{}^8U_a - (\lambda_4 + \xi){}^4U_a - \tau({}^4U_a - {}^4U_x) & \text{(E12)} \\ \dfrac{d^4U_x}{dt} = {}^8\phi_e^x\ \lambda_8{}^8U_x - \lambda_4{}^4U_x + \tau({}^4U_a - {}^4U_x) \quad . & \text{(E13)} \end{cases}$$

Solution

$$U_4{}^a = \sum_{j=1}^{4} g_j e^{x_j t} \quad , \tag{E14}$$

$$U_4{}^x = \sum_{j=1}^{4} g_j \frac{x_j - w_j}{\tau} e^{x_j t} \quad . \tag{E15}$$

where

$$g_j = \lambda_8 h_j \frac{{}^8\phi_e^a(x_j - \ell) + {}^8\phi_e^x(x_j - a)}{x_j{}^2 - (k+\ell)x_j + k\ell - \tau^2} \qquad \text{for } j = 1, 2. \tag{E16}$$

$$g_{3/4} = \frac{(-1)^j}{x_3 - x_4}\ (g_1x_1 + g_2x_2 + ({}^4U_a(o) - g_1 - g_2)x_{4/3} - {}^4E_a(o)) \tag{E17}$$

$$\text{for } j = 3, 4.$$

and $k = -(\tau + \lambda_4 + R\xi)$, (E18)

$\ell = -(\tau + \lambda_4)$, (E19)

$^4E_a(o) = k\,^4U_a(o) + \tau\,^4U_x(o) + {}^8\phi_e^a \lambda_8\,^8U_a(o)$, (E20)

$x_{3/4} = -(\tau + \lambda_4 + \frac{R\xi}{2}) \pm \frac{1}{2}\sqrt{(R\xi)^2 + 4\tau^2}$, (E21)

$$w_j = \begin{cases} k + {}^8\phi^a\ \lambda_8\ \dfrac{h_j}{g_j} & \text{for } j = 1, 2, \\ k & \text{for } j = 3, 4. \end{cases} \quad \text{(E22)}$$

From Equation (48) of Section 4.1,

$d\ U_{CQ}/dt = {}^8\phi_e^{CQ}\ \lambda_8\ {}^8U_{CQ} - (\lambda_4 + R_e\ \xi_{CQ})\ {}^4U_{CQ}$. (E23)

Solution

$$^4U_{CQ} = {}^4U_{CQ}(0)\ \exp(-a_{CQ}t) + \lambda_8\ {}^8\phi_e^{CQ}\ {}^8U_{CQ}(0)$$
$$(\exp(-a_{CQ}\ t) - \exp(-b_{CQ}\ t))/(b_{CQ} - a_{CQ}) , \quad \text{(E24)}$$

where

$$a_{CQ} = \lambda_4 + R\ \xi_{CQ}$$
$$b_{CQ} = \lambda_8 + \xi_{CQ} \quad . \quad \text{(E25)}$$

E3. THORIUM-230

The thorium fractionation in the amorphous and crystalline iron may be calculated from Equations (51) and (52) of Section 4.1, which are set out below:

$$\begin{cases} \dfrac{dI_a}{dt} = {}^4\phi_e^a\ \lambda_4\,^4U_a - \lambda_i I_a - \tau(I_a - I_x) , & \text{(E26)} \\ \dfrac{dI_x}{dt} = {}^4\phi_e^x\ \lambda_4\,^4U_x - \lambda_i I_x + \tau(I_a - I_x) . & \text{(E27)} \end{cases}$$

Solution

$$I^a = \sum_{j=1}^{4} f_j e^{x_j t} + f_5 e^{-\lambda_i t} + f_6 e^{-(2\tau + \lambda_i)t} , \qquad \text{(E28)}$$

$$I^x = \frac{1}{\tau} \sum_{j=1}^{4} [f_j (x_j + \tau + \lambda_i) - {}^4\phi^a \lambda_4 g_j] e^{x_j t} + f_5 e^{-\lambda_i t} -$$

$$- f_6 e^{-(2\tau + \lambda_i)t} , \qquad \text{(E29)}$$

where

$$f_j = \lambda_4 g_j \frac{{}^4\phi_e^a (x_j + \tau + \lambda_i) + {}^4\phi_e^x (x_j - w_j)}{x_j^2 + 2(\tau + \lambda_i) x_j + \lambda_i^2 + 2\lambda_i \tau} \qquad \text{(E30)}$$

for j = 1, ... 4.

$$f_m = -\frac{(-1)^m}{2\tau} q I_a(o) - \frac{(-1)^m}{2\tau} i_{E_a}(o) + \frac{(-1)^m}{2\tau} \sum_{j=1}^{4} (x_j + q) f_j \qquad \text{(E31)}$$

$$q = \lambda_i + 2(6 - m)\tau \qquad \text{for m = 5, 6.}$$

$$i_{E_a}(o) = -(\tau + \lambda_i) I_a(o) + \tau I_x(o) + {}^4\phi^a \lambda_4 (g_1 + g_2 + g_3 + g_4) . \qquad \text{(E32)}$$

The thorium-230 fractionation in the clay/quartz phase may be calculated from Equation (53) of Section 4.1.

$$dI_{CQ}/dt = {}^4\phi_e^{CQ} \lambda_4 {}^4U_{CQ} - \lambda_i I_{CQ} . \qquad \text{(E33)}$$

Solution

$$I_{CQ} = I_{CQ}(0) \exp(-\lambda_i t)$$

$$+ \lambda_4 {}^4\phi_e^{CQ} {}^4U_{CQ}(0) (\exp(-\lambda_i t) - \exp(-a_{CQ} t))/(a_{CQ} - \lambda_i)$$

$$+ \lambda_8 \lambda_4 {}^8\phi_e^{CQ} {}^4\phi_e^{CQ} U_8(0) [(a_{CQ} - b_{CQ}) \exp(-\lambda_i t)$$

$$+ (b_{CQ} - \lambda_i) \exp(-a_{CQ} t) - (a_{CQ} - \lambda_i)$$

$$\exp(-b_{CQ} t)]/[(a_{CQ} - b_{CQ})(b_{CQ} - \lambda_i)(a_{CQ} - \lambda_i)] . \qquad \text{(E34)}$$

APPENDIX F

COMPUTER PROGRAM - MULTIPHASE

```
0060        DIMENSION NAME(2)
0070        IC=73
0080 C
0090 C   MODEL OF URANIUM TRANSPORT IN MULTIPHASE SYSTEM
0100 C
0110 C   PARAMETERS
0120 C    SU,SI = U4/U8,TH/U4 ACT.RATIOS, EG. SUA0= INITIAL U4/U8 IN AMOR-
0130 C              PHOUS PHASE
0140 C    RU,RI = RESPECTIVE EXPERIMENTAL DATA, EG RIX=TH/U4 IN CRYSTALLINE
0150 C              PHASE
0160 C    TAU = CHEMICAL EXCHANGE PARAMETER
0170 C    FI =  REDUCED RECOIL PARAMETER, EG. FI4Q= FI FOR U4 IN CLAY/QUARTZ
0180 C    R =   EFFECTIVE U4/U8 LEACHING/DEPOSITION RATIO
0190 C    E =   LEACHING/DEPOSITION RATE IN [C4] UNITS - AMORPHOUS PHASE
0200 C    EQ = L/D RATE - CLAY/QUARTZ PHASE
0210 C    T =  TIME [KY]
0220 C
0230        HFLAG=1.0
0240        C4=0.693/248
0250        C8=0.693/4510000
0260        CI=0.693/75.2
0270        WRITE(3,1)
0280      1 FORMAT(1H1,20X,39HURANIUM TRANSPORT IN MULTIPHASE SYSTEMS)
0290        CALL SCAN(2,1,IC,FIT,1)
0300        CALL SCAN(2,1,IC,FI8A,1)
0310        CALL SCAN(2,1,IC,FI8X,1)
0320        CALL SCAN(2,1,IC,FI8Q,1)
0330        CALL SCAN(2,1,IC,FI4A,1)
0340        CALL SCAN(2,1,IC,FI4X,1)
0350        CALL SCAN(2,1,IC,FI4Q,1)
0360        CALL SCAN(2,1,IC,SUA0,1)
0370        CALL SCAN(2,1,IC,SIA0,1)
0380        CALL SCAN(2,1,IC,SUX0,1)
0390        CALL SCAN(2,1,IC,SIX0,1)
0400        CALL SCAN(2,1,IC,SUQ0,1)
0410        CALL SCAN(2,1,IC,SIQ0,1)
0420        DO 80 J=1,10
0430        READ(1,3) NAME
0440      3 FORMAT(2A4)
0450        CALL SCAN(2,1,IC,RUA,1)
0460        CALL SCAN(2,1,IC,RUX,1)
0470        CALL SCAN(2,1,IC,RUQ,1)
0480        CALL SCAN(2,1,IC,RIA,1)
0490        CALL SCAN(2,1,IC,RIX,1)
0500        CALL SCAN(2,1,IC,RIQ,1)
0510        WRITE(3,4) NAME,RUA,RUX,RUQ,RIA,RIX,RIQ,SUA0,SIA0,SUX0,SIX0,
0520       1SUQ0,SIQ0,FI8A,FI4A,FI8X,FI4X,FI8Q,FI4Q,FIT
0530      4 FORMAT(1H ,5X,2A4,20X,4HRUA=,F4.2,2X,4HRUX=,F4.2,2X,4HRUQ=,F4.2,
0540       12X,4HRIA=,F4.2,2X,4HRIX=,F4.2,2X,4HRIQ=,F4.2,
0550       2/,20X,5HSUA0=,F4.2,2X,5HSIA0=,F4.2,4X,5HSUX0=,F4.2,5HSIX0=,
0560       3F4.2,4X,5HSUQ0=,F4.2,5HSIQ0=,F4.2,/,20X,5HFI8A=,F4.2,2X,
0570       45HFI4A=,F4.2,4X,5HFI8X=,F4.2,2X,5HFI4X=,F4.2,4X,5HFI8Q=,F4.2,2X,
```


BEST COPY AVAILABLE

```
0580       55HFI40=,F4.2,//,20X,20HALLOWED TOLERANCE = ,F4.2,//)
0590         WRITE(3,5)
0600       5 FORMAT(1HO,5X,4HTIME,2X,4HE-AM,2X,4HE-CO,3X,1HR,4X,3HTAU)
0610 C
0620 C     CALCULATIONS
0630 C     TIME
0640 C
0650         DO 70 K1=1,50
0660         T=2.0*K1
0670         IF(T.LE.20.0) GO TO 50
0680         T=20.0+5.0*K1
0690         IF(T.LE.40.0) GO TO 50
0700         T=40.0+10.0*K1
0710         IF(T.LE.100.0) GO TO 50
0720         T=100.0+20.0*K1
0730         IF(T.LE.300.0) GO TO 50
0740         T=300.0+50.0*K1
0750 C
0760 C     CLAY/QUARTZ PHASE
0770 C
0780       50 DO 70 K2= 1,33
0790         EQ=-10.0+0.3*K2
0800         DO 70 K3=1,10
0810         R=0.5+0.3*K3
0820         EQ=EQ*C4
0830         AQ=C4+R*EQ
0840         BQ=C8+EQ
0850         IF((BQ-AQ).EQ.0.0) GO TO 70
0860         IF((AQ-CI).EQ.0.0) GO TO 70
0870         IF((BQ-CI).EQ.0.0) GO TO 70
0880         EX8=EXP(-AQ*T)
0890         EX9=EXP(-BQ*T)
0900         IF(EX9.LE.0.000001) GO TO 70
0910         U4Q=SUQ0*EX8+C4*FI8Q*(EX8-EX9)/(BQ-AQ)
0920         SUQ=U4Q/EX9
0930         DUQ=(SUQ-RUQ)/RUQ
0940         DUQ=ABS(DUQ)
0950         IF(DUQ.GE.FIT) GO TO 70
0960         EX5=EXP(-CI*T)
0970         TQ1=SIQ0*EX5+CI*FI4Q*(EX5-EX9)/(AQ-CI)
0980         TQ2=C4*CI*FI8Q*FI4Q/SUQ0/(BQ-AQ)/(BQ-CI)/(AQ-CI)
0990         TQ3=(AQ-BQ)*EX5+(BQ-CI)*EX8-(AQ-CI)*EX9
1000         TQ=TQ1-TQ2*TQ3
1010         U4IQ=EX8+C4*FI8Q*(EX8-EX9)/(BQ-AQ)/SUQ0
1020         IF(U4IQ.EQ.0.0) GO TO 70
1030         SIQ=TQ/U4IQ
1040         DIQ=(SIQ-RIQ)/RIQ
1050         DIQ=ABS(DIQ)
1060         IF(DIQ.GE.FIT) GO TO 70
1070 C
1080 C     AMORPHOUS AND CRYSTALINE PHASES
```


BEST COPY AVAILABLE

```
1090 C
1100        DO 70 J1=1,32
1110        E=-10.0+0.3*J1
1120        E=E*C4
1130        DO 70 J2=1,8
1140        TAU=0.5+0.3*J2
1150        TAU=TAU*C4
1160        A1=-(TAU+E+C8)
1170        A2=-(TAU+C4+R*E)
1180        A3=-(TAU+C4)
1190        XA=-TAU-C8-E/2
1200        XB=(E**2+4*TAU**2)**0.5
1210        XC=-TAU-C4-R*E/2
1220        XD=((R*E)**2+4*TAU**2)**0.5
1230        X1=XA+0.5*XB
1240        X2=XA-0.5*XB
1250        X3=XC+0.5*XD
1260        X4=XC-0.5*XD
1270        IF((X4-X3).EQ.0.0) GO TO 70
1280        U8A0=1.0
1290        U8X0=1.0
1300        U4A0=SUA0*U8A0*C8/C4
1310        U4X0=SUX0*U8X0*C8/C4
1320        E8A0=A1*U8A0+TAU*U8X0
1330        IF((X1-X2).EQ.0.0) GO TO 70
1340        H1=-(X2*U8A0-E8A0)/(X1-X2)
1350        H2=(X1*U8A0-E8A0)/(X1-X2)
1360        E4A0=A2*U4A0+TAU*U4X0+FI8A*C8*U8A0
1370        GM=C8*H1*(FI8A*(X1-A3)+FI8X*(X1-A1))
1380        IF(GM.EQ.0.0) GO TO 70
1390        WA=X1**2-(A2+A3)*X1+A2*A3-TAU**2
1400        IF(WA.EQ.0.0) GO TO 70
1410        G1=GM/WA
1420        GN=C8*H2*(FI8A*(X2-A3)+FI8X*(X2-A1))
1430        IF(GN.EQ.0.0) GO TO 70
1440        WB=X2**2-(A2+A3)*X2+A2*A3-TAU**2
1450        IF(WB.EQ.0.0) GO TO 70
1460        G2=GN/WB
1470        IF((G1*G2).EQ.0.0) GO TO 70
1480        GA=G1*X1+G2*X2-E4A0
1490        GB=U4A0-G1-G2
1500        G3=(GA+GB*X4)/(X4-X3)
1510        G4=(GA+GB*X3)/(X3-X4)
1520        EX1=EXP(X1*T)
1530        EX2=EXP(X2*T)
1540        EX3=EXP(X3*T)
1550        EX4=EXP(X4*T)
1560        U8A=H1*EX1+H2*EX2
1570        U4A=G1*EX1+G2*EX2+G3*EX3+G4*EX4
1580        SUA=C4*U4A/C8/U8A
1590        DUA=(SUA-RUA)/RUA
1600        DUA=ABS(DUA)
```


BEST COPY AVAILABLE

```
      IF(DUA.GE.FIT) GO TO 70
      EX5=EXP(-CI*T)
      EX6=EXP(-2*TAU*T-CI*T)
      U8X=H1*EX1*(X1-A1)/TAU+H2*EX2*(X2-A1)/TAU
      U4X=G1*EX1*(X1-Z1)+G2*EX2*(X2-Z2)+G3*EX3*(X3-Z3)+G4*EX4*(X4-Z4)
      U4X=U4X/TAU
      SUX=C4*U4X/C8/U8X
      DUX=(SUX-RUX)/RUX
      DUX=ABS(DUX)
      IF(DUX.GE.FIT) GO TO 70
      THA0=SIA0*SUA0*C8/CI
      THX0=SIX0*SUX0*C8/CI
      EIA0=-(TAU+CI)*THA0+TAU*THX0+FI4A*C4*(G1+G2+G3+G4)
      IF(G1.EQ.0.0) GO TO 70
      IF(G2.EQ.0.0) GO TO 70
      Z1=A2+FI8A*C8*H1/G1
      Z2=A2+FI8A*C8*H2/G2
      Z3=A2
      Z4=A2
      FX1=C4*G1*(FI4A*(X1+TAU+CI)+FI4X*(X1-Z1))
      Y1=X1**2+2*(TAU+CI)*X1+CI*CI+2*CI*TAU
      IF(Y1.EQ.0.0) GO TO 70
      F1=FX1/Y1
      FX2=C4*G2*(FI4A*(X2+TAU+CI)+FI4X*(X2-Z2))
      Y2=X2**2+2*(TAU+CI)*X2+CI*CI+2*CI*TAU
      IF(Y2.EQ.0.0) GO TO 70
      F2=FX2/Y2
      FX3=C4*G3*(FI4A*(X3+TAU+CI)+FI4X*(X3-Z3))
      Y3=X3**2+2*(TAU+CI)*X3+CI*CI+2*CI*TAU
      IF(Y3.EQ.0.0) GO TO 70
      F3=FX3/Y3
      FX4=C4*G4*(FI4A*(X4+TAU+CI)+FI4X*(X4-Z4))
      Y4=X4**2+2*(TAU+CI)*X4+CI*CI+2*CI*TAU
      IF(Y4.EQ.0.0) GO TO 70
      F4=FX4/Y4
      FA=2*TAU+CI
      F5=FA*THA0/2/TAU+EIA0/2/TAU
      F5=F5-(F1*(X1+FA)+F2*(X2+FA)+F3*(X3+FA)+F4*(X4+FA))/2/TAU
      F6=-CI*THA0/2/TAU+(F1*(X1+CI)+F2*(X2+CI)+F3*(X3+CI)+F4*(X4+CI))/2/
     1TAU-EIA0/2/TAU
      THA=F1*EX1+F2*EX2+F3*EX3+F4*EX4+F5*EX5+F6*EX6
      SIA=CI*THA/C4/U4A
      DIA=(SIA-RIA)/RIA
      DIA=ABS(DIA)
      IF(DIA.GE.FIT) GO TO 70
      TT=TAU+CI
      FF=FI4A*C4
      T1=(F1*(X1+TT)-FF*G1)*EX1
      T2=(F2*(X2+TT)-FF*G2)*EX2
      T3=(F3*(X3+TT)-FF*G3)*EX3
      T4=(F4*(X4+TT)-FF*G4)*EX4
```


BEST COPY AVAILABLE

```
2120        THX=(T1+T2+T3+T4)/TAU+F5*EX5-F6*EX6
2130        SIX=CI*THX/C4/U4X
2140        DIX=(SIX-RIX)/RIX
2150        DIX=ABS(DIX)
2160        IF(DIX.GE.FIT) GO TO 70
2170     55 E=E/C4
2180        EQ=EQ/C4
2190        TAU=TAU/C4
2200        WRITE(3,8)T,E,EQ,R,TAU
2210      8 FORMAT(1H ,5X,F5.0,1X,F4.1,3F6.2)
2220        HFLAG=0.0
2230        EQ=EQ*C4
2240        E=E*C4
2250        TAU=TAU*C4
2260     70 CONTINUE
2270        IF(HFLAG.EQ.0.0) GO TO 80
2280        WRITE(3,9)
2290      9 FORMAT(1H0,38X,44HNO CORRELLATION WAS FOUND FOR THESE SETTINGS)
2300     80 CONTINUE
2310        STOP
2320        END
```


BEST COPY AVAILABLE

APPENDIX G

LIST OF SYMBOLS

a	$\lambda_4 + R\xi$
a_{m_i}	activity of ith chain member
b	$\lambda_8 + \xi$
c	$\lambda_5 + \xi$
c_{m_i}	concentration of i^{th} chain member
F_o	uranium flux factor
h_I, h_{II}, h_{III}	heights above the zones I/II, II/III and III/IV respectively
H	Heaviside function
g_{m_i}	function related to c_{m_i}
I	^{230}Th
K_d	adsorption coefficient
K_d^r	adsorption coefficient of reference isotope
K_{m_i}	distribution coefficient
L	migration distance
m_i	mass number of i^{th} chain member
Pa	^{231}Pa
q	Darcy velocity
R	$^{234}U/^{238}U$ ratio of the leachate (or of the depositing material) - usually activity ratio found in groundwater adjacent to the deposit
R_4	distribution coefficient
Ra	^{226}Ra
R_{CQ}	$^{234}U/^{238}U$ AR in C/Q
Re	recoil factor, e.g. $^aRe^x$ - recoil from amorphous to crystalline

R_{geol}	rate of leaching (or deposition) or radium - allogenic component
R_{m_i}	retardation factor for mass number m_i
Su, Si, Sp	$^{234}U/^{238}U$, $^{230}Th/^{234}U$, $^{231}Pa/^{235}U$
a_S^x	contact area between amorphous and crystalline iron
t	elapsed time
t_o	initial time
Tu_x	average concentration of uranium in the crystalline rock undergoing weathering
U_4, U_5, U_8	^{234}U, ^{235}U, ^{238}U
W	rate of advance of the weathering front
λ_{m_i}	decay constant of i^{th} chain member
λ_4, λ_5, λ_8	decay constants of ^{234}U, ^{235}U, ^{238}U
λ_i, λ_p, λ_r	decay constant of ^{230}Th, ^{231}Pa, ^{226}Ra
λ_o	decay constant associated with the uranium flux F(0) (uranium trend model, J.N. Rosholt)
ξ	rate of leaching (+ve) or deposition (-ve)
τ	rate of exchange between amorphous and crystalline iron
ρ	density
$\emptyset$	porosity
$\emptyset_e^a$	$1 - R_e\Theta(S,p)$, recoil parameter
(S,p)	function of the contact surface area

NRC FORM 335 (2-84) NRCM 1102, 3201, 3202

U.S. NUCLEAR REGULATORY COMMISSION

BIBLIOGRAPHIC DATA SHEET

SEE INSTRUCTIONS ON THE REVERSE

1 REPORT NUMBER (Assigned by TIDC, add Vol. No., if any)

NUREG/CR-5060
AAEC/C49

2 TITLE AND SUBTITLE

An Approach to the Mathematical Modelling of the Uranium Series Redistribution Within Ore Bodies

3 LEAVE BLANK

4 DATE REPORT COMPLETED

MONTH: June | YEAR: 1986

5 AUTHOR(S)

P.L. Airey, C. Golian and D.A. Lever

6 DATE REPORT ISSUED

MONTH: December | YEAR: 1987

7 PERFORMING ORGANIZATION NAME AND MAILING ADDRESS (Include Zip Code)

Australian Atomic Energy Commission
Lucas Heights Research Laboratories
Lucas Heights NSW 2234 Australia

8 PROJECT/TASK/WORK UNIT NUMBER

9 FIN OR GRANT NUMBER

B6661

10 SPONSORING ORGANIZATION NAME AND MAILING ADDRESS (Include Zip Code)

Division of Engineering
Office of Nuclear Regulatory Research
U.S. Nuclear Regulatory Commission
Washington, D.C. 20555

11a TYPE OF REPORT

Topical

b PERIOD COVERED (Inclusive dates)

12 SUPPLEMENTARY NOTES

13 ABSTRACT (200 words or less)

The distributions of the uranium series isotopes in the Koongarra ore body were "predicted" by a simple one-dimensional model of isotopic migration parameters. Controlling the "predictions" were the retardation factors and the groundwater flow rates. The conditions modelled were a groundwater flow rate of 1 meter per year, retardation factors of 1 x 10^4 for ^{238}U and of 1.2 x 10^4 for ^{234}U, and ^{230}Th is immobile. For this set of conditions, an exceptionally good agreement was observed between field-measured isotope ratios and "predicted" isotope ratios.

A multiphase model adequately describes the redistribution of uranium and daughter radionuclides in the weathered zone of the ore bodies. It redistributes U, Th and Ra isotopes among an aqueous phase, an amorphous iron phase, a crystalline phase and a "phase" of clay and quartz.

14 DOCUMENT ANALYSIS – a. KEYWORDS/DESCRIPTORS

Uranium Ore Body, Natural Analogue, High-Level Waste Transport Model Validation, transport modelling, uranium decay series, isotope fractionation, radionuclide migration

b. IDENTIFIERS/OPEN-ENDED TERMS

15 AVAILABILITY STATEMENT

Unlimited

16 SECURITY CLASSIFICATION

~~Unclassified~~

~~Unclassified~~

17 NUMBER OF PAGES

18 PRICE

*U.S. GOVERNMENT PRINTING OFFICE: 1987- 202-292:60316

BEST COPY AVAILABLE

UNITED STATES
NUCLEAR REGULATORY COMMISSION
WASHINGTON, D.C. 20555

OFFICIAL BUSINESS
PENALTY FOR PRIVATE USE, $300

SPECIAL FOURTH CLASS RATE
POSTAGE & FEES PAID
USNRC
PERMIT No. G-67

BEST COPY AVAILABLE